The Application of Remotely Sensed Inner-core Rainfall and Surface Latent Heat Flux in Typhoon Intensity Forecast

GAO, Si

A Thesis Submitted in Partial Fulfillment

of the Requirement for the Degree of

Doctor of Philosophy

in

GeoInformation Science

The Chinese University of Hong Kong

August 2010

Thesis/Assessment Committee

Professor Yee LEUNG (Chair)

Professor Long-Sang CHIU (Thesis Supervisor)

Professor Yuan-Zhi ZHANG (Committee Member)

Professor Gin-Rong LIU (External Examiner)

ABSTRACT

Abstract of thesis entitled:

The Application of Remote Sensed Inner-core Rainfall and Surface Latent Heat Flux in Typhoon Intensity Forecast

Submitted by GAO, Si

for the degree of Doctor of Philosophy

at The Chinese University of Hong Kong in July 2010

Despite improvements in statistical and dynamic models in recent years, the prediction of tropical cyclone (TC) intensity still lags that of track forecasting. Recent advances in satellite remote sensing coupled with artificial intelligence techniques offer us an opportunity to improve the forecasting skill of typhoon intensity.

In this study rapid intensification (RI) of TCs is defined as over-water minimum central pressure fall in excess of 20 hPa over a 24-h period. Composite analysis shows satellite-based surface latent heat flux (SLHF) and inner-core rain rate (IRR) are related to rapid intensifying TCs over the western North Pacific, suggesting SLHF and IRR have the potential to add value to TC intensity forecasting.

Several linear regression models and neural network models are developed for the intensity prediction of western North Pacific TC at 24-h, 48-h, and 72-h intervals. The datasets include Japan Meteorological Agency (JMA) Regional Specialized Meteorological Center Tokyo (RSMC Tokyo) best track data, the National Centers for Environmental Prediction (NCEP) Global Forecasting System Final analysis, the Tropical Rainfall Measuring Mission (TRMM) Microwave Imager sea surface temperature (SST), the Objectively Analyzed Air-sea Fluxes (OAflux) SLHF and TRMM Multisatellite Precipitation Analysis (TMPA) rain rate data. The models

include climatology and persistence (CLIPER), a model based on Statistical Typhoon Intensity Prediction System (STIPS), which serves as the BASE model, and a model of STIPS with additional satellite estimates of IRR and SLHF (STIPER). A revised equation of TC maximum potential intensity (MPI) is derived using TMI Optimally Interpolated Sea Surface Temperature data (OISST) with higher temporal and spatial resolutions. Analysis of the resulting models indicates that the STIPER model reduces the mean absolute intensity forecast error by 6% for TC intensity forecasts out to 72 h compared to the CLIPER and BASE. Neural network models with the same predictors as STIPER can provide up to 28% error reduction compared to STIPER. The largest improvement is the intensity forecasts of the rapidly intensifying and rapidly decaying TCs.

A logistic regression model (LRRI) and a neural network model (NNRI) for RI forecasting of TCs are developed for the period 2000–2007. The five significant predictors are intensity change in the previous 12 h, intensification potential, lower-level relative humidity, eddy flux convergence at 200 hPa, and vertical wind shear. The verification of forecasts in 2008 typhoon season shows that NNRI outperforms LRRI for RI detection.

摘 要

盡管用于熱帶氣旋強度預報的統計和動力模式在近年來有一定改進，然而熱帶氣旋強度預報仍落后于路徑預報。近來衛星遙感和人工智能技術方面的進展，為提高臺風強度預報水平提供了契機。

本文定義熱帶氣旋的迅速增強為海面上熱帶氣旋24小時中心最低氣壓下降≥20 hPa。合成分析結果顯示，基于衛星的海氣潛熱通量和內核區降水率與西太平洋熱帶氣旋迅速增強有關。因此，有可能利用海表潛熱通量和內核區降水率改進熱帶氣旋強度預報。

本文建立了一系列線性回歸模型和神經網絡模型用于 24 小時、48 小時和72 小時西太平洋熱帶氣旋強度預報。計算預報因子所使用的數據包括日本氣象廳（JMA）東京區域專責气象中心（RMSC Tokyo）的最佳路徑數據、美國國家環境預報中心（NCEP）全球預報系統的最終分析資料、熱帶降雨觀測計劃（TRMM）衛星微波成像儀（TMI）的海表溫度數據、美國 Woods Hole 海洋研究所客觀分析海氣通量（OAFlux）項目提供的海氣潛熱通量數據和 TRMM 多衛星降雨分析（TMPA）數據。建立的線性回歸模型包括氣候持續性模型（CLIPER）、基于統計臺風強度預報方案（STIPS）的模型（該模型作為基本模型（BASE））及添加了衛星觀測的海氣潛熱通量和內核區降水率為預報因子的STIPS 模型（STIPER）。利用更高時空分辨率的 TMI 最優插值的海表溫度修訂了熱帶氣旋最大潛在強度（MPI）方程。模型分析結果表明，相對于 BASE 模型，STIPER 模型的 24 至 72 小時強度預報平均絕對誤差下降最高達到 6%。與STIPER 模型比較，使用同樣預報因子的神經網絡模型的平均絕對預報誤差下降高達 28%。對迅速增強和迅速減弱熱帶氣旋的強度預報改進最大。

為預報熱帶氣旋是否迅速增強，利用 2000–2007 年的數據建立了邏輯回歸模型（LRRI）和神經網絡模型（NNRI）。五個顯著預報因子包括過去 12 小時的強度變化、增強潛勢、低層相對濕度、200 hPa 渦流通量輻合和垂直風切變。對2008 臺風季節的模型預報驗證表明 NNRI 模型優于 LRRI 模型。

ACKNOWLEDGEMENTS

First of all, I would like to express my sincere gratitude to my supervisor, Prof. Long Sang Chiu, for his instructive advice and valuable suggestions on my dissertation, without him this work would not have been completed. The encouragement he gave me and the research methodologies and life attitude I learned from him will be beneficial in my future career and life.

Thanks are extended to my committee members, Prof. Yee Leung, Prof. Yuanzhi Zhang, and Prof. Gin-Rong Liu for their help and advice. Thanks also go to Dr. Chung-Lin Shie, Dr. Roongroj Chokngamwong for the helpful discussion and suggestions. I would also like to thank Prof. Johnny Chan and Prof. William Rossow for their useful comments and suggestions on my presentation in a conference. I also appreciate the encouragement from Prof. Hui Lin during my study.

I am indebted to many colleagues in the Institute of Space and Earth Information Science (ISEIS) and the Department of Geography and Resource Management. A lot of wonderful memories remind me the times spent with Mr. Biao Liu, Mr. Shengxiao Wang, Mr. Shilai Cheng, Mr. Hongshuo Wang, Mr. Yu Zhou, Mr. Wei Zhang, Mr. Kai Wang, Mr. Kai Cao, Mr. Yong Xu, Ms. Hongyan Xi, Ms. Qing Zhao, Ms. Xuehua Gao, Ms. Chunlan Guo and other graduate students. Thanks go to them for any help they gave me.

I am very grateful to my parents and other relatives for their unselfish support and love. No matter where I go, I will always miss them and love them.

This work is supported by a CUHK Direct Grant. Thanks for the graduate scholarship from CUHK/ISEIS.

TABLE OF CONTENTS

LIST OF TABLES

LIST OF FIGURES

CHAPTER 1 Introduction

A tropical cyclone (TC) is a warm-core, non-frontal, synoptic-scale cyclone that originates over tropical or subtropical oceans and is driven principally by heat transfer from the ocean. Usually for the purpose of issuing useful warnings, TCs are categorized according to their maximum wind speed, defined as the maximum speed of the wind at an altitude of 10 m, averaged over 10 min except in the United States where a 1 min average is conventional. TCs in their formative stage, with maximum winds of 17 m s^{-1} (33 knots) or less, are known as tropical depressions; when their maximum wind speeds are in the range of 18 to 32 m s^{-1} (34 to 63 knots), they are called tropical storms, whereas TCs with maximum winds of 33 m s^{-1} (64 knots) or greater are called hurricanes in the western North Atlantic and eastern North Pacific, typhoons in the western North Pacific, and severe TCs elsewhere such as in the Indian Ocean and South Pacific (Emanuel 2003).

TCs have some major benefits. These storms play a very important role in balancing the earth's heat by transporting great amounts of heat from tropical oceans to the polar regions of the globe. They also provide beneficial rains to many areas that would otherwise be affected by drought so as to save farmers and water supplies in many communities.

However, the devastating TC seasons of recent years have highlighted the importance of TC forecasting. The extensive damage and loss of life caused by TCs result from a lot of natural hazards, such as storm surge (a rapid, local rise in sea

level associated with storm landfall), strong winds, heavy rains and their associated flash flood, landslides, mudflows and so on. For example, Hurricane Katrina and the accompanying flood due to the collapse of the levees in Louisiana of the 2005 Atlantic hurricane season was the largest natural disaster in the history of the United States. Estimated total damage was $81 billion (2005 USD, Knabb et al. 2005), making it the most costly storm in United States since the 1926 Great Miami Hurricane (Pielke et al. 2008). Over 1,800 people died in the actual hurricane and in the subsequent floods, making it the deadliest U.S. hurricane since the 1928 Okeechobee Hurricane. The Galveston storm of 1900 was ranked the deadliest in US, the storm resulted in 8000–12000 death. And Super Typhoon Nina was a short-lived but intense 1975 super typhoon that caused major damage and deaths in China, mainly due to the collapse of the Banqiao Dam. Over 100,000 people lost their lives because of the resulting floods, making it one of the deadliest TCs recorded in history. Recently Cyclone Nargis in 2008 was a strong TC that caused the worst natural disaster in the recorded history of Myanmar. Official death toll estimates exceed 138,000 fatalities. Damage estimates at over $10 billion made it the most damaging cyclone ever recorded in the Indian Ocean Basin (Fritz et al. 2009).

Zhang et al. (2009) examined the direct economic losses and human casualties caused by TCs that made landfall in China during 1983–2006 using the dataset released by the Department of Civil Affairs of China. On average, seven TCs made landfall over mainland China and Hainan Island, leading to 472 deaths and direct economic losses of 28.7 billion yuan (2006 RMB) per year.

Accurate forecasting of TC track and intensity is therefore essential to minimize economic losses and human casualties caused by the disasters associated with TCs. While track forecasting skill has made relatively steady improvement over the years with improved numerical models (Kurihara et al., 1998), satellite (Soden et al. 2001; Goerss 2009) and dropsonde (Burpee et al. 1996; Tuleya and Lord, 1997; Aberson and Franklin, 1999; Wu et al. 2005; Weissmann 2010) observation, the prediction of TC intensity or maximum sustained surface winds still lags far behind that of track forecasts and remains a big challenge in all TC basins (Knaff et al. 2005).

At present there are three primary kinds of TC intensity guidance techniques: 1) the simple Statistical Hurricane Intensity Forecast (SHIFOR) or Statistical Typhoon Intensity Forecast (STIFOR) model (Jarvinen and Neumann 1979; Chu 1994; Knaff et al. 2003), which makes a prediction based on climatology and persistence (CLIPER). [See Panofsky and Brier (1968) for a basic discussion about meteorological forecast verification.] Climatology refers to climatological averages, and persistence is a forecast that the current conditions will continue.], the predictors contain Julian date information, latitude, longitude, translational speed current intensity and 12-h intensity change in the previous 12 h of the storm,; 2) the dynamical models such as the Geophysical Fluid Dynamics Laboratory (GFDL) hurricane model (Kurihara et al. 1998; Bender et al. 2007), Japanese Meteorological Agency limited area typhoon model (JTYM) (Tatsumi 1986) and Hurricane Weather Research and Forecasting (HWRF) model (Davis et al. 2008; Surgi et al. 2008; Xiao et al. 2009); 3) statistical-dynamic models such as the Statistical Hurricane

Intensity Prediction Scheme (SHIPS) (DeMaria and Kaplan 1994a; DeMaria and Kaplan 1999; DeMaria et al. 2005) and the Statistical Typhoon Intensity Prediction Scheme (STIPS) (Knaff et al. 2005), which usually produce the best forecasts among the three kinds of techniques because they employ the strengths of both statistical models and dynamical models, and combine parameters related to CLIPER and synoptic-environmental parameters derived from numerical weather forecasts. The synoptic-environmental parameters are mainly composed of 200-hPa eddy momentum flux convergence, maximum potential intensity that depends on sea surface temperature (SST), 850–200-hPa vertical wind shear, 200-hPa temperature, higher and lower level relative humidity and 850-hPa relative vorticity. The SHIFOR (or STIFOR) model is primarily used as a baseline for evaluating the skill of the official intensity forecasts and those from the objective models.

DeMaria et al. (2007) evaluated the National Hurricane Center and Joint Typhoon Warning Center operational TC intensity forecasts for the three major northern hemisphere TC basins (Atlantic, eastern North Pacific, and western North Pacific) for the past two decades, and found that there had been some marginal improvement at 24 and 48 h for the Atlantic and at 72 h for the eastern and western Pacific. The intensity forecasts had significant skill out to 96 h in the Atlantic and out to 72 h in the eastern and western Pacific. The skill of the intensity forecasts was comparable at 12 h with that of the track forecast, but the track forecasts were 2 to 5 times more skillful by 72 h. The comparison results of track and intensity forecast error trends for the two-decade period showed that the percentage track forecast improvement

was almost an order of magnitude larger than that for intensity, indicating that intensity forecasting still has a long way to go. Especially, the rapid intensity changes associated with TCs are nearly impossible to predict in current forecast models (Elsberry et al. 2007; Blackerby 2005).

In general, the relatively low skill of intensity forecasts and the inability to forecast RI are primarily due to the complexity of the TC intensity change processes and our limited understanding of these processes. In the past, the impact of the ocean (e.g. SST, ocean heat content), inner-core processes (e.g. eyewall replacement, inner-core asymmetry, sea spray), and environmental interactions (e.g. vertical wind shear, flow pattern, upper tropospheric trough) on TC intensity change have been examined (Willoughby et al. 1982; Shay et al. 2000; Wang 2002; Kaplan and DeMaria 2003; Yu and Kwon 2005; Ventham and Wang 2007; Yang et al. 2007; Mainelli et al. 2008). Some of those have been considered as potential predictors in current operational TC intensity forecasting models.

The SHIPS has been refined by including some satellite-based predictors. Fitzpatrick (1997) was the first to attempt to add infrared satellite observations of western North Pacific TCs into a linear regression scheme similar to that used by DeMaria and Kaplan (1994a). The resulting model showed competitive skill with the operational intensity forecasts issued in 1983 by the Joint Typhoon Warning Center. DeMaria et al. (2005) tried to include brightness temperature from Geostationary Operational Environmental Satellite (GOES) infrared (10.7 μm) imagery and ocean heat content (OHC, which were only available in Atlantic) from satellite-based

altimetry into SHIPS during 2003 and 2004 Atlantic and eastern Pacific TC seasons. At 12–72 h, the Atlantic forecasts were improved by up to 3.5% due to the inclusion of OHC and GOES brightness temperature, and the eastern North Pacific forecasts were improved by up to 7% because of the addition of GOES data.

One major limitation of infrared images is that low-level TC characteristics are often obscured by cirrus shields (Lee et al. 2002). Therefore Jones et al. (2006) further enhanced SHIPS by adding some new predictors derived from passive microwave imagery (SHIPS-MI). These new predictors were calculated within a radius of 100 km centered at the best-track defined TC position using brightness temperature converted from passive microwave imagery, which were collected from the Defense Meteorological Satellite Program (DMSP) and Tropical Rainfall Measuring Mission (TRMM) satellites. The relevant sensors include the Special Sensor Microwave Imager (SSM/I; Hollinger et al. 1987) aboard the DMSP satellites and the TRMM Microwave Imager (TMI; Kummerow et al. 1998). A 2%–8% improvement was produced for the Atlantic and eastern North Pacific TC intensity forecasts out to 72 h. The improvement in both basins was largest for rapidly intensifying or weakening TCs. That is to say, SHIPS-MI does partially solve the problem of inability to predict rapid intensification (RI) of TCs.

More recently, the OHC estimation was applied to operational forecast of the intensity of category 5 hurricanes during 2003-2005 hurricane seasons (Mainelli et al. 2008). The OHC input can reduce the average intensity errors of the SHIPS forecasts by up to 5% for all cases of these intense storms, and up to 20% for individual

hurricanes, although the addition of OHC only produced up to 1% improvement on the intensity forecast for all the dependent TC samples during about 10 years.

However, the TC intensity forecasting still has much room to improve. Wind-induced surface heat exchange (WISHE; Emanuel 1986) has been considered as one of the major mechanisms for cyclone intensification. Surface latent heat flux (SLHF), which is the amount of energy exchange between the surface and the air due to evaporation or condensation, is one of the major energy sources for TC development; however few studies examined its role in TC RI using analyzed or observational data quantitatively. Only two case studies can be found. Gautam et al. (2005) used National Centers for Environmental Prediction (NCEP) reanalysis data and found that SLHF was strongly coupled and was associated with the intensity variations of hurricane Isabel (2003). And most recently Lin et al. (2009) employed satellite-derived data and showed that SLHF was the primary contributor to the total enthalpy during the RI period of Cyclone Nargis (2008). Although SST has been utilized to estimate the maximum potential intensity (MPI, e.g., DeMaria and Kaplan 1994; Whitney and Hobgood 1997) which is already a predictor in statistical typhoon intensity prediction schemes (e.g., Knaff et al., 2005), SLHF is a nonlinear combination of near-surface wind speed and the difference of surface humidity (Qs) and near-surface humidity, where Qs depends on SST.

The latent heat release (LHR) through condensation and precipitation processes, especially in the inner core (radius of 110 km from storm center), is vital to the development and maintenance of TCs (Charney and Eliassen 1964; Kuo 1965). The

rainfall as a proxy of condensational heating is a good indicator of typhoon strength. Many case studies (e.g., Riehl and Malkus 1961; Rao and Macarthur 1994; Rodgers et al. 1994; Chang et al. 1995; Rodgers and Pierce 1995; Rodgers et al. 1998; Simpson et al. 1998; Rodgers et al. 2000; Heymsfield et al. 2001; Jiang et al. 2008) have showed examples that the strength of TC intensity is significantly correlated with rainfall intensity within the inner cores of TCs using satellite or aircraft observation data.

The operational satellite-enhanced TC intensity prediction schemes are only available in Atlantic and eastern North Pacific at present. To further improve TC intensity prediction, especially RI prediction in western North Pacific, we will add two new satellite-based predictors (SLHF and inner-core rain rate) and employ more sophisticated statistical techniques such as neural networks and logistic regression. Neural network model has shown better performance than linear regression model in TC intensity prediction (Baik and Hwang 2000; Jin et al. 2008). Logistic regression model has been applied to predict TC formation (Mundhenk 2009; Fu et al. 2010) and can also be used in TC RI forecasting.

Data and methodology is described in chapter 2. Chapter 3 provides SLHF and rainfall associated with rapidly intensifying TCs over western North Pacific and demonstrates that SLHF and inner-core rain rate have the potential to be new predictors. Development of statistical typhoon intensity prediction schemes using multiple linear regression and neural networks by adding SLHF and inner-core rain rate is presented in chapter 4. In chapter 5, neural network model and logistic

regression model for typhoon RI prediction are developed. Finally, conclusion and discussion are given in chapter 6.

CHAPTER 2 Data and Methodology

2.1 Data

2.1.1 Tropical cyclone best track

The TC best track data containing position and intensity information used in this study is collected from Japan Meteorological Agency (JMA) Regional Specialized Meteorological Center Tokyo (RSMC Tokyo). This post analysis best track data consist of 6-h estimates of position (latitude and longitude), minimum central pressure (MCP), and 10-min maximum sustained wind speed (MWS) for all named TCs in western North Pacific (WNP) basin including the South China Sea (SCS) from 1951 to the present.

RSMC Tokyo employed the original Dvorak (1982, 1984) technique to estimate TC position and intensity till 1990 and a modified version of Dvorak technique by Koba et al. (1990) has been utilized since 1990. The MWS is rounded to the nearest 5 kt (1 kt = 0.5144 m s^{-1}), the MCP is rounded to the nearest millibar, and latitude and longitude of the position are rounded to the nearest tenth.

Those non-developing tropical depressions which did not reach the strength of tropical storm were not recorded in the dataset.

Joint Typhoon Warning Center (JTWC) of U.S. Naval Pacific Meteorology Oceanography Center in Hawaii (in Guam before 1999) also provides TC best track data over the WNP; the difference is that at JTWC 1-min MWS is determined using original Dvorak technique as well as improved techniques such as the objective

Dvorak technique (Velden et al. 1998) and advanced objective Dvorak technique (Olander and Velden 2007). A comparison study by Song et al. (2010) showed that JTWC data have higher intensity estimates for typhoons, but lower intensity estimates for tropical depressions than RSMC Tokyo data. Yu et al. (2007) developed simple linear regression models based on CLIPER and found that the model using RSMC Tokyo MWS estimates produced smaller error than the model using JTWC MWS estimates. Therefore RSMC Tokyo dataset is used in this study.

2.1.2 Rain rate

The rainfall dataset used in this study is the Tropical Rainfall Measuring Mission (TRMM) Multisatellite Precipitation Analysis (TMPA) (Huffman et al., 2007). TMPA at fine resolutions (0.25° × 0.25° and 3 hourly) combines precipitation estimates from multiple satellites, as well as land surface rainfall gauge analyses when possible. The precipitation data sources from satellites include TMI and Precipitation Radar (PR) on TRMM (Kummerow et al. 1998; Haddad et al. 1997), SSM/I (Wentz and Spencer 1998) on DMSP satellites, Advanced Microwave Scanning Radiometer Earth Observing System (AMSR-E; Wilheit et al. 2003) on the AQUA satellite, Advanced Microwave Sounding Unit-B (AMSU-B; Weng et al. 2003) on the National Oceanic and Atmospheric Administration (NOAA) satellites, and infrared data of geosynchronous earth orbit satellites (Janowiak et al. 2001) and Geostationary Operational Environmental Satellite (GOES) Precipitation Index (GPI; Arkin and Meisner 1987) estimates. Both research-quality and real-time TMPA

products are available. At present the gauge analyses are merged into the research-quality product only. The dataset covers the area between 50°N and 50°S for the period from 1998 to the present. The latency in the real-time product is on the order of 2–3 h.

2.1.3 Surface latent heat flux

A number of semi-operational SLHF products are examined for this study. For satellite-based products, such as the National Aeronautics and Space Administration (NASA)/Goddard Space Flight Center Satellite-based Surface Turbulent Flux (GSSTF) dataset (Chou et al. 1997, 2003; Shie et al. 2009), the Japanese Ocean Flux utilizing Remote Sensing Observations (J-OFURO) (Kubota et al., 2002) and the Hamburg Ocean-Atmospheric Parameter Set (HOAPS) (Grassl et al., 2000). They are deemed inadequate due to either coarse resolution, missing data around the TC center or insufficient temporal coverage. The third release of the Objectively Analyzed Air-sea Fluxes (OAflux) (Yu et al. 2008) daily SLHF product is utilized due to its global ocean coverage and availability for the relatively long period from 1985 to 2008. OAFlux dataset is gridded on a 1.0° latitude-longitude resolution for the global ocean basins that are free from ice. The SLHF, Q_{LH}, is based on the state-of-the-art Coupled Ocean-Atmosphere Response Experiment (COARE) bulk flux algorithm 3.0 (COARE 3.0; Fairall et al. 2003), viz

$$Q_{LH} = \rho L_e c_e U(q_s - q_a) = \rho L_e c_e U \Delta q \tag{2.1}$$

where ρ is the density of air, L_e is the latent heat of evaporation, c_e is the turbulent

exchange coefficients for latent heat flux, U is the wind speed relative to the sea surface at the height of 10 m, $\Delta q = q_s - q_a$ where q_s and q_a denote the surface and near-surface (i.e. 2 m) atmospheric specific humidity, respectively. q_s is computed from the saturation humidity, q_{sat}, for pure water at SST T_s,

$$q_s = 0.98 q_{sat}(T_s) \tag{2.2}$$

where a multiplier factor of 0.98 is used to take into account the reduction in vapor pressure caused by a typical salinity of 34 psu. It is worth pointing out that the extrapolated values of c_e in COARE 3.0 from 19 m s^{-1} through 36 m s^{-1} are in good agreement with the results from Coupled Boundary Layer Air-Sea Transfer Experiment (CBLAST; Black et al. 2007) and the Humidity Exchange Over the Sea (HEXOS; DeCosmo et al. 1996; modified as per Fairall et al. 2003). This suggests that c_e is constant with wind speed up to hurricane-force winds of 33 m s^{-1}.

The difference of OAFlux SLHF product from other flux products is that it is not derived from one single data source, but determined by objectively blending the multiple data sources from satellite and numerical weather prediction (NWP) model outputs while using in situ observations to assign the weights. Three variables (U, T_s, q_a) are needed for OAFlux synthesis of SLHF. Input data sources of satellite wind speed are from SSM/I (Wentz 1997), the Quick Scatterometer (QuikSCAT; Lungu 2001) and AMSR-E (Wentz and Meissner 2000) available from the Remote Sensing System (RSS) website at http://www.ssmi.com. These wind data at twice daily and quarter-degree resolution are averaged to daily and 1-degree resolution of OAFlux. Satellite near surface humidity fields at 10 m above sea level from 1988 to 2000

obtained from version 2 of GSSTF (GSSTF2; Chou et al. 2003) was employed to estimate daily near surface humidity at 1-degree resolution from SSM/I data (Chou et al. 1995, 1997). SST input dataset is NOAA Optimally Interpolated (OI) daily SST analysis at quarter-degree resolution produced by Reynolds et al. (2007). There are two products for this SST analysis, one is Advanced Very High Resolution Radiometer (AVHRR) infrared SST available from January 1985 to present and the other is the combination of AVHRR infrared SST and AMSR-E microwave SST available from June 2002 to present. Both products use in situ observations from buoys and ships to adjust satellite bias. The AVHRR only SST product was averaged onto 1-degree grid to develop OAFlux dataset for the consistency of the time series. However, satellite observations do not cover 100% global ocean on daily basis, so daily-averaged and linearly interpolated surface meteorological data at 1-degree resolution from the 40-yr European Centre for Medium-Range Weather Forecasts (ECMWF) Re-Analysis (ERA-40; Uppala et al. 2005), and the National Centers for Environmental Prediction (NCEP) reanalysis (Kalnay et al. 1996; Kanamitsu et al. 2002) were used to fill in the information that satellites cannot provide and to fill in the missing gaps between swaths. Consistent with the NWP model outputs, the synthesis produced U at 10 m, q_a at 2 m, and T_s at the sea surface. A height adjustment was applied to those input datasets that do not have the specified reference heights.

OAFlux also provides daily U, q_s, and q_a data that are used to calculate SLHF.

2.1.4 NCEP analysis

NCEP Global Forecasting System (GFS) Final (FNL) analysis (Yang et al. 2006) at 1-degree and 6-hourly resolution is used to derive environmental predictors in STIPS (Knaff et al. 2005) for the development of typhoon intensity prediction models. Specifically, the environmental data include air temperature, wind, relative humidity data at 200, 250, 300, 350, 400, 450, 500, 550, 600, 650, 700, 750, 800 and 850 hPa. Divergence, relative eddy flux convergence and relative vorticity at each grid are calculated using wind field information and central difference method. All the environmental predictors are computed by averaging corresponding data within some specific radius; the details will be introduced in chapter 4.

NCEP reanalysis is not used because of the relatively course 2.5° × 2.5° resolution.

2.1.5 Sea surface temperature

TMI Optimum Interpolation (OI) daily SST (Gentemann et al. 2004) at 0.25° × 0.25° resolution together with RSMC Tokyo best track data are used to estimate MPI, which is one of important predictors in TC intensity prediction models such as SHIPS and STIPS, whereas only weekly SST (Reynolds et al. 2002) or climatological SST analysis (Levitus 1982) data were used in SHIPS or STIPS. High-resolution daily SST could represent important temporal and spatial variability such as cold wake which is not resolved by low-resolution SST analysis, and hence shows potential to improve the SHIPS forecasts in Atlantic and eastern North Pacific

(Berg et al. 2004; Gentemann et al. 2007).

TMI OI SST analysis is available from the RSS website at http://www.ssmi.com and covers the latitude band 40°S–40°N from January 1998 to present. AMSE-R OI SST analysis and combined TMI+AMSR-E OI SST analysis are also available globally from June 2002 to present. These SST data sets are not used due to their short duration, but can be incorporated rather easily in future developments.

Table 2.1 summarizes the availability of aforementioned datasets, including temporal and spatial coverage and resolution.

Table 2.1 Datasets used in this study and the temporal and spatial coverage and resolution.

Dataset	Spatial resolution	Temporal resolution	Spatial coverage	Temporal coverage
RSMC Tokyo best track	0.1°	6 hourly	Northwest Pacific and the South China Sea	1951–2009
NCEP analysis	1.0°	6 hourly	global	2000–present
TMPA rain rate	0.25°	3 hourly	40°N to 40°S	1998–present
OAFlux SLHF	1.0°	daily	global ocean	1985–2008
TMI OI SST	0.25°	daily	40°N to 40°S	1998–present

2.2 Methodology

2.2.1 Multiple linear regression

Multiple linear regression (Wilks 2006) is used to model the relationships between TC intensity changes at six forecast ranges, namely 12, 24, 36, 48, 60 and 72 hours

(hr), with various meteorological parameters. The multiple linear regression equation is given below,

$$y = b_0 + b_1 x_1 + b_2 x_2 + \cdots + b_k x_k \tag{2.4}$$

where the dependent variable y is the intensity change (predictand) from initial time (t = 0) to forecast times (t = 12, 24, 36, 48, 60 or 72 hr). The independent variables x_1, x_2, …, x_k are predictors such as meteorological parameters, b_1, …, b_k are the regression coefficients for corresponding predictors related to TC intensity change, and b_0 is the regression constant.

Eq. (2.4) is solved by least squares, which yields regression constant and coefficients estimates that minimize the sum squares of errors $|\varepsilon^2|$ (differences between observed and predicted intensity change), where $\varepsilon_i = y_i - \hat{y}_i$. The resulting forecasting equation is

$$\hat{y} = \hat{b}_0 + \hat{b}_1 x_1 + \hat{b}_2 x_2 + \cdots + \hat{b}_k x_k \tag{2.5}$$

where the variables are the same as those in (2.4) except that "^" represents estimated values.

Two measures, mean absolute error (MAE) and adjusted R^2, are used to evaluate the regression models. They are given by (2.6) and (2.7), respectively.

$$MAE = \frac{1}{n}\sum_{i=1}^{n}|y_i - \hat{y}_i| \tag{2.6}$$

$$\overline{R}^2 = 1 - \frac{n-1}{n-K-1}\frac{\sum_{i=1}^{n}(y_i - \hat{y}_i)^2}{\sum_{i=1}^{n}(y_i - \bar{y})^2} \tag{2.7}$$

where n is the number of observations, K is the number of predictors, y_i and $\hat{y}_i$

are observed and predicted values of predictand, respectively, and $\bar{y}$ is the mean value of y_i.

The conventional measure for the proportion of variance explained by regression, R^2, is not used since the linear regression models with different number of predictors are compared in this study and the R^2 value will increase although the regression may not improve if the number of predictors is increased.

When developing a multiple linear regression model, one commonly uses a method to select a good set of predictors based upon their combined ability to predict the dependent variable or predictand. For our models a stepwise procedure is used to select variables from the potential predictor pool at each forecast time (see Wilks 2006). The significance of individual predictors is based on F test (Bulmer 1979). A 99% statistical significance level is required for an individual predictor to be included initially in the model. Once in the model, a predictor can only be removed if its significance level becomes less than 98% after the addition/removal of another predictor. The stepwise procedure identifies important predictors at each forecast time, which sometimes results in erratic forecasts. To avoid this problem, all of the predictors chosen for any forecast period through the stepwise selection procedure are included in the final group of predictors. Using the predictors in this final group, a single multiple regression model is created for each forecast time.

2.2.2 Neural networks

With the development of the artificial intelligence technique, neural network, or

more precisely artificial neural network, which has excellent performance in self-adaptive learning and nonlinear mapping, have been applied successfully in many disciplines. In the atmospheric sciences, many applications have been found in research areas such as short-range climate prediction, interpretation and application of numerical prediction products, air pollution prediction, rainfall estimation from satellite imagery, and pattern examination of long-term climate data (Grimes et al. 2003; Jin 2004; Ali 2004). Moreover, NN has been started to apply in typhoon intensity prediction (Baik and Hwang 2000; Jin et al. 2008).

The back-propagation (BP) algorithm (Rumelhart et al. 1986) is known to be most useful when one tries to solve a problem in which the relationship between input and output is nonlinear and training data are abundant (Hinton 1992). A BP neural network with one hidden layer is constructed in this study. That is, the neural network has three layers: one input layer, one hidden layer and one output layer. Figure 2.1 indicates the neural network architecture. There are M nodes in the input layer, K nodes in the hidden layer, and one node in the output layer. The nodes in input and output layer represent the predictors and predictand, respectively. Determination of the number of hidden nodes is usually determined empirically to optimize performance for the particular situation. The network is fully connected. This means that a node in any layer of the network is connected to all of the nodes in the previous layer.

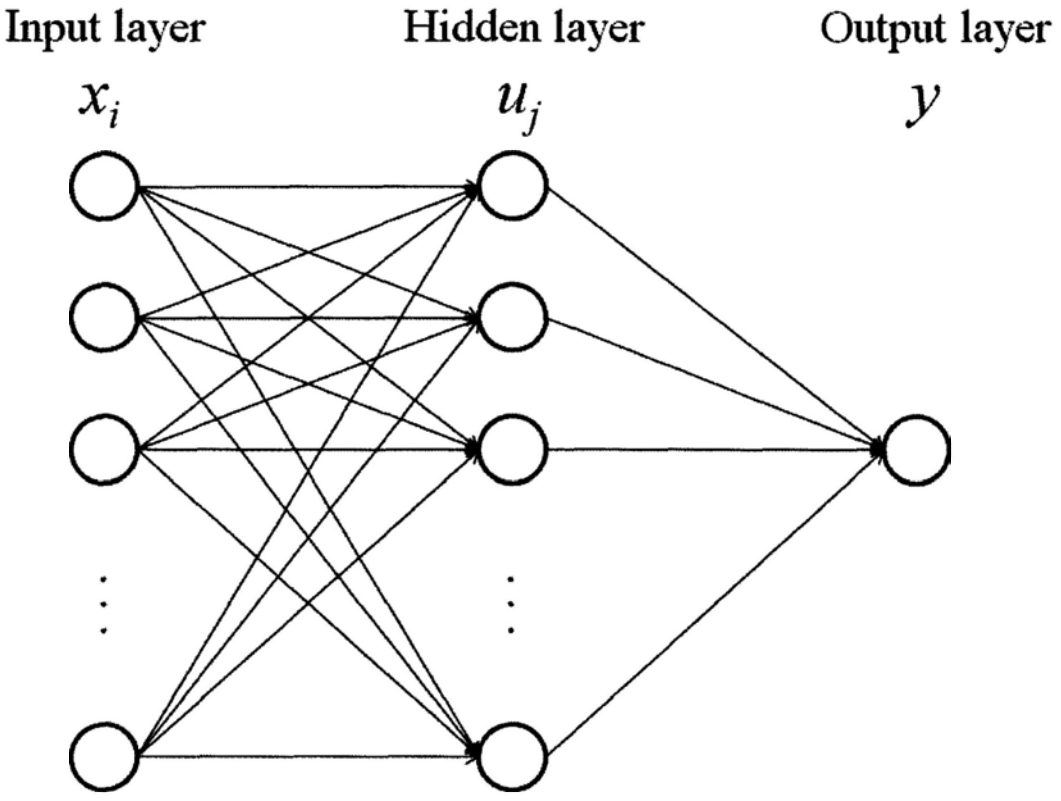

Figure 2.1 Architectural graph of a neural network with one hidden layer.

The connection between node i in input layer and node j in hidden layer can be represented by a weight, w_{ij}. The connection between node j in hidden layer and the one node in output layer can be represented by a weight, w_j. w_{ij} and w_j indicates the importance of that connection between the two nodes. Node j in hidden layer and the one node in output layer are associated with bias parameters, i.e. b_j and b, respectively. The transfer functions f_1 and f_2 are used from input layer to hidden layer and from hidden layer to output layer, respectively. Therefore, the value u_j for node j in hidden layer is given in terms of the input variables x_i by

$$u_j = f_1\left(\sum_{i=1}^{M} w_{ij} x_i + b_j\right) \tag{2.9}$$

The output node $\hat{y}$ is calculated by

$$\hat{y} = f_2\left(\sum_{i=1}^{K} w_j u_i + b\right) \tag{2.10}$$

Generally, there are three transfer functions: log-sigmoid transfer function, tan-sigmoid transfer function and linear transfer function. The three functions can generate output between 0 and 1, between −1 and 1, and within the range ±∞, respectively, as the input varies from negative to positive infinity. The choice of the transfer function depends on particular application.

The training phase of the neural network, called neuro-learning, is an iterative process for optimizing appropriate weights and biases which are generated randomly at first. Learning of the network with training matrix samples by tuning weight and bias parameters using the learning algorithm continues until mean-squared error (MSE) is converged to an acceptably small value, ε. MSE is obtained from

$$MSE = \frac{1}{n}\sum_{i=1}^{n}(y_i - \hat{y}_i)^2 \tag{2.11}$$

where n is the number of training samples, y_i is the target output, and $\hat{y}_i$ is the actual output. BP learning is from output layer toward input layer.

Neural network training has an overfitting problem. The problem occurs when the actual outputs after training match the target outputs from the noisy training samples well, but when new independent data is added to the network the error becomes large. "Early stopping" is used to deal with this problem. This technique is provided in Matlab Neural Network Toolbox (Demuth et al. 2009). In this technique the input data are randomly divided into three subsets: 60% of the samples are the training set, 20% the validation set, and 20% the test set. The MSE on the validation set is

checked during the training process. The validation MSE normally reduces during the initial training phase, as does the MSE on the training set. But the validation MSE begins to increase when the network starts to overfit the training samples. When the validation MSE increases for a specified number of iterations, the training is stopped, and the weights and biases at the minimum of the validation MSE are returned. The resulting network can be used to make predictions by feeding new independent data.

2.2.3 Logistic regression

Logistic regression (Wilks 2006) is useful to describe the relationship between some independent variables (predictors) and a binary dependent variable (predictand). It has been widely used in the atmospheric sciences to predict precipitation, lightning, TC formation (Chiu and Kadem 1990; Applequist et al. 2002; Mazany et al. 2002; Ramirez-Beltran et al. 2007; Mundhenk 2009; Fu et al. 2010).

In this study, a binary logistic regression model is developed to identify whether a TC sample intensifies rapidly or not, since rapid intensification of TCs is most interesting and is also a big challenge. The predictand y is set to one if the TC sample undergoes rapid intensification (RI), and y is set to zero if not. y is expressed in terms of the predictors $x_1, x_2, \ldots, x_k$ according to the nonlinear equation

$$y = \frac{1}{1+\exp[-(a_0 + a_1x_1 + a_2x_2 + \cdots + a_kx_k)]} \tag{2.12}$$

where a_0 is the intercept and $a_1, a_2, \ldots, a_k$ are the regression coefficients associated with the predictors. The intercept and regression coefficients are to be estimated from

the training samples by maximum likelihood method. The resulting forecasting equation is

$$\pi = \frac{1}{1+\exp[-(\hat{a}_0 + \hat{a}_1 x_1 + \hat{a}_2 x_2 + \cdots + \hat{a}_k x_k)]} \tag{2.13}$$

where π is the probability of forecast undergoes RI, and the parameters with "^" above represents optimal estimates. The exponential function limits the outcome π to lie between zero and one. The forecasts base on new inputs of predictors are then categorized into 0 or 1 by comparing the probability to a probability threshold, τ

$$\hat{y} = \begin{cases} 0, & if\ \pi < \tau \\ 1, & if\ \pi \geq \tau \end{cases} \tag{2.14}$$

where $\hat{y}$ is the final forecasts. $\hat{y} = 1$ denotes a predicted RI event, while $\hat{y} = 0$ means a predicted non-RI event.

Table 2.2 shows a 2 × 2 contingency table for categorical forecast verification. These *a* forecast-observation pairs are called *hits*, represent the events are forecast to occur and did occur. *b* instances are called *false alarms*, the events were forecast to occur but did not occur. *c* instances of the events occurred despite not being forecast, called *misses*. There are also *d* instances of the events did not occur and not being forecast, called *correct negatives*.

Table 2.2 A 2 × 2 contingency table for categorical forecast verification

Rapid intensification or not		Observed		Total
		Yes	No	
Forecast	Yes	*a*	*b*	*a* + *b*
	No	*c*	*d*	*c* + *d*
Total		*a* + *c*	*b* + *d*	*a* + *b* + *c* + *d*

Four scores are used to measure the performance of the binary logistic regression model (Wilks 2006). Probability of detection (POD) is the fraction of the observed RI events that were correctly forecast. False alarm ratio (FAR) is the proportion of forecast RI events actually did not occur. Critical success index (CSI) is the number of correct RI forecasts divided by the total number of occasions when RI event was forecast and/or observed. CSI is particularly useful when the RI event to be forecast occurs substantially less frequently than the non-RI event. The three scores (POD, FAR, and CSI) are expressed as the following equations

$$POD = \frac{a}{a+c} \tag{2.15}$$

$$FAR = \frac{b}{a+b} \tag{2.16}$$

$$CSI = \frac{a}{a+b+c} \tag{2.17}$$

The CSI is somewhat sensitive to the climatology of the event, tending to give poorer scores for rare events. A related score, the equitable threat score (ETS) is designed to help offset this tendency. The ETS is given by

$$ETS = \frac{a-a_r}{a+b+c-a_r} \tag{2.18}$$

where $a_r = \frac{(a+b)(a+c)}{a+b+c+d}$.

CHAPTER 3 Surface Latent Heat Flux and Rainfall Associated with Rapidly Intensifying Tropical Cyclones over the Western North Pacific

Current operational guidance techniques tend to under-forecast TC intensification (Elsberry et al. 2007; Blackerby 2005), hence forecasting of TC rapid intensification (RI) is a great challenge. As mentioned in chapter 1, several factors related to ocean characteristics, inner-core processes, and environmental interactions are found to be favorable for TC intensification.

A few studies focused directly on TC RI. Holliday and Thompson (1979) revealed that underlying warm waters were necessary conditions for typhoon RI and RI was usually associated with eye contraction. Bosart et al. (2000) demonstrated that RI of Hurricane Opal (1985) resulted from high upper-level divergence, low vertical wind shear and the enhanced moisture and heat due to a warm ocean eddy. Kaplan and DeMaria (2003) employed composite analysis to examine a number of environmental conditions favorable for rapid intensifying Atlantic TCs. Among these conditions, Yang et al. (2008) utilized data mining techniques and identified that the combination (high latitude, low longitude, the TC being in an intensification phase, an initial intensity far away from the maximum potential intensity, high steering layer value, and low relative eddy flux convergence) can be considered as a sufficient condition for RI of Atlantic TCs.

Although some case studies (e.g., Rodgers et al. 1994; Chang et al. 1995; Gautam

et al. 2005; Lin et al. 2009) have emphasized the importance of SLHF and inner-core rainfall on TC RI, it has not been confirmed for a large dataset. The goal of the study in this chapter is to quantify the role of SLHF and rainfall in TC intensification using RSMC Tokyo best track, OAFlux SLHF and TMPA rain rate data during the period 1998–2006. We will concentrate on samples when cyclones underwent RI. A composite analysis will be performed for the RI and non-RI samples and the significance of the difference tested using a Student *t* test.

Variables (SLHF and rain rate) were evaluated at the beginning (t = 0 h) of each 24-h period provided that the system remained both over water and tropical (e.g., extra-tropical samples were excluded and landfall effect was left out of account) during 24-h period. The 24-h intensity change in MCP (ΔP_{24}) were determined for each 24-h time period by subtracting MCP at t + 24 h from MCP at the initial (t = 0 h) time.

There were 209 named TCs [91 tropical storms (18 m s^{-1} ≤ MWS ≤ 33 m s^{-1}) and 118 typhoons (MWS ≥ 34 m/s)]. It should be noted that the TCs are defined based on the maximum intensity during the life of the TCs, hence no tropical depression (MWS ≤ 17 m s^{-1}) are recorded in the dataset. These TCs contributed a total of 5077 samples (e.g., 24-h period differences) that were subsequently employed in the statistical analysis discussed in section 3.1.

To determine if SLHF conditions associated with the RI samples were significantly different from those non-RI samples, a composite analysis on initial (t = 0 h) rainfall and SLHF characteristics in a 20°×20° square region centered at TC

position for RI samples and non-RI samples was utilized. Student t tests (Bulmer 1979) was used to perform significance tests for the difference between RI and non-RI samples.

Section 3.1 provides the climatology of western North Pacific TC 24-h intensity changes. Composites of the rainfall and SLHF are presented in section 3.2 and section 3.3, respectively. Finally, conclusions and discussions are offered in section 3.4.

3.1 Intensity change distribution

Figure 3.1 shows the frequency distribution of ΔP_{24} as a function of the initial (t = 0 h) intensity of all 5077 samples. Slow intensification (–9 hPa $\leq \Delta P_{24} \leq$ 0) was the most frequently observed 24-h intensity change for tropical depressions. The figure indicates that a higher fraction of the tropical storm sample than of the typhoon or tropical depression sample exhibited ΔP_{24} fall exceeding 10 hPa. This finding may be attributed to a few factors, as Kaplan and DeMaria (2003) proposed. First, tropical storms are further from their maximum potential intensity than typhoons and, consequently, have the potential to intensify faster. Second, tropical storms may intensify more rapidly than tropical depressions because they are better organized. Conversely, figure 3.1 indicates that typhoons are likely to decay at a faster rate than either tropical storms or tropical depressions, because of their high intensities.

The cumulative frequency distribution of ΔP_{24} for each intensity category (figure 3.2) indicates that TC decay ($\Delta P_{24} > 0$) occurs for ~70% of all typhoon samples,

however, it only occurs in 17% of the tropical depression samples, 43% of the tropical storm samples, and 44% of all TC samples.

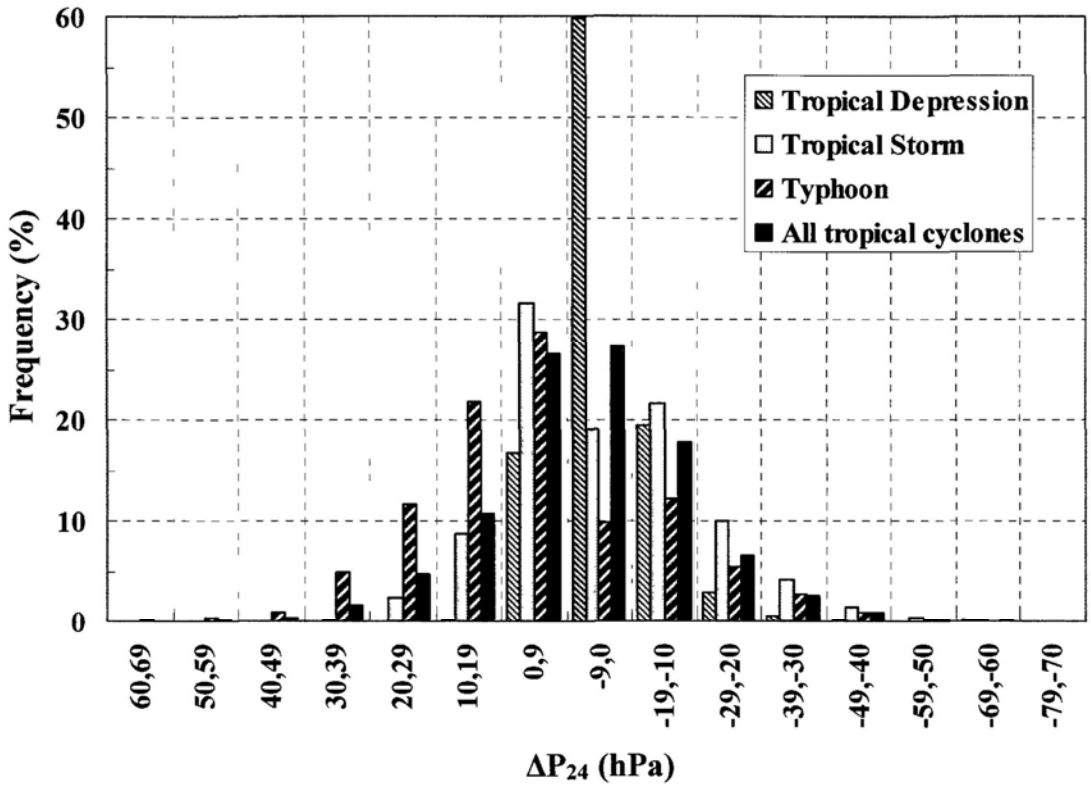

Figure 3.1 The frequency distributions of 24-h intensity change (ΔP_{24}) stratified by tropical cyclone intensity at time t = 0 h. The distributions are provided for tropical depressions, tropical storms, typhoons, and all tropical cyclones.

To separate RI and non-RI samples, RI is defined as the 90th percentile of ΔP_{24} for all of the TC samples used in this study. Correspondingly, samples with ΔP_{24} fall $\geq$ 20 hPa are RI samples and the others are non-RI samples. It is interesting to note that the Holliday and Thompson's (1979) definition for RI of a 24-h pressure fall of $\geq$ 42 hPa is equivalent to the 98.8th percentile of all of the 24-h pressure changes of the TCs in the current study sample.

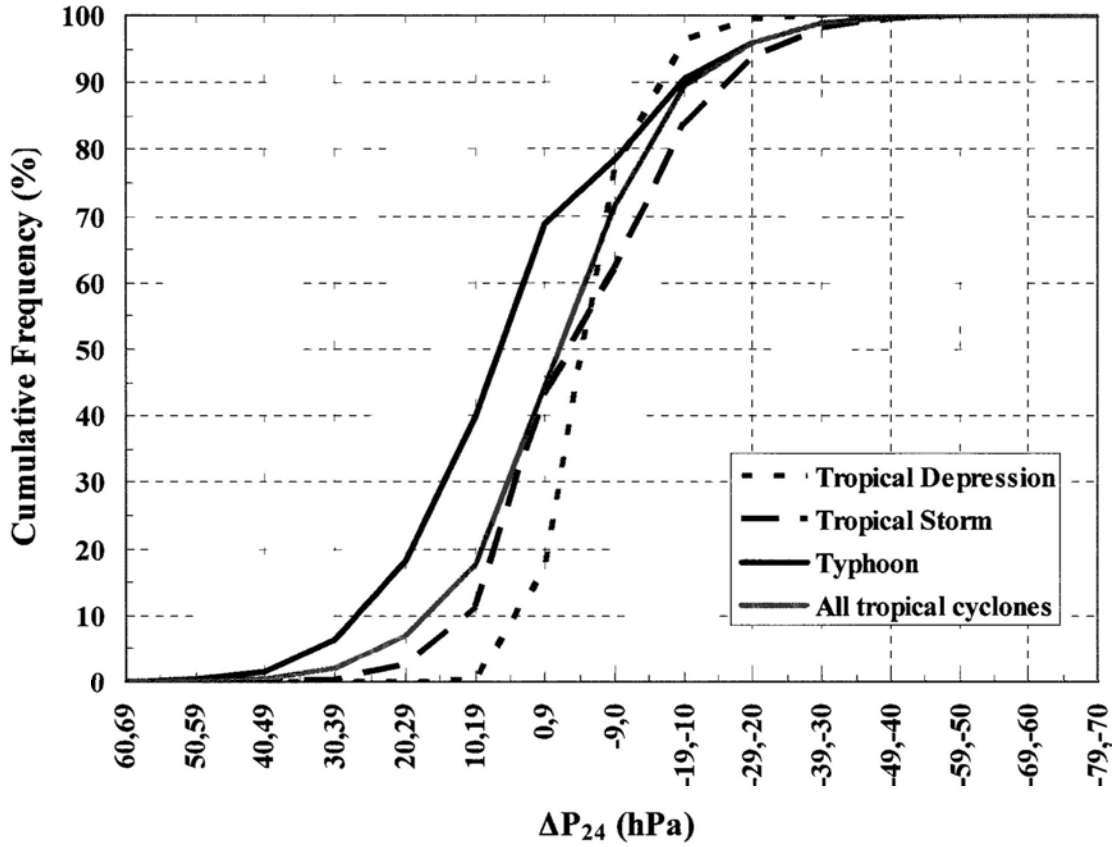

Figure 3.2 Same as figure 3.1 except for cumulative frequency distribution.

The percentage of systems that underwent RI at least once during their lifetime is also analyzed. Our result shows that 86% of all typhoons, 95% of all super-typhoons (MWS $\geq$ 51 m s^{-1}) underwent RI at least once during their lifetime. Overall, 51% of all named WNP TCs underwent RI during their life time.

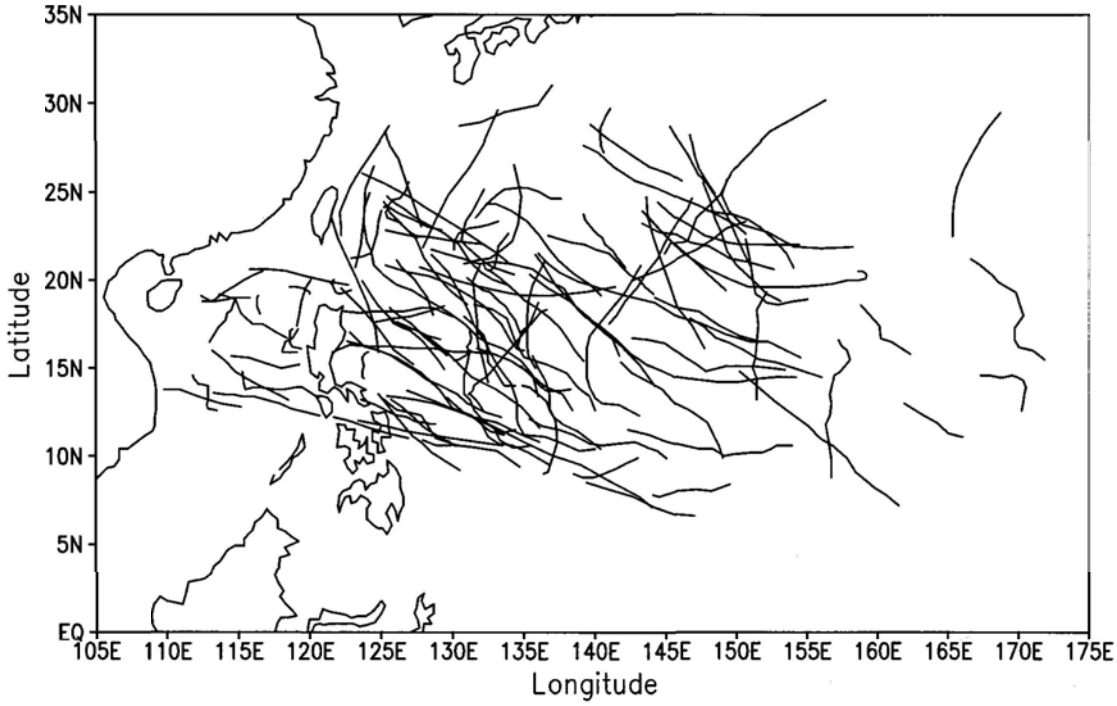

Figure 3.3 The 24-h tracks of the 1998–2006 rapid intensification samples.

Figure 3.3 shows the 24-h tracks of the 533 RI samples. Because RI may occur continuously over a 24-h time periods, some of the tracks overlap. The figure shows that RI generally occurred in regions between 10°N and 25°N. There was no RI case occurring in coastal ocean area with exceptions for those in the vicinity of Taiwan and the Philippines. The lowest latitude for RI is 7°N. Both Taiwan and the Philippines are located at the lower latitudes surrounded by open sea which is favorable for RI. At latitudes too close to the equator (5°N to 5°S), the small Coriolis force does not provide a favorable condition for RI.

Figure 3.4 shows the seasonal distribution of the RI samples. The vast majority (73%) of the RI samples occurred from July to October, and RI occurred most frequently in September. This is a slight delay for the RI compared to that in the Atlantic (Kaplan and DeMaria, 2003), which shows the vast majority of the RI

samples occur in August and September.

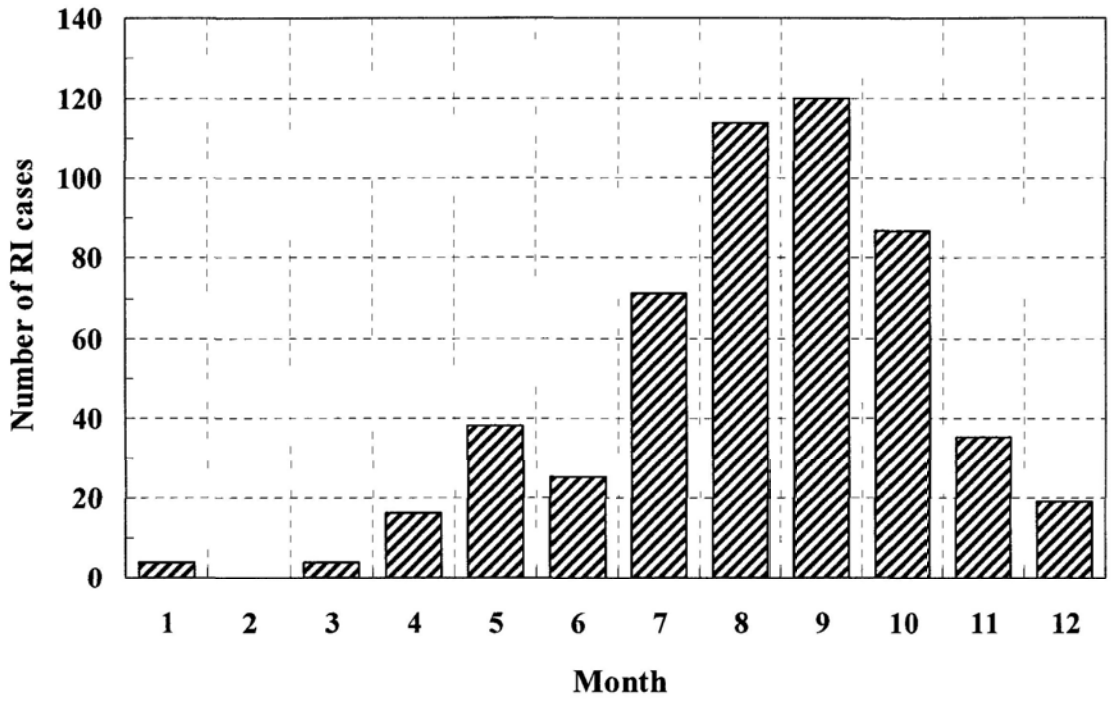

Figure 3.4 The seasonal distribution of RI samples (1998–2006).

3.2 Rainfall pattern

In this section, the rainfall distributions at the start of each of the RI samples are compared to the non-RI samples. Each sample corresponds to a 24-hour displacement. Figure 3.5 shows the composite of rainfall for RI samples, non-RI samples, and their difference. The areas with statistically significant difference at 95% confidence level determined by a *t*-test are shaded.

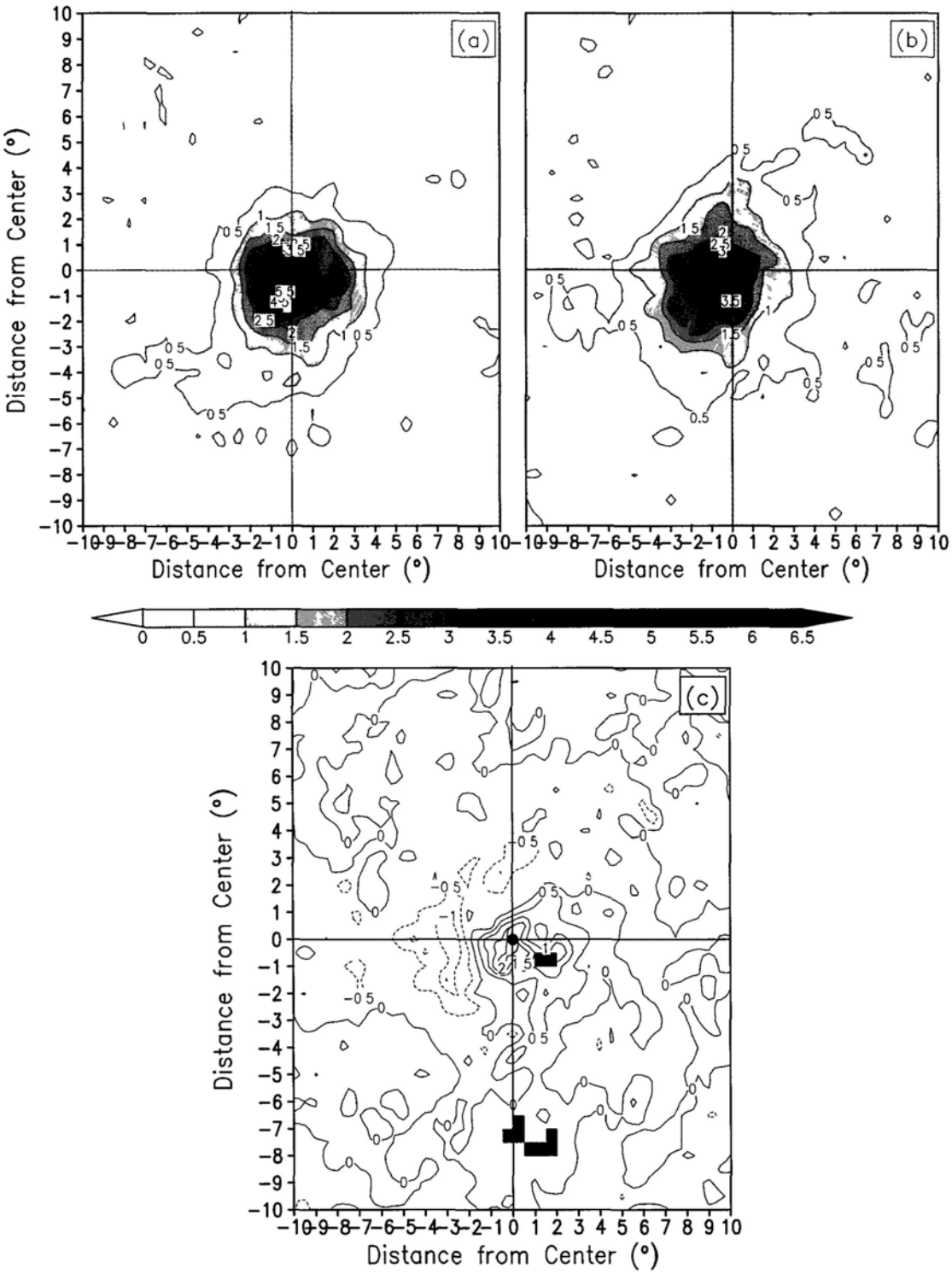

Figure 3.5 The composite initial rainfall distribution of: (a) RI samples; (b) non-RI samples; (c) difference between RI and non-RI samples (RI samples – non-RI samples) for all the samples. Areas with statistically significant difference at the 95% confidence level are shaded. The origin denotes the tropical cyclone center at t=0h. The x and y ordinates represent east and north, respectively. (Unit: mm hour^{-1})

It is seen clearly from Figure 3.5 that composite rainfall of RI samples is higher than that of non-RI samples in the areas near TC center, with a maximum of ~6.5 mm $hour^{-1}$ within inner-core regions compared to ~4.0 mm $hour^{-1}$ for non-RI samples.

3.3 SLHF pattern

In this section, the SLHF conditions present at the start of each of the RI samples are compared to the non-RI samples. Figure 3.6 shows the composite of SLHF for RI samples, non-RI samples, and their difference between RI and non-RI the samples. The areas with statistically significant difference at 95% confidence level determined by a *t*-test are shaded. The SLHF associated with RI samples tend to be higher than the non-RI samples, with a maximum of ~190 W m^{-2} to the north of the TC center compared to ~150 W m^{-2} to the north of the TC center for the non-RI samples. There is significant difference between RI and non-RI samples to the north of TC center.

Near-surface wind speed (U) and air-sea humidity difference (Δq) are two major components to compute SLHF, to compare their effects of on the SLHF pattern, composite analysis are performed on U and Δq separately. Figure 3.7 show the composite of U. The patterns for RI samples (Figure 3.7a) and non-RI samples (Figure 3.7b) are nearly the same, with the maxima to the northeast of the storm center and the decreasing wind speed around the maxima. The maximum wind speed for RI samples is ~10.5 m s^{-1} while it is ~10 m s^{-1} for non-RI samples. Figure 3.7c shows that the higher wind speed difference between RI and non-RI samples is

located to the north of the center with a maximum difference of 0.6 m s^{-1}, however, the difference is insignificant.

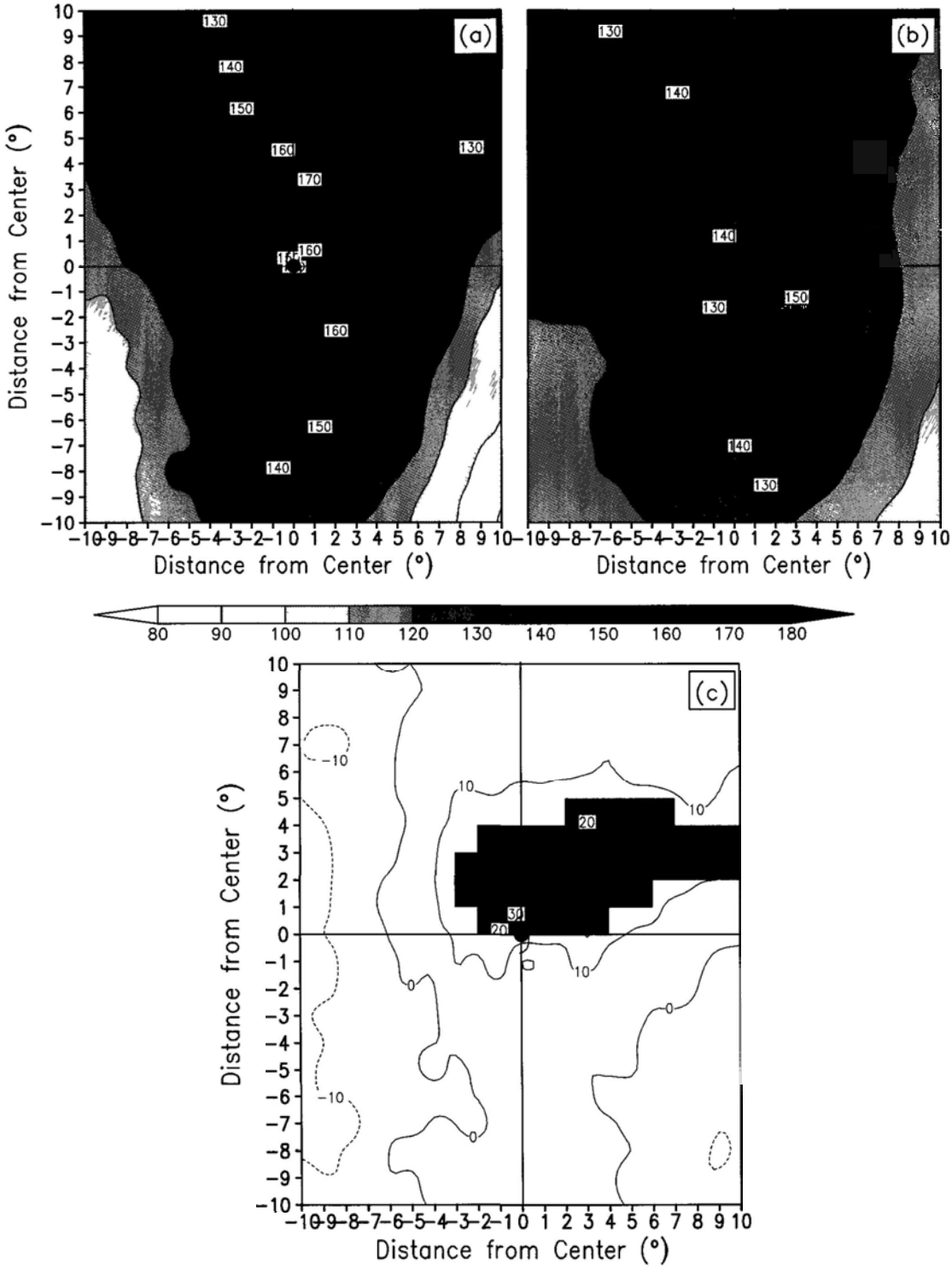

Figure 3.6 Same as Figure 3.5 except for SLHF. (Unit: W m^{-2}).

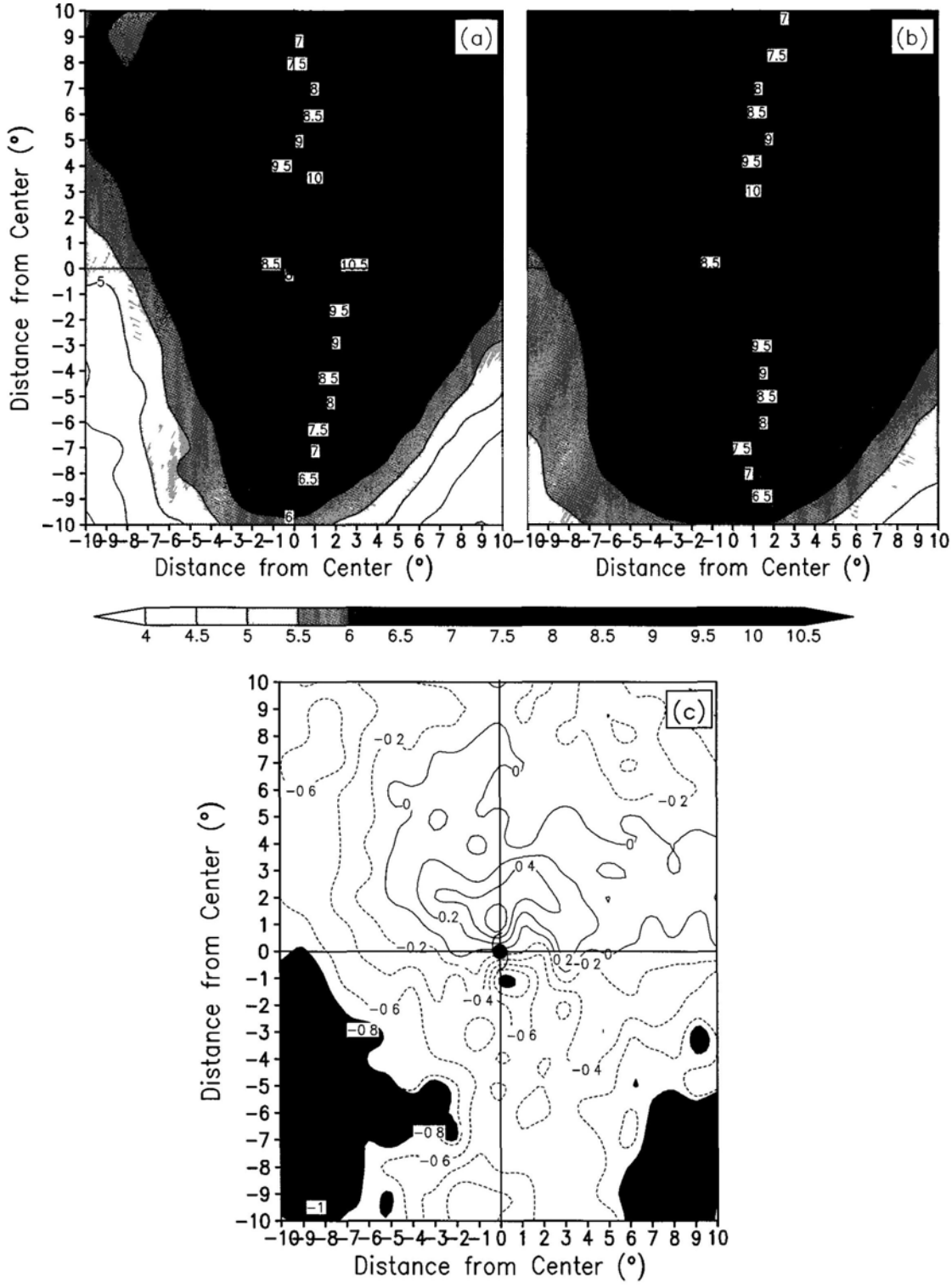

Figure 3.7 Same as Figure 3.6 except for near-surface wind speed. (Unit: m s^{-1})

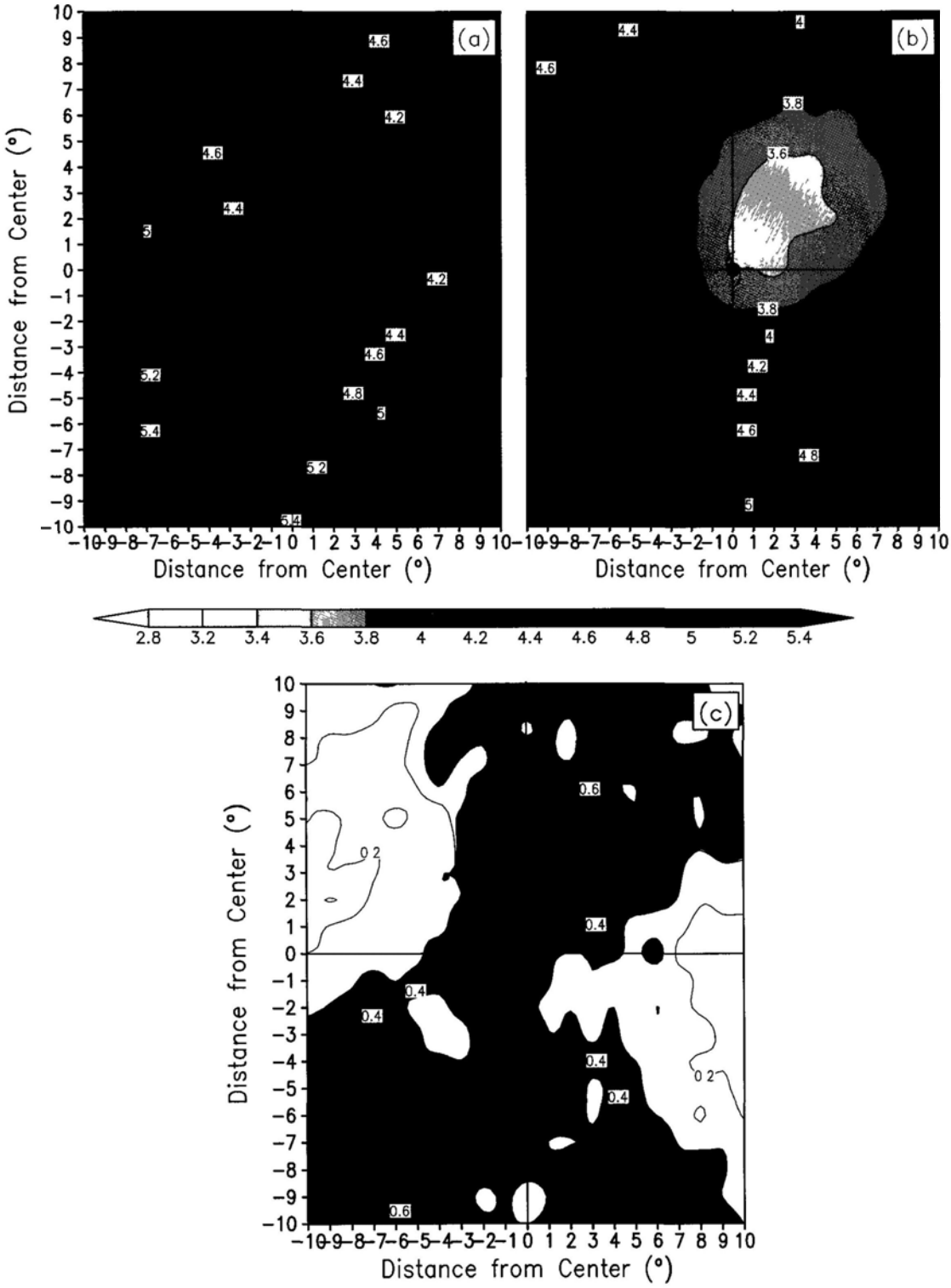

Figure 3.8 Same as Figure 3.6 except for air-sea humidity difference. (Unit: g kg^{-1})

Figure 3.8 shows the composite of Δq. Both of the composite for RI samples and non-RI samples have the similar pattern, with a minimum to the northeast of the

storm center. The minimum Δq for RI samples is ~4.0 g kg^{-1}, while it is ~3.6 g kg^{-1} for non-RI samples. The Δq associated with RI samples is higher than that associated with non-RI samples, and the maximum difference occurs to the northeast of the cyclone center. More importantly, the maximum difference is significant, suggesting that air-sea humidity difference dominates the significantly higher SLHF to the northeast of the storm center.

Table 3.1 The sample sizes of four categories stratified by moving direction. The number of RI and non-RI samples and the percentage of RI samples for each category are also presented.

	Total sample number (%)	***RI***	***Non–RI***	***Percent RI***
Westward moving	1263 (26.9)	154	1109	12.2
Northwestward moving	1706 (36.3)	227	1479	13.3
Northward moving	786 (16.7)	72	714	9.1
Northeastward moving	945 (20.1)	58	887	6.1
All	**4700 (100.0)**	**511**	**4189**	**10.9**

The pattern of high SLHF to the north of the TC center for RI samples suggests there is directionality of SLHF for RI. Hence all samples are divided into four categories according to the TC moving direction over each 24-h time period (see Figure 3.9). Table 3.1 summarizes the number of RI and non-RI 24-h displacement samples for each direction. Overall there is roughly 1 in 9 (10.9%) chance for RI. The chance for RI is the highest for northwestward moving samples (13.3%) and the least for northeastward moving samples (6.1%), with comparable chance for westward and northward moving samples (12.2% and 9.1%, respectively).

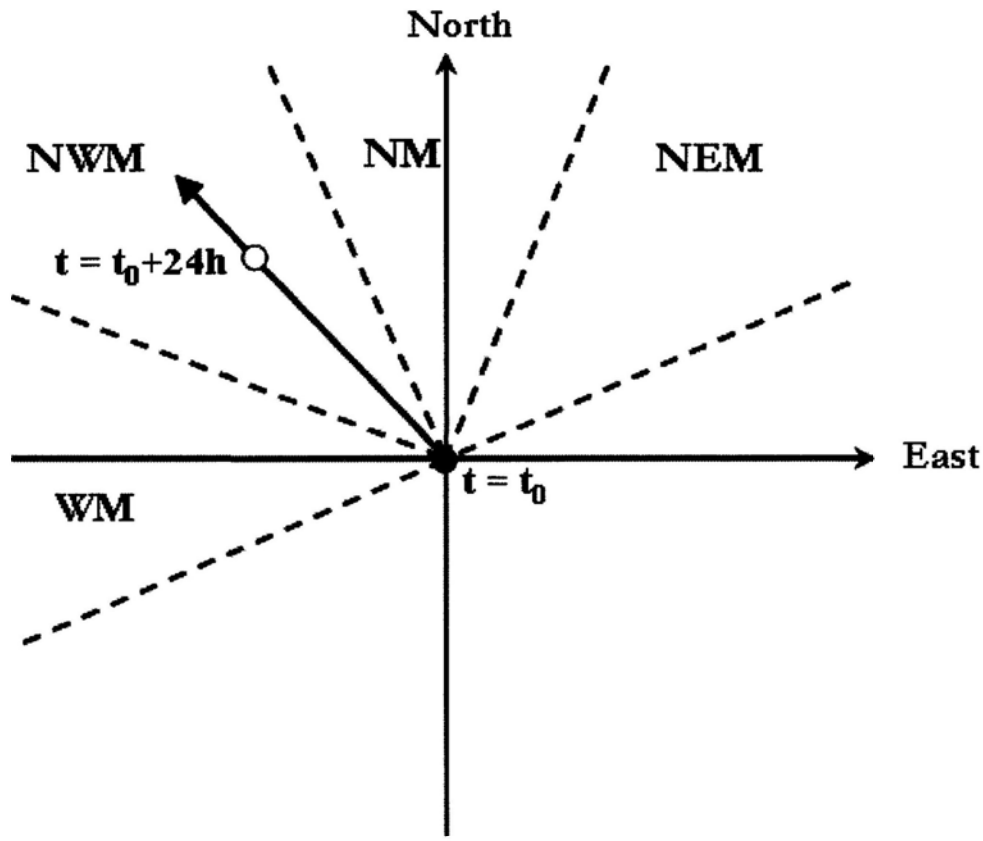

Figure 3.9 Four categories based on moving direction: westward moving category (WM), northwestward moving category (NWM), northward moving category (NM), northeastward moving category (NEM). The filled circle and the unfilled circle denote tropical cyclone positions at $t = t_0$ and at $t = t_0+24h$, respectively. Each of four angles is 45°.

Composite analyses on SLHF were performed for the overall samples first and then for each moving directions separately. Figure 3.10 shows the composite of SLHF for RI samples, non-RI samples, and their difference for westward moving category. The areas with statistically significant difference at 95% confidence level determined by a *t*-test are shaded. The SLHF associated with RI samples tend to be higher than the non-RI samples, with a maximum to the north-northwest of the TC center of ~190 W m^{-2} compared to ~160 W m^{-2} for the non-RI samples. The maximum SLHF is roughly located to the right of the moving direction for both RI

and non-RI samples. Significant difference between RI and non-RI samples exists for an area around the TC centers (Figure 3.10(*c*)).

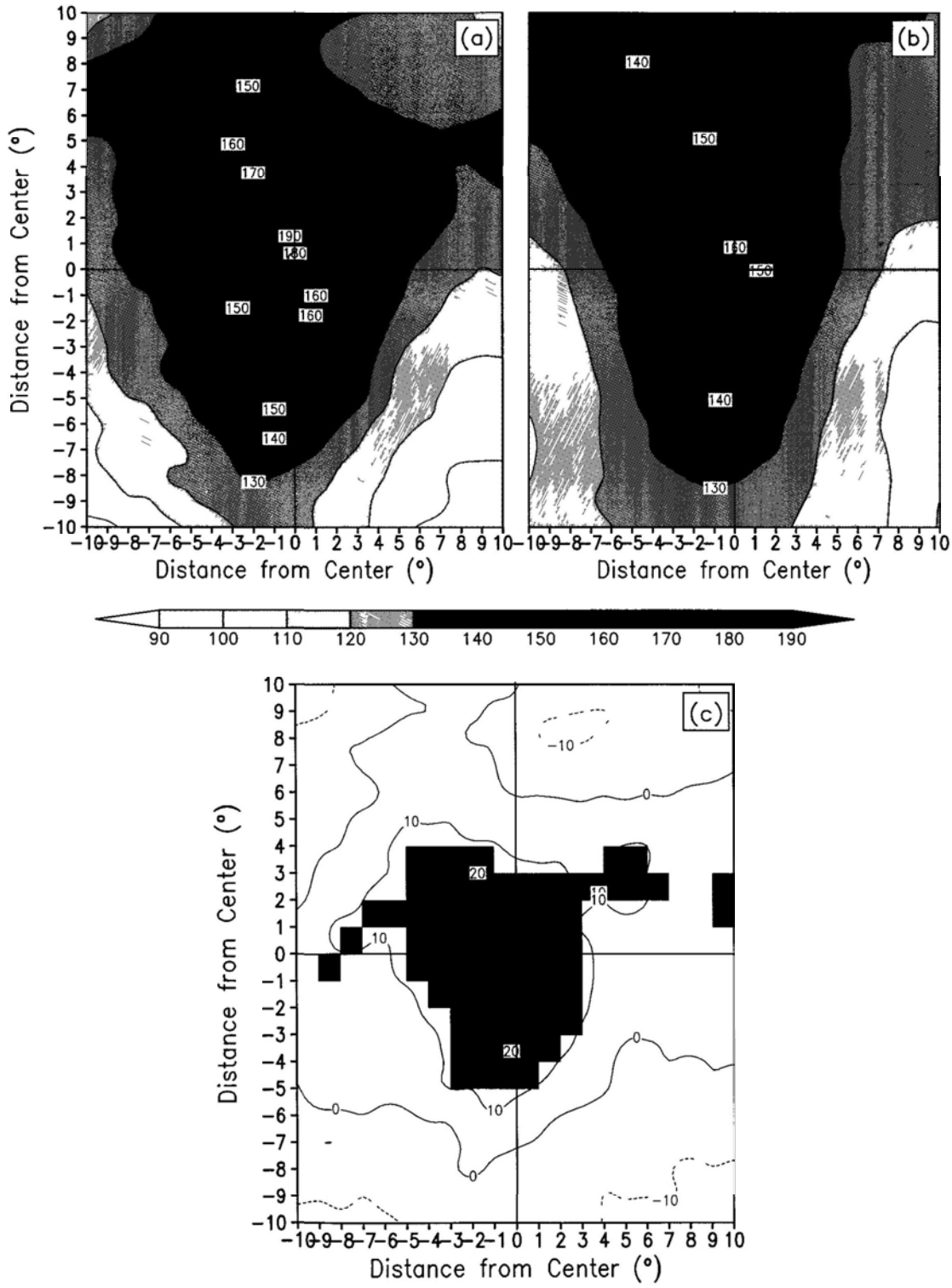

Figure 3.10 Same as Figure 3.6 except for westward moving category.

For northwestward moving category the maximum of ~180 W m^{-2} for RI samples (Figure 3.11(*a*)) and ~170 W m^{-2} for non-RI samples (Figure 3.11(*b*)) shift to the north of the TC center, and the maximum also locate roughly on the right-hand side of moving direction. The significant difference between RI and non-RI samples exists over an area to the northwest of the TC centers (Figure 3.11(*c*)).

Figure 3.12 is similar to Figure 3.8, except it is for northward moving category. The maximum of ~180 W m^{-2} for RI samples (Figure 3.12(*a*)) and ~170 W m^{-2} for non-RI samples (Figure 3.12(*b*)) shift to the east of the TC center, and the maximum also locate roughly on the right-hand side of moving direction. The significant difference between RI and non-RI samples exists over an area to the north of the TC centers (Figure 3.12(*c*)).

For northeastward moving category there exist the maximum of ~170 W m^{-2} for RI samples (Figure 3.13(*a*)) and ~150 W m^{-2} for non-RI samples (Figure 3.13(*b*)) both on the right-hand side of moving direction; And there are maximum to the northwest of the TC centers for both RI and non-RI samples, where the difference of SLHF between RI and non-RI samples is not significant. The significant difference does exist over an area to the northeast of the TC centers (Figure 3.13(*c*)).

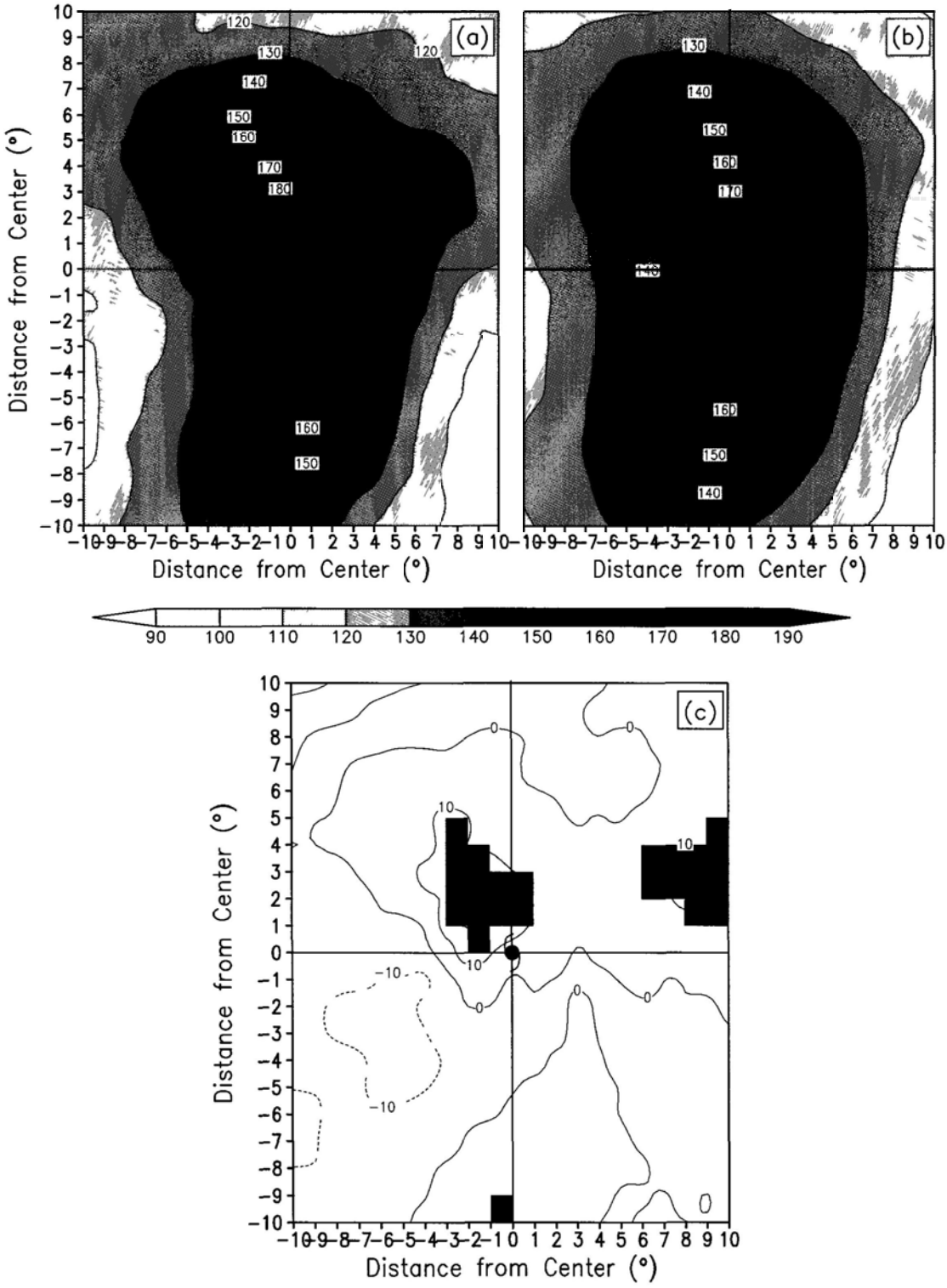

Figure 3.11 Same as Figure 3.6 except for northwestward moving category

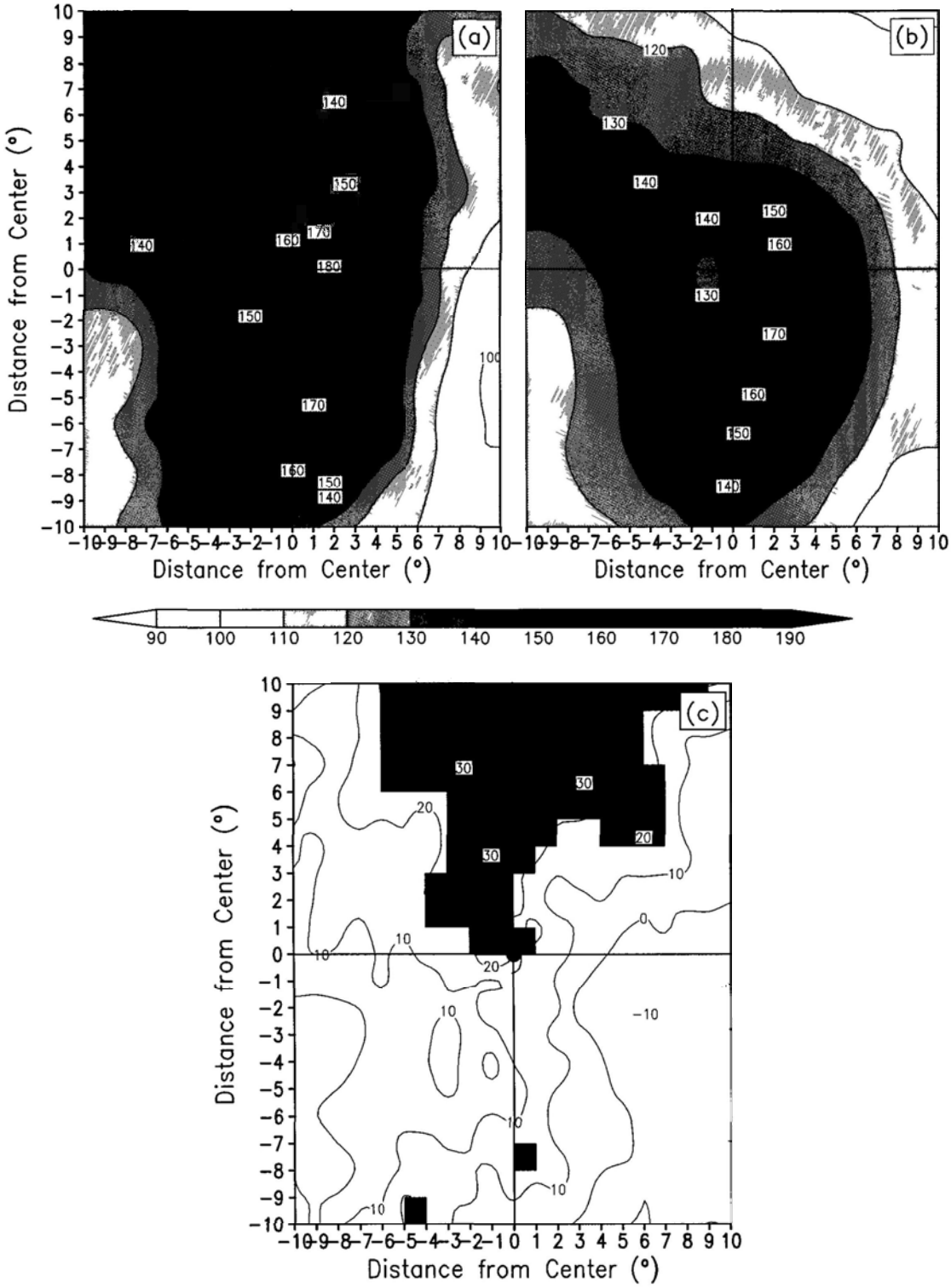

Figure 3 12 Same as Figure 3.6 except for northward moving category

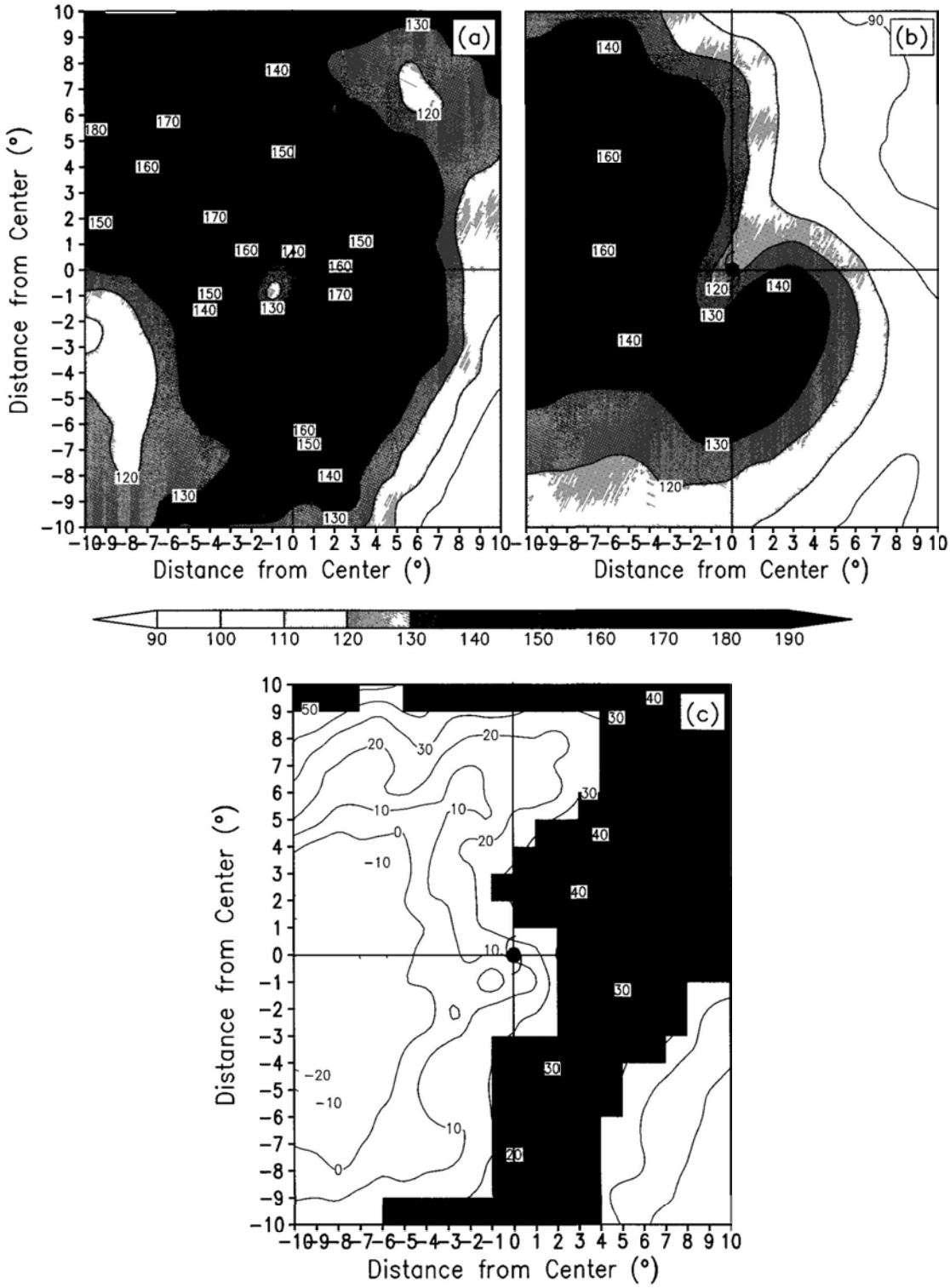

Figure 3.13 Same as Figure 3.6 except for northeastward moving category.

The maxima of SLHF locate on the right-hand side of TC track for all the four categories are mainly due to the cyclonic circulation of TC that results in the largest

resultant wind speed on the right-hand side, because they move in the same direction on the right-hand side of TC. These results demonstrate that TCs move to higher SLHF areas tend to intensify rapidly, suggesting that SLHF provides the energy and moisture for TC rapid intensification.

3.4 Summary and discussion

The primary findings of this chapter are as follows.

(a) In this study, RI was defined as approximately the 90th percentile of all 24-h over-water intensity changes of western North Pacific and South China Sea TCs from 1998 to 2006. This is equal to a minimum central pressure falls of 20 hPa over a 24-h period.

(b) Of the 209 named TCs that comprise the 1998–2006 samples, 51% of all named TCs, 86% of all typhoons, and 95% of super typhoons undergo RI at least once during their lifetime.

(c) The rainfall within inner-core regions of RI samples is higher than that of non-RI samples.

(d) The SLHF associated with RI and non-RI samples show general similar patterns for all four categories. There are maxima of SLHF to the right of TC track. The significant difference of SLHF for RI and non-RI samples occurs on TCs' pathway, suggesting that SLHF, which provide moisture and energy from ocean surface for TC development, is an important factor in TC rapid intensification.

SLHF is a nonlinear combination of U and the difference of Qs and Qa, where Qs

depends on SST. Correlation analysis shows that TC intensity is more significantly correlated with IRR than outer-core (radius of 110 km from storm center) rain rate, thus average rain rate within inner-core region is adapted in this study. Although SST has been utilized to estimate the maximum potential intensity (MPI) which is already a predictor in statistical typhoon intensity prediction scheme (e.g., Knaff et al., 2005), our result shows that SLHF and inner-core rainfall have the potential to be new predictors for TC intensity forecasting. The work in the following chapters will focus on investigating whether SLHF and inner-core rainfall (IRR) can be employed to improve the intensity forecast, especially for RI estimates. Besides multiple linear regression and logistic regression methods, more sophisticated statistical techniques, such as neural networks, will also be employed.

CHAPTER 4 Development of Statistical Typhoon Intensity Prediction: Application to Satellite Observed Rain Rate and Surface Evaporation

Based on the traditional predictors (independent variables) in STIPS (Knaff et al. 2005) and two new satellite-based potential predictors (SLHF and IRR) proposed in the last chapter, statistical typhoon intensity prediction models using linear regression and neural network are developed in this chapter. The dependent variables (predictands) are over-water intensity (i.e. MWS) change from the initial forecast time (DELV) at 24-h interval.

$$DELV = \Delta MWS = MWS(t_0 + T) - MWS(t_0) \tag{4.1}$$

where T are 24, 48, and 72 h. Models beyond 72 h are not created, since a snapshot of satellite observation (i.e., SLHF and IRR) is unlikely to influence intensity change significantly beyond 3 days (Fitzpatrick 1997).

All the datasets are collected over the period from 2000 to 2008 for model development. This period represents an intersection of all available data used in this study. RSMC Tokyo best track data, NCEP GFS FNL environmental data and TMPA rain rate data are collected twice daily at 0000 and 1200 UTC. Only over-water TC samples are considered since land effects on TC intensity change are not taken into account in this work and OAFlux SLHF and TMI SST data are available over the ocean only.

Section 4.1 describes the computation of the potential predictors. The predictor

selection procedure and development and evaluation of linear regression models are presented in section 4.2. Neural network models are assessed in section 4.3. The summary of this chapter is given in section 4.4.

4.1 Potential predictors

Table 4.1 summarizes the predictors (including 16 original and two new satellite-based predictors, SLHF and IRR) used in this study. The computation of the traditional climatological and environmental predictors follows the approach in Knaff et al. (2005). All of the environmental predictors are obtained using a "perfect prog" approach (Kalnay 2003). Both the NCEP GFS FNL analysis and the actual TC best track (by the RSMC Tokyo) are used to develop the models. The predictors that are evaluated at the beginning of the forecast period are static, such as those predictors related to climatology and persistence; and predictors that are averaged along the track of the storm from the initial observation to the forecast time are time dependent, providing the mean conditions for the storm, such as those predictors related to SST, moisture and wind fields.

Table 4.1 Potential climatological, environmental, and satellite-based predictors. The predictors that are evaluated at the beginning of the forecast period are static (S), and the predictors that are averaged along storm track from the initial time to the forecast time are time dependent (T).

Predictor	Description	Static (S) or time dependent (T)
Climatology and persistence		
MWS0	Initial maximum wind speed	S
DMWS	Maximum wind speed during the past 12 h	S
JDAY	Absolute value of (Julian day – 248)	S
SPD	Strom translational speed	S
LAT	Latitude of storm center	S
LON	Longitude of storm center	S
Environmental		
POT	Maximum potential intensity based on Eq. (1) minus initial maximum wind speed	T
RHLO	Area-averaged (200–800 km) relative humidity at 850–700 hPa	T
RHHI	Area-averaged (200–800 km) relative humidity at 500–300 hPa	T
U200	Area-averaged (200–800 km) zonal wind at 200 hPa	T
T200	Area-averaged (200–800 km) temperature at 200 hPa	T
δ200	Area-averaged (0–1000 km) divergence at 200 hPa	T
REFC	Relative eddy flux convergence within 600 km at 200 hPa	T
SHR	Area-averaged (200–800 km) 200–850-hPa wind shear	T
USHR	Area-averaged (200–800 km) 200–850-hPa zonal wind shear	T
ζ850	Area-averaged (0–1000 km) 850-hPa relative vorticity	T
Satellite-based		
SLHF	Area-averaged (5° × 5° box) surface latent heat flux	S
IRR	Area-averaged (0-110 km) inner-core rain rate	S

4.1.1 MPI estimation

The MPI is defined as the upper bound of TC intensity for given atmospheric and oceanic thermal conditions (Camp and Montgomery 2001). It can be estimated theoretically (e.g., Miller 1958; Emanuel 1988; Holland 1997) or empirically (e.g., Merrill 1987; DeMaria and Kaplan 1994b; Whitney and Hobgood 1997; Knaff et al. 2005; Zeng et al. 2007) over Atlantic, eastern North Pacific and western North Pacific. Only MPI in eastern North Pacific shows linear relationship with SST. The nonlinear relationship over Atlantic and western North Pacific is partly due to rapid recurvature of some TCs over colder SSTs and a lag before the circulation spins down as suggested by Whitney and Hobgood (1997). However, over the eastern North Pacific the TCs generally move more slowly and the storm strength has more direct correlation with the SST. Lack of aircraft observations of extremely high wind speeds may also contribute to the linear relationship between maximum intensity and SST over eastern North Pacific.

Following the empirical approach, the MPI is determined as an exponential function of SST, the interpolated 1° × 1° monthly SST climatology (Levitus 1982) or 1° × 1° weekly SST analysis (Reynolds et al. 2002) used in previous studies is replaced as the high-resolution daily SST data retrieved from TMI in this study. Daily SSTs are expected to provide more precise thermal information of the ocean. SST were stratified into SST bins with mid-points from 16.5°C to 32.5°C at 0.5°C interval, and each observation is assigned to the nearest SST midpoint. Table 4.2 shows maximum intensity and numbers of observation for each SST group. 91% of

the observations are assigned to warmer SST groups (≥26.0°C). This is only slightly lower than the 92% found by Zeng et al. (2007) for the western North Pacific storms, and higher than the 76% found by Whitney and Hobgood (1997) and the 82% found by DeMaria and Kaplan (1994b) for the Atlantic systems. The strongest typhoon in the record is Typhoon Jangmi that occurred in 2008 and the peak intensity 115 kt is assigned to 28.0°C category. The SST categories from 28.5°C to 31.0°C have the same maximum intensity 110 kt. For the categories higher than 31.0°C, it shows a decline of maximum intensity.

The empirical exponential MPI function described by Eq. (4.2) is derived with a SST cutoff of 28.5°C since the flattening or decrease of maximum wind over the warmest waters at this SST. The Curve Fitting Toolbox of Matlab (Demuth et al. 2009) is used to fit the MPI equation. This parametric equation is not contained in the toolbox library hence a custom MPI equation is created. The Non-linear Least Squares method and Trust-Region algorithm in the toolbox are employed. The resulting coefficients are given by A = 29.59 kt, B = 108.1 kt, C = 0.1292 °C^{-1} and T_0 = 30.0 °C.

$$MPI = A + Be^{C(T-T_0)} \tag{4.2}$$

Figure 4.1 shows this MPI function as well as the data used for its development. The highest MPI is given as 140 kt. The intense TCs are located only over high SST regions. A lot of weak storms over high SSTs are those observations in the early development stages of TCs, and a small number of weak storms occurred over SSTs below 26.0°C shows that they can survive over colder waters, as suggested by Zeng

et al. (2007).

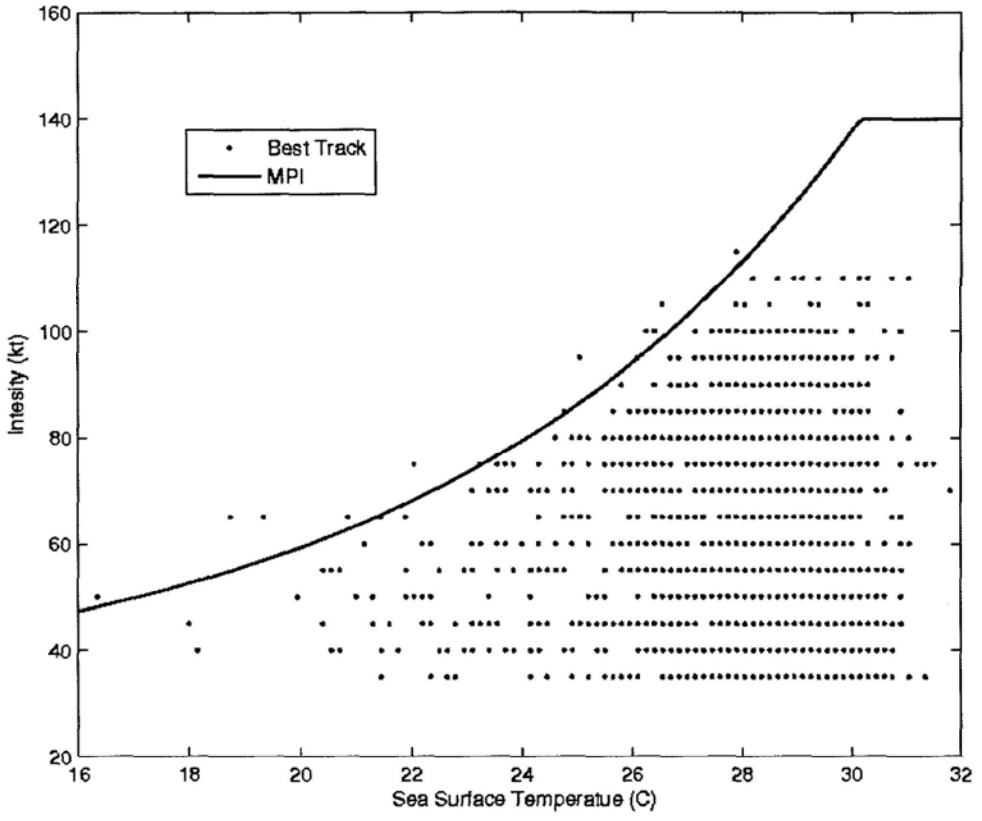

Figure 4.1 The empirical relationship between maximum potential intensity (MPI, kt) and sea surface temperature (°C). The relationship is derived from data of 9 yr (2000–2008) and the individual data points used for its development are also shown.

4.1.2 Other potential predictors

Those potential static predictors in relation to climatology and persistence contain initial intensity (MWS0), intensity change in the previous 12 h (DMWS), absolute value of Julian date anomaly from 248 [JDAY; 248 is the peak of seasonal TC activity over western North Pacific (Neumann 1993)], average storm translational speed in the previous 12 h (SPD), latitude (LAT) and longitude (LON) of current storm location.

Table 4.2 SST group properties.

SST midpoint (°C)	Number of Observations	Maximum intensity (kt)
16.5	1	50
18.0	2	45
18.5	1	65
19.5	1	65
20.0	1	50
20.5	8	55
21.0	3	65
21.5	7	65
22.0	11	75
22.5	10	60
23.0	17	75
23.5	15	75
24.0	11	75
24.5	28	85
25.0	31	95
25.5	37	85
26.0	72	100
26.5	93	105
27.0	100	100
27.5	188	100
28.0	186	115
28.5	226	110
29.0	424	110
29.5	244	110
30.0	150	110
30.5	78	110
31.0	15	110
31.5	3	75
32.0	1	70

The potential predictors related to moisture are mean upper-level relative humidity (RHHI) at 850–700 hPa layer and mean mid-level relative humidity (RHLO) at 500–300 hPa layer, in an annulus of 200–800 km from storm center. The inner regions within 200-km radius of the TC are removed from the analysis since synthetic observations are often assimilated to the global dynamic models to initialize the TC (e.g., Goerss and Jefferies 1994).

The area-averaged zonal wind at 200 hPa (U200), air temperature at 200 hPa (T200), 200 – 850 hPa wind shear (SHR), and zonal component of the shear (USHR) within the same 200–800 km annulus are examined as potential predictors. SHR and USHR are calculated using Eq. (4.3) and (4.4), respectively.

$$SHR = \sqrt{(u_{200} - u_{850})^2 + (v_{200} - v_{850})^2} \tag{4.3}$$

$$USHR = u_{200} - u_{850} \tag{4.4}$$

where u and v are zonal and meridional wind components of wind velocity, the subscripts denote the atmospheric layers in hPa.

The divergence at 200 hPa (δ200) and the relative vorticity at 850 hPa (ζ850) are calculated based on central difference method for grids center around the TC center, using Eq. (4.5) and (4.6), respectively. The divergence and vorticity are then averaged within 1000 km radius.

$$\delta 200_{i,j} = \frac{\partial u}{\partial x} + \frac{\partial v}{\partial y} = \frac{u_{i+1} - u_{i-1}}{D_x} + \frac{v_{j+1} - v_{j-1}}{D_y} \tag{4.5}$$

$$\zeta 850_{i,j} = \frac{\partial v}{\partial x} - \frac{\partial x}{\partial y} = \frac{v_{i+1} - v_{i-1}}{D_x} - \frac{u_{j+1} - u_{j-1}}{D_y} \tag{4.6}$$

where u and v are the same as those in Eq. (4.3), the subscripts i and j represent zonal

and meridional grid numbers, D_x is the distance between grid (i+1, j) and grid (i–1, j), and D_y is the distance between grid (i, j+1) and grid (i, j–1).

The relative eddy flux convergence (REFC) at 200 hPa is calculated at 100-km radical intervals from 100 to 600 km using Eq. (4.7):

$$REFC = -r^{-2}\frac{\partial}{\partial r}\left(r^2\overline{U_L'V_L'}\right) \tag{4.7}$$

where U is the radial wind, V is the tangential wind, r is radius. The overbar denotes an azimuthal average; the primes represent a departure from the azimuthal average, and the subscript L indicates that the calculation is done along the storm track. The storm translational speed is removed from the horizontal wind components to determine U and V. REFC is a measure of the momentum flux and accounts for positive interactions between the storm and synoptic-scale systems, it is only evaluated at 200 hPa since the interactions is more likely to present in the upper levels as suggested by Holland and Merrill (1984) in a theoretical study. At lower atmosphere, the large inertial stability of the rapidly rotating storm circulation limits the interactions with the environment.

Table 4.3 Correlation coefficients between 24-h minimum central pressure (ΔP_{24}) change and area-averaged SLHF within different size of boxes. The number of samples during the period 2000–2008 is 1728.

Size of box	Correlation coefficients between ΔP_{24} and area-averaged SLHF
3° × 3°	–0.128
5° × 5°	–0.132
7° × 7°	–0.122
9° × 9°	–0.100

SLHF and IRR predictors are computed as the average within a box of 5° × 5° and within a radius of 100 km centered at TC position, respectively. SLHF parameter is also calculated from larger or smaller boxes. The correlation coefficients between area-averaged SLHF within different size of boxes and 24-h minimum central pressure change (ΔP_{24}) using samples during the period 2000–2008 are shown in Table 4.3, the other size of boxes are disregarded since they have lower correlations with ΔP_{24} than does the 5° × 5° averaged SLHF. For the operational purpose, SLHF and IRR are deemed to be static predictors, since it is impossible to acquire satellite remote sensed information in "future".

A stepwise regression procedure is used to select parameters from the potential predictor pool. A 99% statistical significance level based on an *F* test (e.g., Wilks 2006) is the threshold for an individual predictor to be added initially in the model. Once selected, a predictor can only be removed if its significance level becomes less than 98% after the addition/removal of another predictor. The stepwise procedure continues until none of the selected predictors can be removed and none of the remaining potential predictors can be added.

4.2 Linear regression models

To assess the contribution of SLHF and IRR on the intensity change prediction, three kinds of regression models are developed. The first serves as a control. The stepwise procedure is applied on the 16 STIPS original predictors to select significant predictors and create a base regression model (hereafter referred to as

BASE). The second kind of model is developed by adding the two new satellite-based predictors SLHF and IRR into the base regression model (hereafter referred to as STIPER). The stepwise procedure is also employed on the 6 predictors related to climatology and persistence to create another kind of regression model called CLIPER, which is generally a baseline to evaluate the skill of operational models. A model can be considered to produce skillful intensity forecast if it has smaller error than CLIPER.

Assuming the independence of annual statistics, the samples in one year are used for verification and the samples in the other years are used for model development. For example, to predict 2003 TC intensity over western North Pacific, the samples of 2000–2002 and 2004–2008 are used to construct the models. As a result, for each CLIPER, BASE and STIPER model there are totally nine regression equations, which may contain different sets of significant predictors due to different training samples. All of the predictors identified for any regression equation are included in the final group of predictors. The final CLIPER, BASE and STIPER models are created using the final group of predictors. The predictand as well as the predictors are normalized by subtracting their means and dividing by their standard deviations before regression, the resulting coefficients can be used to compare the relative contribution of each predictor directly.

4.2.1 24-h intensity prediction

a. Model interpretation

Table 4.4 lists the normalized coefficients associated with each predictor for each

STIPER 24-h forecast equation. The number of samples used to develop the regression equations are shown in parentheses at the top of the table. There are around 1100 samples for training every single model. The STIPER models for 24-h intensity forecast contain 10 important predictors: MWS0, DMWS, JDAY, LAT, POT, RHLO, RHHI, SHR, SLHF and IRR. Among these predictors, MWS0, DMWS, JDAY, and LAT are used to create the CLIPER models; MWS0, DMWS, JDAY, LAT, POT, RHLO, RHHI, and SHR are included in the BASE models.

In all these models, the four most important predictors are POT, DMWS, SHR and MWS0. As expected, the persistence term DMWS is associated with a positive regression coefficient, since storms that have intensified in the previous 12 h tend to intensify in the next 24 h (Knaff et al. 2005). Intensity change is negatively correlated with the MWS0 because weak storms are further from their MPI and hence have more potential to intensify. Vertical wind shear has a negative impact on the intensification of TCs. One explanation for this is that the heat and moisture at upper levels are advected in a different direction relative to the low-level cyclonic circulation and therefore the "ventilation" of heat away from the circulation inhibits the development of the storm (Gray 1968). DeMaria (1996) proposed an alternate explanation, the tilt of the upper and lower level potential vorticity due to vertical wind shear produces a mid-level temperature increase near the vortex center, and this mid-level warming is hypothesized to reduce the convective activity and thus inhibit storm development.

The coefficient of JDAY is negative since this variable indicates the number of

days from the peak of the typhoon season. LAT is negatively correlated with intensity change since the SST generally decreases toward the north in the western North Pacific basin. RHLO and RHHI can affect TC intensification rates because high relative humidity in the middle atmosphere reduces the entrainment of dry air into cumulus convection which is direct source of TC's energy. Nearly the same positive coefficients associated with the two new satellite-based predictors suggest that latent heat release in the atmosphere and latent heat transfer at the ocean-atmosphere interface have comparable effects on TC development in 24 hrs.

Table 4.4 STIPER predictor normalized regression coefficients in different verification years for 24-h forecasts. The predictors are listed on the left side of the table and the verification years are listed at the top with the number of dependent samples (N) used to develop the equation shown in parentheses.

Year (N) / Predictor	2000 (1126)	2001 (1102)	2002 (1065)	2003 (1097)	2004 (1039)	2005 (1108)	2006 (1111)	2007 (1144)	2008 (1176)
1) MWS0	–0.15	–0.17	–0.17	–0.14	–0.15	–0.15	–0.13	–0.16	–0.14
2) DMWS	0.29	0.31	0.30	0.30	0.30	0.30	0.30	0.28	0.28
3) JDAY	–0.12	–0.10	–0.12	–0.11	–0.12	–0.10	–0.10	–0.12	–0.11
4) LAT	–0.11	–0.09	–0.10	–0.10	–0.13	–0.10	–0.09	–0.13	–0.12
5) POT	0.31	0.29	0.29	0.31	0.30	0.30	0.33	0.29	0.32
6) RHLO	0.07	0.04	0.05	0.04	0.05	0.04	0.05	0.06	0.06
7) RHHI	–0.01	0.02	0.03	0.04	0.01	0.04	0.01	0.00	–0.01
8) SHR	–0.17	–0.18	–0.17	–0.18	–0.18	–0.16	–0.17	–0.18	–0.18
9) SLHF	0.05	0.06	0.05	0.03	0.04	0.04	0.05	0.05	0.05
10) IRR	0.04	0.07	0.04	0.07	0.03	0.06	0.05	0.05	0.04

b. Dependent model statistics

Table 4.5 shows mean absolute error (MAE) and percent variance explained (R^2) of CLIPER, BASE, and STIPER estimated from dependent data for 24-h model training. MAE and R^2 represent the potential forecast capability of the models. The CLIPER models have the largest MAE of about 7.6 kt and smallest R^2 of about 0.47, the STIPER models have the smallest MAE of about 7.0 kt and the largest R^2 of about 54%, and the BASE models have MAE and R^2 between the other two kinds of models. The results indicate that the addition of synoptic predictors can enhance the model capability of intensity prediction and the inclusion of two satellite-based predictors on heat source can improve the capability further.

Table 4.5 Developmental statistics of CLIPER, BASE and STIPER models for 24-h forecast. Mean absolute error (MAE, kt) of the model estimate and percent variance explained (R^2) are shown.

Year	CLIPER		BASE		STIPER	
	MAE	R^2	MAE	R^2	MAE	R^2
2000	7.60	47.4	7.14	53.8	7.11	54.1
2001	7.66	46.7	7.17	53.0	7.13	53.5
2002	7.59	47.1	7.15	53.5	7.11	53.8
2003	7.61	46.3	7.13	53.0	7.11	53.5
2004	7.47	48.0	7.00	54.4	6.99	54.5
2005	7.51	46.4	7.02	52.8	6.98	53.3
2006	7.54	46.3	7.04	52.9	7.01	53.3
2007	7.32	47.0	6.91	52.8	6.89	53.1
2008	7.46	46.0	6.99	52.4	6.97	52.7

c. Model evaluation

The models developed above are evaluated in this section. Table 4.6 shows MAE and R^2 of CLIPER, BASE and STIPER 24-h forecasts for different verification years. The best model for every verification year is indicated in bold italics. The numbers of samples used to verify are also shown. There are 70 samples for verification year 2008 and up to 207 samples for verification year 2004. Both of the BASE and STIPER models can produce better forecasts than CLIPER. Among 9 verification cases, STIPER has the lowest MAE and the highest R^2 for 6 cases. The MAEs of the STIPER models are 1%–3% smaller than those of the corresponding BASE models for the 6 cases. As a result, STIPER is skillful for 24-h intensity forecast and the inclusion of satellite-based predictors SLHF and IRR provides 1%–3% improvement compared with the model without satellite information.

Table 4.6 also shows that the MAE in 2005, 2007 and 2008 verification years are larger than the other verification years. Some statistics of 24-h observations and forecasts from STIPER are shown in Table 4.7. On average 23 TCs contribute to 138 observations of 24-h intensity change per year during period 2000–2008. The maximum and the minimum 24-h intensity change during the period 2000–2008 are 50 kt per day and –45 kt per day. The high variances of intensity change observations in year 2005, 2007, and 2008 result in the bad model performance in these years.

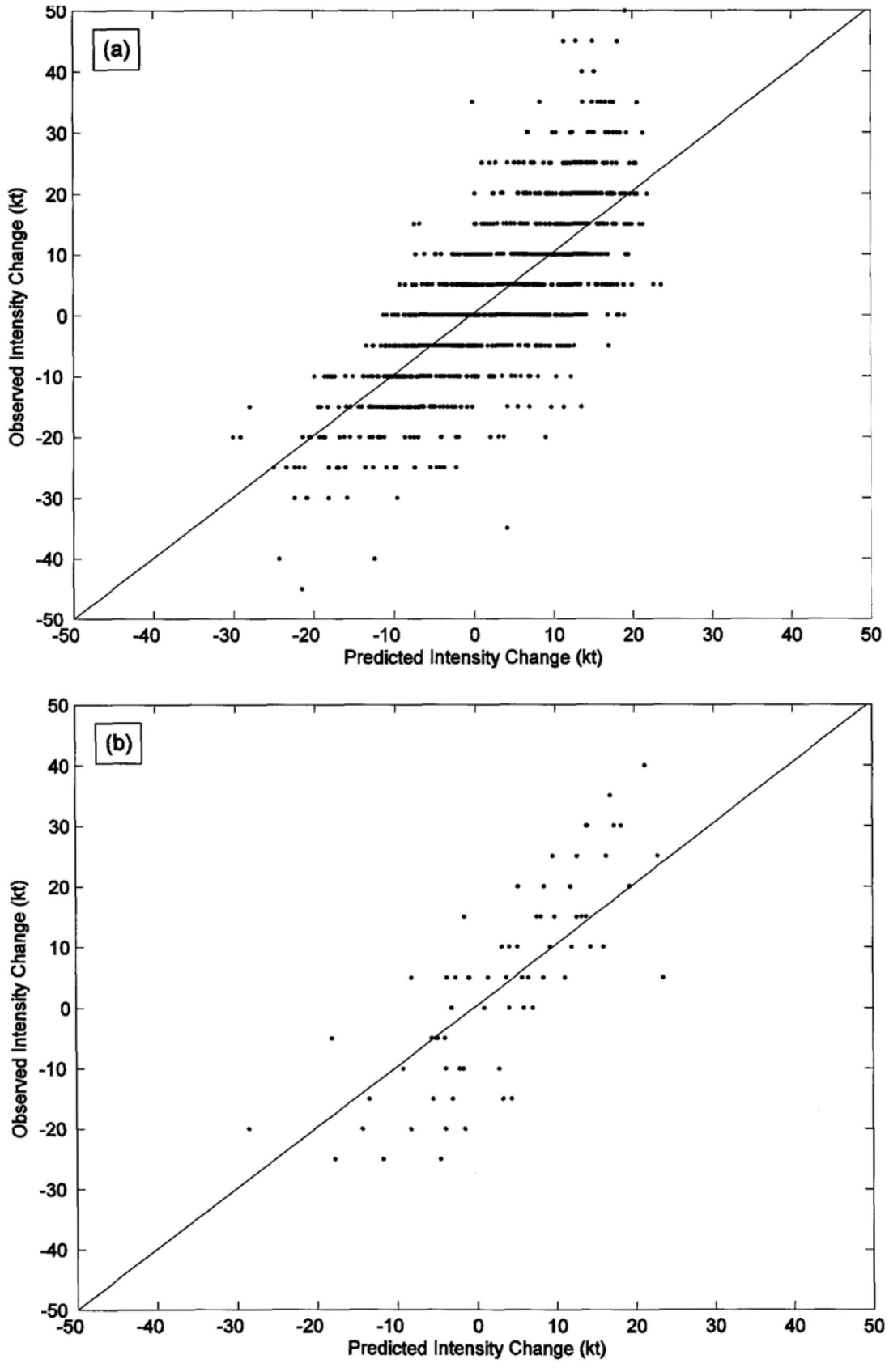

Figure 4.2 Scatter plots of STIPER predicted intensity change and observed intensity change for (a) dependent training samples during 2000–2007, (b) independent verification samples in 2008.

Table 4.6 Mean absolute errors (MAE, kt) and percent variances explained (R^2) for CLIPER, BASE, and STIPER 24-h forecasts in different verification years with number of samples (N). The best model for each verification year is indicated in bold italics.

Year	N	CLIPER		BASE		STIPER	
		MAE	R^2	MAE	R^2	MAE	R^2
2000	120	7.01	37.5	6.54	43.8	***6.49***	***44.0***
2001	144	6.51	47.5	***6.33***	***54.0***	6.46	52.4
2002	181	7.30	42.6	6.77	48.7	***6.76***	***49.5***
2003	149	6.94	50.5	***6.73***	***53.4***	6.73	52.6
2004	207	7.94	39.5	7.58	45.5	***7.37***	***46.7***
2005	138	7.60	49.3	***7.47***	***54.6***	7.60	54.3
2006	135	7.43	50.5	7.18	54.6	***7.18***	***54.7***
2007	102	9.87	44.3	8.67	54.6	***8.59***	***55.1***
2008	70	8.67	55.5	8.09	60.8	***8.05***	***61.7***

Figure 4.2 indicates the scatter plots of STIPER predicted 24-h intensity change and observed 24-h intensity change for dependent training samples during period 2000–2007 and independent verification samples in 2008. The STIPER model is shown to under-estimate the rapid intensification rates and over-estimate the intensity in rapidly decaying events. This is consistent with the evaluation study by Elsberry et al. (2007) and confirms the conclusion of Knaff et al. (2005) that linear regression model can not predict extremes.

To examine and compare the performance in specific stage of TCs of the BASE and STIPER models, mean absolute error is stratified by initial TC intensity and 24-h intensity change for the 2008 verification case as an example. Figure 4.3a shows mean absolute error as a function of initial intensity classified in 5-kt bins. The

STIPER model outperforms the BASE model for typhoons with intensity between 45 kt and 85 kt. The BASE model produces better forecasts (lower MAE) for 35–40 kt bin and 85–90 kt bin, however, the sample size for the two bins are very small. Figure 4.3b indicates mean absolute error binned as a function of 24-h intensity change. Most of the samples are located within the intensity range of ±20 kt. Mean absolute error for the STIPER model is not larger than that for the BASE model for all intensity change bins except between 5–10 kt. The MAE becomes higher with increasing magnitude of intensity change. It is worthy to point out that STIPER performs much better for substantially intensifying samples (with 24-h intensity change larger than 20 kt) than the BASE model, suggesting that the addition of satellite information could reasonably improve the forecasts of rapidly intensifying samples.

Table 4.7 Statistics of 24-h observations and forecasts from the STIPER model. The unit of intensity change is kt day^{-1}, the unit of intensity is kt, and the unit of variance is kt^2 day^{-2}.

	2000	2001	2002	2003	2004	2005	2006	2007	2008
Min intensity change	–20	–35	–30	–25	–45	–40	–30	–40	–25
Max intensity change	40	35	30	30	40	45	45	50	40
Max intensity	100	105	100	105	110	105	105	110	105
Number of storms	23	24	25	20	28	22	23	24	22
Variance of observations	133	162	146	172	162	208	201	270	262
Variance of forecasts	86	105	96	128	96	101	79	85	119
Variance of forecast error	32	35	30	34	33	36	38	46	35

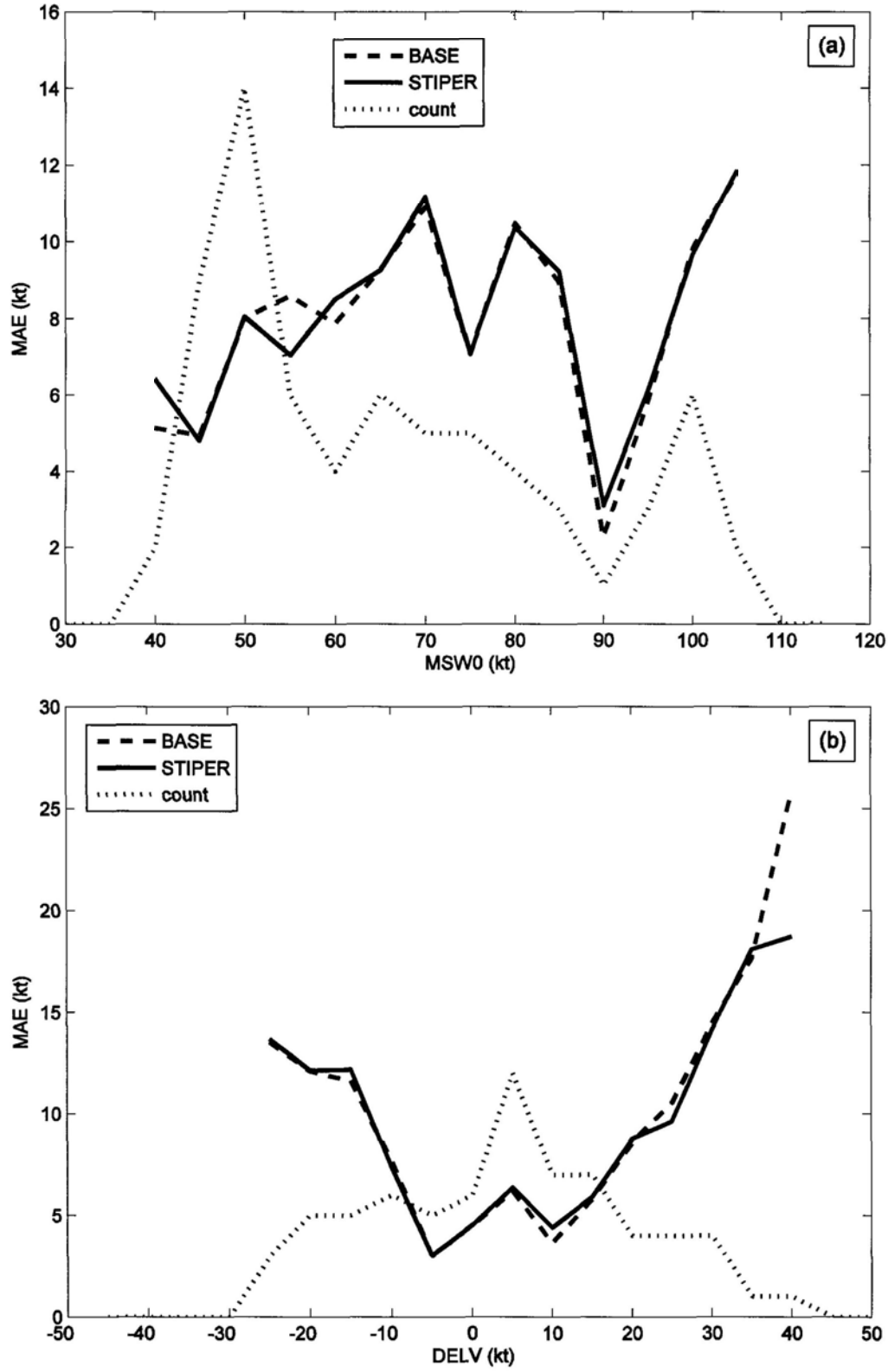

Figure 4.3 BASE model and STIPER model mean absolute error (MAE) (a) stratified by best-track initial intensity (MWS0) in 5-kt bins for 24-h forecasts and (b) stratified by 24-h intensity change (DELV) in 5-kt bins. Lower values of mean absolute error represent better forecasts. Dotted lines represent the number of valid observations within a particular bin.

4.2.2 48-h intensity prediction

a. Model interpretation

The important predictors in STIPER selected from the potential predictor pool for 48-h intensity forecast contain MWS0, DMWS, JDAY, LAT, POT, RHLO, RHHI, REFC, SHR, USHR, SLHF and IRR (Table 4.8). There are around 700 samples for 48-h model training. The CLIPER models for 48-h intensity prediction have the same predictors as the one of 24-h version, and the BASE models and the STIPER models for 48-h intensity forecast have two more predictors (REFC and USHR) than those for 24-h version of STIPER.

The predictors related to SST and vertical wind shear (POT and SHR) are most important. The contribution of the persistence term DMWS is weaker than 24-h version of STIPER since the persistence variable is more important for shorter-term forecasts. Relative to 24-h intensity change, initial SLHF has lower impact on 48-h intensity change, however, the other satellite-based predictor IRR has larger normalized regression coefficient, suggesting that inner-core latent heating plays a more important role in 48-h intensification process.

The positive regression coefficients associated with USHR indicate that westerly shear (and westerly 200-hPa winds) is favorable for TC intensification. This positive relationship is consistent with the finding in STIPS, but different from the negative relationships found in the east Pacific Basin and the Atlantic Basin (DeMaria and Kaplan 1994a; DeMaria and Kaplan 1999). There are two possible explanations for this: 1) The accompanying westerly winds of tropical upper tropospheric troughs

(TUTTs; Sadler 1976, 1978) or mid-latitude troughs on the north side of TCs weaken the easterly shear normally observed over the storm center and result in weak westerlies within the 200–800-km annulus where the vertical wind shear is computed. This mechanism is likely more effective in the western North Pacific Basin where most of the tropical cyclogenesis are associated with monsoon troughs (Zehr 1992; Briegel and Frank 1997; Ritchie and Holland 1999), which often has intense upper-level easterlies (Wang and Xu 1997) that inhibit storm intensification. 2) An empirical observation that typhoon peak intensity is often at or near recurvature (Riehl 1972; Evans and McKinley 1998; Knaff 2009).

The positive relationships between the momentum flux predictor REFC and 48-h intensity change is expected, since REFC tends to be large when a TC is moving towards an upper-level trough in the midlatitude westerlies or interacting with a upper-level cold lows in low latitudes, and the large REFC that makes the upper-level circulation more cyclonic could result in the increase of the storm intensification rate (Holland and Merrill 1984; Molinari and Vollaro 1989; DeMaria et al. 1993).

b. Dependent model statistics

Table 4.9 shows mean absolute error (MAE) and percent variance explained (R^2) of CLIPER, BASE, and STIPER estimated from dependent data for 48-h model training. The CLIPER models have the largest MAE of about 10.7 kt and smallest R^2 of about 54%, the STIPER models have the smallest MAE of about 9.3 kt and the

largest R^2 of about 64%, and the BASE models have MAE and R^2 between the other two kinds of models. The results indicate that the addition of synoptic predictors can enhance the model capability of intensity prediction and the inclusion of two satellite-based predictors on heat source can improve the capability further.

Table 4.8 STIPER predictor normalized regression coefficients with explained variances (R^2, %) statistic at the bottom in different verification years for 48-h forecasts. The predictors are listed on the left side of the table and the verification years are listed at the top with the number of dependent samples (N) used to develop the equation shown in parentheses.

Year (N) / Predictor	2000 (759)	2001 (736)	2002 (702)	2003 (726)	2004 (684)	2005 (738)	2006 (744)	2007 (770)	2008 (837)
1) MWS0	–0.11	–0.16	–0.11	–0.09	–0.16	–0.13	–0.12	–0.16	–0.13
2) DMWS	0.14	0.16	0.15	0.15	0.15	0.15	0.16	0.15	0.15
3) JDAY	–0.15	–0.13	–0.17	–0.13	–0.16	–0.13	–0.13	–0.15	–0.14
4) LAT	–0.13	–0.07	–0.12	–0.11	–0.16	–0.11	–0.09	–0.13	–0.11
5) POT	0.56	0.50	0.55	0.57	0.51	0.53	0.53	0.51	0.53
6) RHLO	0.05	0.01	–0.00	0.02	0.02	0.01	0.02	0.04	0.02
7) RHHI	–0.05	–0.02	0.03	0.01	–0.04	0.02	–0.01	–0.05	–0.01
8) REFC	0.09	0.12	0.11	0.06	0.11	0.08	0.10	0.10	0.10
9) SHR	–0.16	–0.21	–0.19	–0.20	–0.22	–0.18	–0.18	–0.20	–0.19
10) USHR	0.08	0.09	0.13	0.09	0.12	0.11	0.08	0.10	0.10
11) SLHF	0.02	0.03	–0.01	–0.00	–0.01	–0.00	0.02	0.02	0.01
12) IRR	0.09	0.13	0.11	0.12	0.09	0.13	0.10	0.10	0.10

Table 4.9 Developmental statistics of CLIPER, BASE and STIPER models for 48-h forecast. Mean absolute error of the model estimate and percent variance explained (R^2) are shown.

Year	CLIPER		BASE		STIPER	
	MAE	R^2	MAE	R^2	MAE	R^2
2000	10.61	54.8	9.37	64.4	9.28	65.1
2001	10.86	52.3	9.56	62.4	9.40	63.8
2002	10.73	53.6	9.46	63.8	9.32	64.6
2003	10.78	51.5	9.55	61.4	9.46	62.4
2004	10.49	54.8	9.19	65.3	9.12	65.8
2005	10.78	52.4	9.56	61.7	9.41	62.9
2006	10.75	52.1	9.53	61.8	9.44	62.6
2007	10.28	55.7	9.21	63.6	9.14	64.4
2008	10.67	53.3	9.45	62.9	9.35	63.8

c. Model evaluation

The 48-h models are evaluated in this section. Table 4.10 shows MAE and R^2 of CLIPER, BASE and STIPER 48-h forecasts for different verification years. The best model for every verification year is indicated by bold italics. The numbers of samples used to verify are also shown. There are 40 samples for verification year 2008 and up to 153 samples for verification year 2004. Both of the BASE and STIPER models can provide better forecasts than CLIPER. Among 9 verification cases, STIPER has the lowest MAE and the highest R^2 except for 2001 and 2005. The MAEs of the STIPER models are 1%–3% smaller than those of the corresponding BASE models for the 7 cases. As a result, STIPER is skillful for 48-h intensity forecast and the inclusion of satellite-based predictors SLHF and IRR provides 1%–3% improvement

compared with the model without satellite information.

Table 4.10 Mean absolute errors (MAE, kt) and percent variances explained (R^2) for CLIPER, BASE, and STIPER 48-h forecasts in different verification years with number of samples (N). The best model for each verification year is indicated in bold italics.

Year	N	CLIPER		BASE		STIPER	
		MAE	R^2	MAE	R^2	MAE	R^2
2000	78	10.92	33.3	10.21	40.9	***9.89***	***43.9***
2001	101	9.37	60.9	***8.93***	***66.7***	9.42	62.1
2002	135	10.42	50.9	9.73	55.6	***9.68***	***56.8***
2003	111	10.03	64.2	8.86	70.9	***8.62***	***71.0***
2004	153	11.62	45.8	10.92	50.1	***10.55***	***52.2***
2005	99	10.00	60.5	***8.87***	***70.9***	9.20	69.0
2006	93	10.35	61.4	9.09	70.1	***8.92***	***71.3***
2007	67	14.78	31.0	11.97	55.0	***11.56***	***56.9***
2008	40	12.57	59.3	12.24	62.1	***11.85***	***63.9***

4.2.3 72-h intensity prediction

a. Model interpretation

MWS0, DMWS, JDAY, LAT, LON, POT, RHHI, REFC, SHR, USHR, SLHF and IRR are selected as the important predictors in STIPER from the potential predictor pool for 72-h intensity forecast contain (Table 4.11). Around 500 samples are utilized for 72-h model training. The CLIPER models for 72-h intensity prediction have one more predictor (LON) than the 24-h and 48-h versions. In addition to LON, the BASE models and the STIPER models for 72-h intensity forecast also have two more predictors (REFC and USHR) than those for 24-h version of STIPER, while RHLO

is eliminated in 72-h models.

Table 4.11 STIPER predictor normalized regression coefficients with explained variances (R^2, %) statistic at the bottom in different verification years for 72-h forecasts. The predictors are listed on the left side of the table and the verification years are listed at the top with the number of dependent samples (N) used to develop the equation shown in parentheses.

Year (N) / Predictor	2000 (522)	2001 (505)	2002 (470)	2003 (489)	2004 (464)	2005 (509)	2006 (509)	2007 (536)	2008 (572)
1) MWS0	–0.13	–0.19	–0.21	–0.24	–0.24	–0.22	–0.20	–0.26	–0.21
2) DMWS	0.10	0.12	0.09	0.09	0.09	0.09	0.11	0.09	0.10
3) JDAY	–0.15	–0.13	–0.16	–0.16	–0.16	–0.11	–0.13	–0.14	–0.14
4) LAT	–0.11	–0.02	–0.09	–0.14	–0.14	–0.08	–0.08	–0.11	–0.09
5) LON	0.05	0.01	0.07	0.06	0.06	0.07	0.03	0.04	0.05
6) POT	0.64	0.57	0.53	0.52	0.52	0.53	0.54	0.49	0.55
7) RHHI	–0.04	–0.01	0.02	–0.06	–0.06	0.02	–0.01	–0.02	–0.01
8) REFC	0.08	0.14	0.12	0.13	0.13	0.08	0.11	0.10	0.11
9) SHR	–0.12	–0.19	–0.16	–0.21	–0.21	–0.15	–0.16	–0.17	–0.17
10) USHR	0.06	0.09	0.08	0.11	0.11	0.07	0.06	0.06	0.07
11) SLHF	0.01	0.02	0.01	–0.03	–0.03	0.01	0.02	0.01	0.01
12) IRR	0.12	0.13	0.12	0.11	0.11	0.15	0.12	0.12	0.13

The predictors related to SST and vertical wind shear (POT and SHR) and the initial intensity (MWS0) are the most important, while the persistence term DMWS is less important than 24-h version and 48-h version of STIPER. Just as 48-h intensity change, initial SLHF also has lower impact on 72-h intensity change than the 24-h case. The other satellite-based predictor IRR has comparable normalized

regression coefficient as 48-h models, suggesting that inner-core latent heating plays almost the same role for 48-h and 72-h intensification process.

The positive regression coefficients associated with USHR and REFC indicate that westerly shear (and westerly 200-hPa winds) and large upper-level momentum flux is also favorable for TC intensification in 72 h. The positive regression coefficient of LON indicates that the intensification rate would be higher if the storms are at higher longitude. This may be because those storms travel longer over the ocean and could obtain more heat from the underlying warm water.

Table 4.12 Developmental statistics of CLIPER, BASE and STIPER models for 72-h forecast. Mean absolute error of the model estimate and percent variance explained (R^2) are shown.

Year	CLIPER		BASE		STIPER	
	MAE	R^2	MAE	R^2	MAE	R^2
2000	11.15	63.6	9.64	72.9	9.52	73.9
2001	11.33	60.5	9.83	70.4	9.65	71.8
2002	11.56	62.2	10.07	71.3	9.86	72.4
2003	11.22	59.6	10.05	68.2	9.91	69.5
2004	11.03	63.7	9.45	73.8	9.27	74.8
2005	11.42	60.7	10.13	69.1	9.91	70.8
2006	11.36	60.4	9.99	69.1	9.89	70.3
2007	10.85	63.9	9.75	70.8	9.61	71.8
2008	11.26	61.7	9.92	70.5	9.76	71.7

b. Dependent model statistics

Table 4.12 shows mean absolute error (MAE) and percent variance explained (R^2)

of CLIPER, BASE, and STIPER estimated from dependent data for 72-h model training. The CLIPER models have the largest MAE of about 11.3 kt and smallest R^2 of about 62%, the STIPER models have the smallest MAE of about 9.8 kt and the largest R^2 of about 72%, and the BASE models have MAE and R^2 between the other two kinds of models. The results indicate that the addition of synoptic predictors can enhance the model capability of intensity prediction and the inclusion of two satellite-based predictors on heat source can improve the capability further.

Table 4.13 Mean absolute errors (MAE, kt) and percent variances explained (R^2) for CLIPER, BASE, and STIPER 72-h forecasts in different verification years with number of samples (N). The best model for each verification year is indicated in bold italics.

Year	N	CLIPER		BASE		STIPER	
		MAE	R^2	MAE	R^2	MAE	R^2
2000	50	***11.99***	***22.4***	12.43	17.8	12.16	21.1
2001	67	***10.76***	***69.2***	11.34	68.7	11.50	68.3
2002	102	10.48	55.9	9.61	62.8	***9.56***	***65.2***
2003	83	11.82	70.4	9.62	80.3	***9.45***	***80.6***
2004	108	13.00	51.0	12.45	51.4	***12.17***	***53.1***
2005	63	10.62	68.7	***8.79***	***79.8***	9.51	76.9
2006	63	10.82	70.2	9.57	79.3	***8.95***	***80.8***
2007	36	16.11	26.0	12.08	63.9	***11.44***	***67.8***
2008	26	***9.60***	***67.5***	9.64	67.1	11.58	54.5

There is an increase of variances explained as a function of time from 24 h to 72 h. This increase does not represent an enhancement in model skill at longer forecast times. Instead, it simply reflects that the variability of intensity change increases as a

function of time.

c. Model evaluation

The evaluation results of 72-h CLIPER, BASE and STIPER models are shown in Table 4.13. The best model for every verification year is indicated by bold italics. The numbers of samples used to verify are also shown. There are 26 samples for verification year 2008 and up to 108 samples for verification year 2004. Among the 9 verification cases, 5 STIPER models, 3 CLIPER models and 1 BASE model provide the best forecasts. The MAEs of the STIPER models are 1%–6% smaller than those of the corresponding BASE models for 5 cases. As a result, STIPER is skillful for 72-h intensity forecast and the inclusion of satellite-based predictors SLHF and IRR provides 1%–6% improvement compared with the model without satellite information. However, the 72-h models are less stable than shorter-term forecast models for 24-h and 48-h intensity prediction.

The increasing MAEs with the longer forecast time intervals (as shown in Table 4.6, Table 4.10 and Table 4.13) is primarily due to the inclusion of some predictors related to CLIPER, which have more impact on intensity change in shorter time periods.

4.3 Neural network models

The nonlinear response of the linear regression models suggests the use of non-linear models can be beneficial. The back-propagation neural network (NN)

models for 24-h, 48-h and 72-h intensity prediction (NN24, NN48, and NN72) are developed using the same predictors from the linear regression model STIPER. The input layers of NN24, NN48, and NN72 models contain ten neurons, twelve neurons, and twelve neurons, respectively, which correspond to those predictors used in the linear regression forecasting models for the same time period. All of the NN models have seven neurons in the hidden layers and one neuron in the output layers. The only neuron in the output layers corresponds to the predictand (24-h, 48-h or 72-h intensity change). The log-sigmoid transfer function is selected from the input layer to the hidden layer and the linear transfer function is used from the hidden layer to the output layer in all of above NN models. Same as linear regression models, the NN models are developed by using 8-year data samples for training and 1-year data samples for verification.

Table 4.14 indicates the verification statistics of NN24, NN48, and NN72 models. The mean absolute errors of NN24 model range from 5.97 kt in 2001 to 8.04 kt in 2007. The mean absolute errors of NN48 model are larger than those of NN24 model; they range from 7.81 kt in 2003 to 10.45 kt in 2007. Surprisingly, NN72 model has smaller mean absolute error than NN48 model except for 2000, 2001 and 2004. Figure 4.4, Figure 4.5 and Figure 4.6 offer us the direct comparison of the three linear regression models (CLIPER, BASE, and STIPER) and the NN models at three forecasting intervals (24 h, 48 h, and 72 h) in the nine verification years from 2000 to 2008.

Table 4.14 Mean absolute errors (MAE, kt) and percent variances explained (R^2) of neural network modes (NN24, NN48, and NN72) for 24-h, 48-h, and 72-h intensity forecasts in different verification years.

Year	NN24		NN48		NN72	
	MAE	R^2	MAE	R^2	MAE	R^2
2000	6.02	47.2	8.29	53.6	10.03	52.6
2001	5.97	62.7	8.10	70.8	9.61	74.0
2002	6.27	55.9	8.43	62.9	8.23	72.8
2003	6.21	58.8	7.81	74.4	7.79	83.0
2004	6.95	51.1	9.13	61.9	10.26	62.5
2005	6.91	57.2	8.71	69.3	8.26	81.3
2006	6.72	59.0	8.52	73.3	8.51	80.0
2007	8.04	59.1	10.45	63.6	8.72	74.4
2008	7.21	67.2	9.78	72.7	8.70	75.5

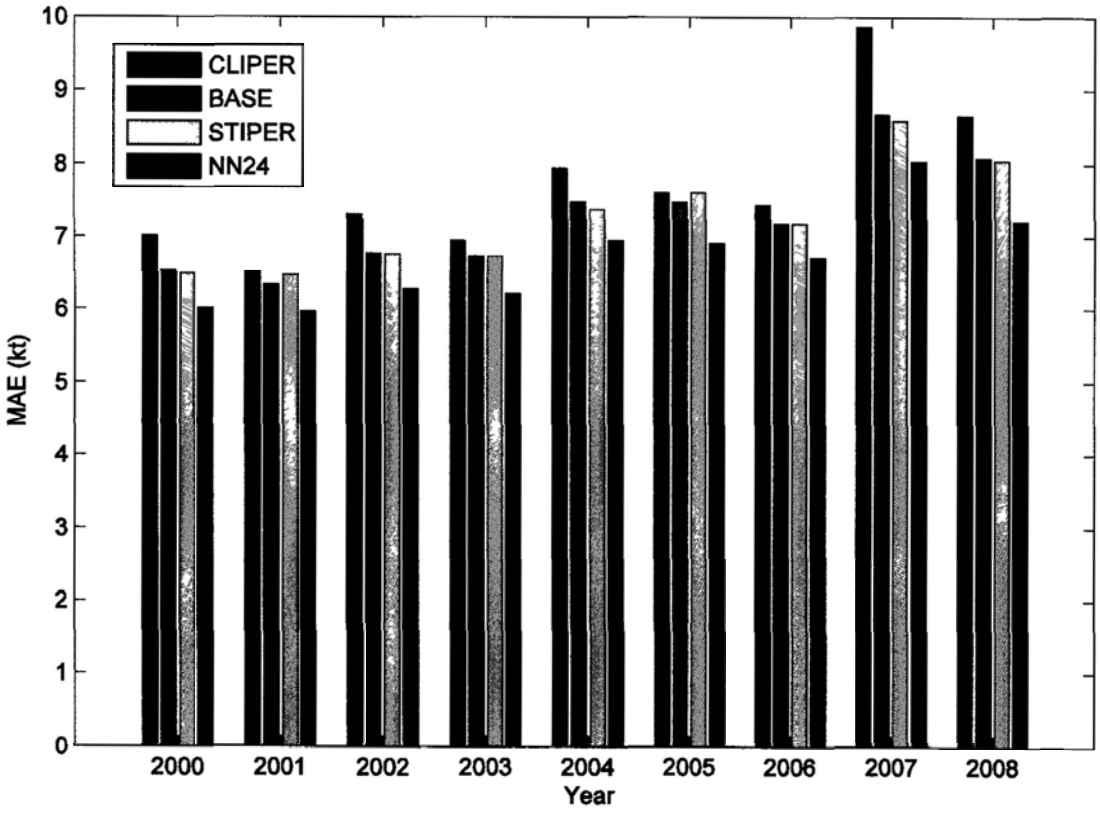

Figure 4.4 The mean absolute errors (MAE, kt) of four regression models (CLIPER, BASE, STIPER, and NN24) in different verification years at 24-h forecast time.

For the 48-h forecasts (Figure 4.5), the NN48 model has 4–17% improvement compared to the STIPER model and 14–29% improvement compared to the CLIPER model.

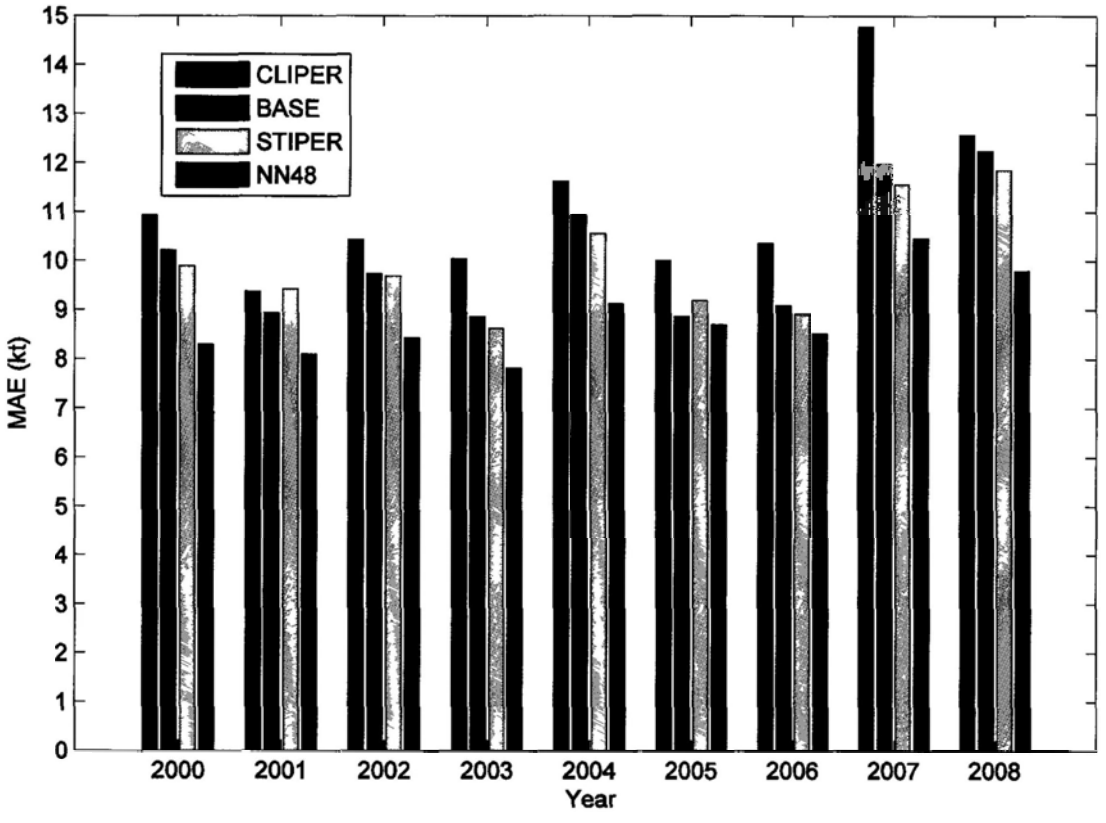

Figure 4.5 The mean absolute errors (MAE, kt) of four regression models (CLIPER, BASE, STIPER, and NN48) in different verification years at 48-h forecast time.

At 72-h forecast time (Figure 4.6), the NN72 model 6–28% improvement compared to the STIPER model and 9–46% improvement compared to the CLIPER model.

Figure 4.7 indicates the scatter plots of NN24 predicted 24-h intensity change as well as observed 24-h intensity change for dependent training samples during period 2000–2007 and independent verification samples in 2008, STIPER results are also

shown for comparison. Generally, NN24 has lower absolute errors both for the developmental samples and the verification samples than STIPER. The mean absolute errors are then stratified by initial TC intensity and 24-h intensity change of NN24 model and the 24-h STIPER model in the verification year 2008 (Figure 4.8). It is indicated that the NN24 model outperforms the 24-h STIPER model almost in all the TC stages and intensity change bins. The largest error reduction of NN24 model occurs for the rapidly intensifying or rapidly decaying storms, especially for the sample intensifying by 40 kt, the forecast error decreases by 7 kt.

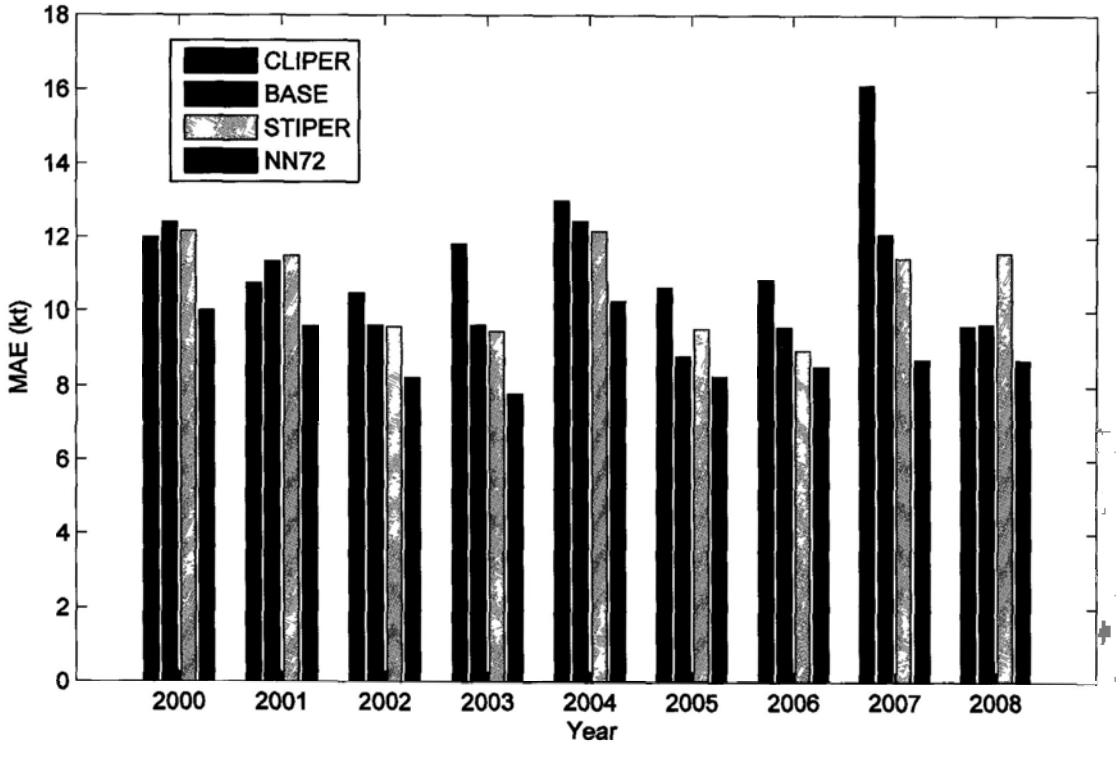

Figure 4.6 The mean absolute errors (MAE, kt) of four regression models (CLIPER, BASE, STIPER, and NN72) in different verification years at 72-h forecast time.

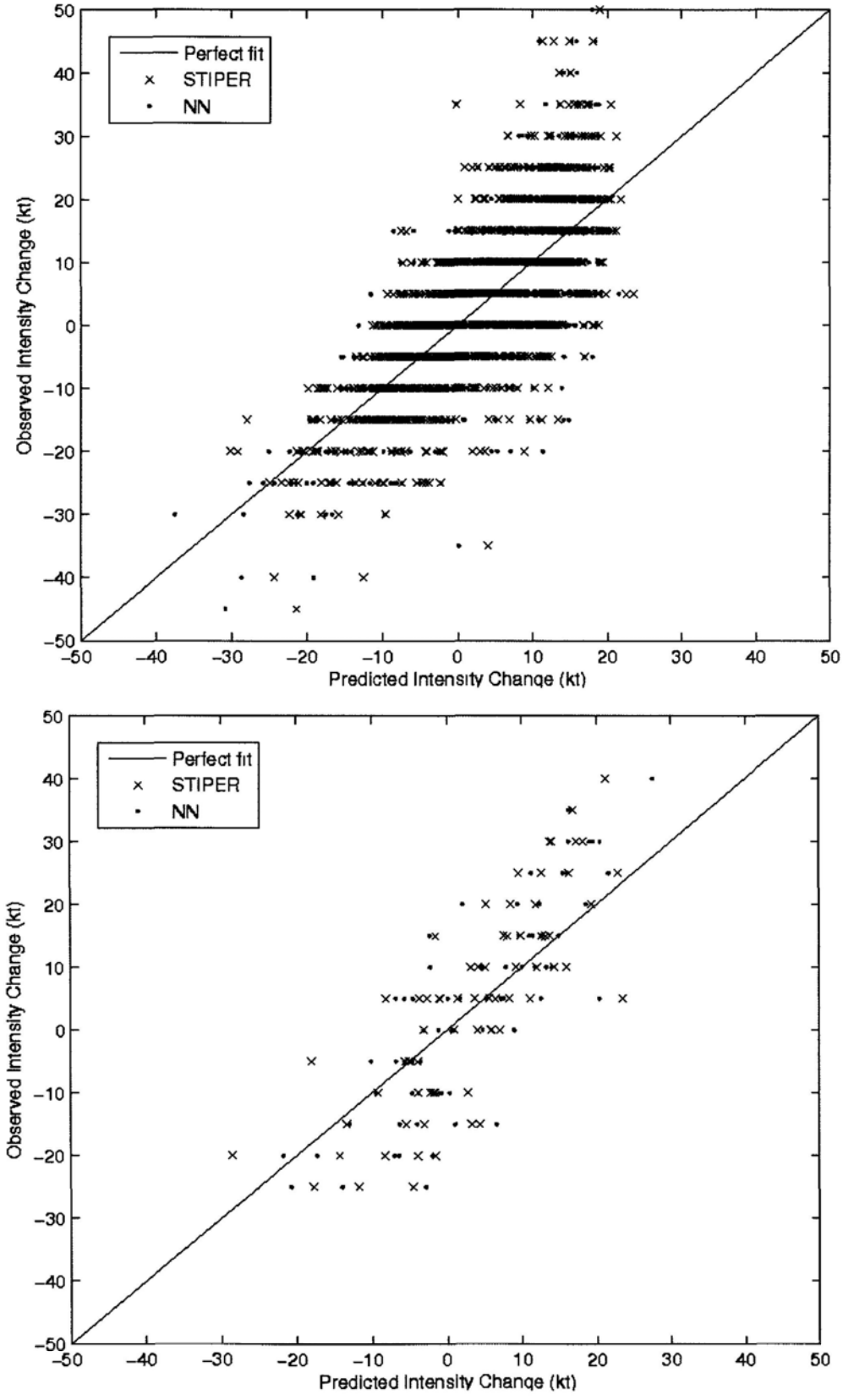

Figure 4.7 Scatter plots of STIPER and NN24 predicted 24-h intensity change versus observed 24-h intensity change for (a) dependent training samples during 2000–2007, (b) independent verification samples in 2008.

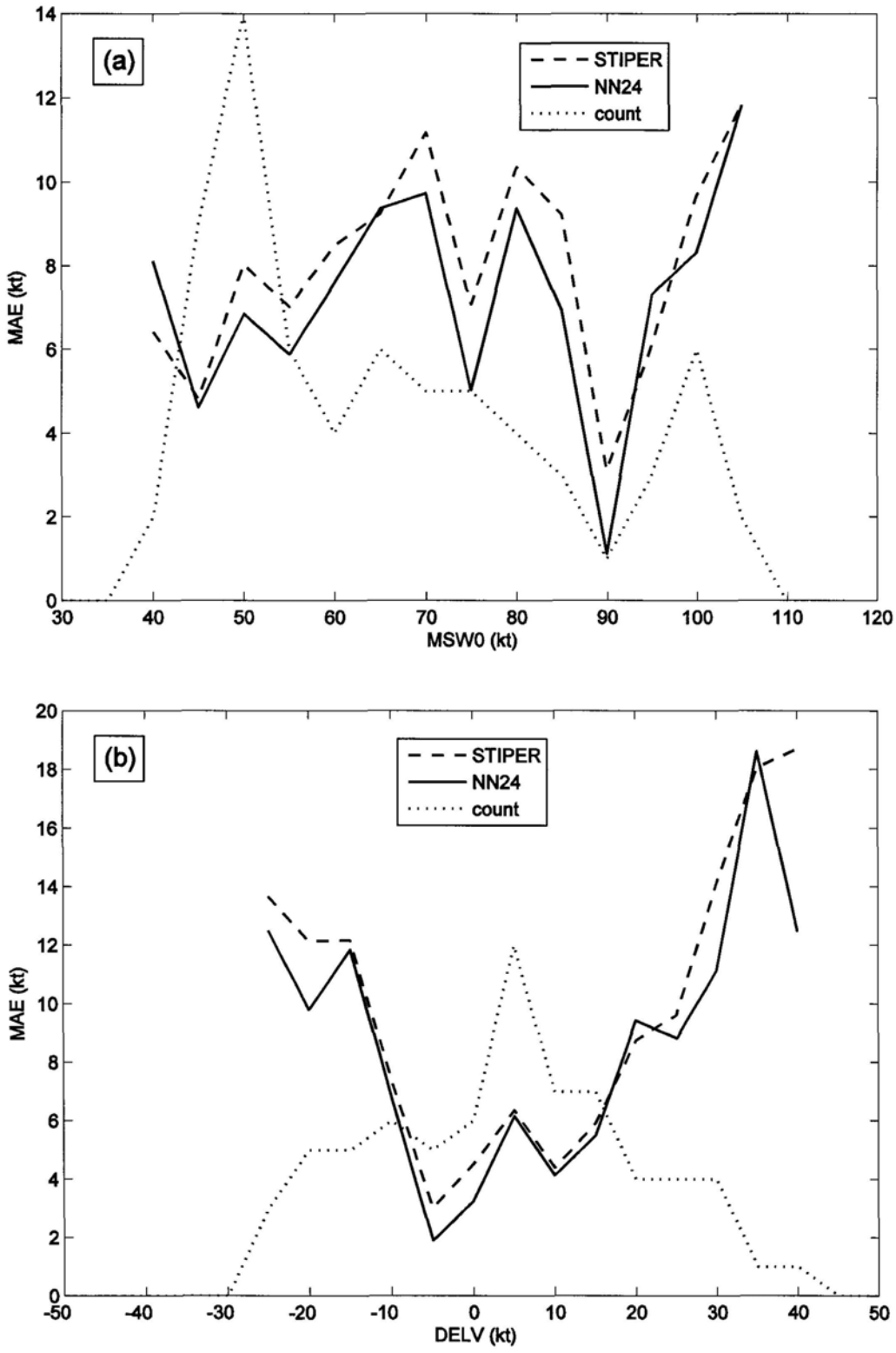

Figure 4.8 NN24 model and STIPER model mean absolute error (MAE) (a) stratified by best-track initial intensity (MWS0) in 5-kt bins for 24-h forecasts and (b) stratified by 24-h intensity change (DELV) in 5-kt bins. Lower values of mean absolute error represent better forecasts. Dotted lines represent the number of valid observations within a particular bin.

The NN models are clearly superior to the corresponding linear regression models. This is probably because the NN models are constructed using artificial intelligence nonlinear fitting, which has capabilities of strong nonlinear mapping and self-adaptation learning by including nonlinear transfer function and therefore better captures the nonlinear evolutionary characteristics of TC intensity.

4.4 Summary

A new maximum potential intensity equation is derived using TMI OI sea surface temperature data with high temporal and spatial resolution (daily and a quarter degree). This equation together with environmental information obtained from NCEP GFS FNL analysis, best track taken from RSMC Tokyo and SLHF and IRR derived from satellite data are then utilized to develop multiple linear regression models and neural network models for western North Pacific TC intensity forecasting at 24-h, 48-h, and 72-h intervals.

Compared to the multiple linear regression models (BASE) with climatology, persistence and environmental predictors only, the linear regression models that include additional satellite-based SLHF and IRR (STIPER) provides 1–3% improvement in 24-h and 48-h forecasting and 1–6% improvement in 72-h forecasting. The largest improvement of the satellite-enhanced STIPER model occurs for those rapidly intensifying storms.

The neural network (NN) models developed using the same predictors as those used in the STIPER models outperform the STIPER models. The improvement is up

to 10%, 17%, and 28% at 24-h, 48-h, and 72-h forecast time, respectively. The error reduction exists for all the TC stages and intensity change magnitudes, and forecasts of the rapidly intensifying and rapidly decaying storms have the largest improvement. If compared to the control model CLIPER, the neural network models can provide up to 19%, 29%, and 46% reduction in MAE at 24-h, 48-h, and 72-h forecast time, respectively.

CHAPTER 5 Typhoon Rapid Intensification Forecasting Using Logistic Regression and Neural Networks

Rapid intensification (RI) of TCs is the most interesting and the most important part. Predicting TC rapid intensification is a challenge, since rapidly intensifying storms contribute the major error source in the intensity forecasting models as mentioned in chapter 4 as well as in the previous studies (Blackerby 2005; Elsberry et al. 2007).

Some attempts to forecast RI of the Atlantic and Eastern Pacific TCs have been made. Kaplan and DeMaria (2003) developed a simple RI index to estimate RI probability over the succeeding 24 h for Atlantic hurricanes by comparing the parameters with the corresponding threshold values. This index with 5 predictors provided up to 41% accuracy of RI detection, i.e., 41 RI events took place among 100 events which satisfied the corresponding threshold values of the 5 predictors. Yang et al. (2007, 2008) applied the association rule in data mining techniques (Agrawal et al. 1993) to the same dataset used in Kaplan and DeMaria's (2003) analysis. They found that a combination of the following attributes, such as the position of the TC being at a high latitude and low longitude, the TC being in an intensification phase, with an initial intensity far away from the maximum potential intensity, high steering layer value, and low relative eddy flux convergence offers a high RI probability of detection of 86%. While the combination of these attributes is a sufficient but not necessary condition for the occurrence of RI, and only a small

proportion of all the RI events take place under these conditions, hence a large number of RI events would be missed.

As a follow-up study, Kaplan et al. (2010) used more a sophisticated linear discriminant analysis method (Wilks 2006) to develop a revised RI index and extended the study area to include the eastern North Pacific. Their verification results showed a probability of detection (POD) of up to 59% and 73%, however, a large false alarm ratio (FAR) as high as 85% and 79% for the 2006 and 2007 hurricane seasons was also noted.

Logistic regression is widely used for categorical prediction, whose outcome is the probability of occurrence of an event. The difference between linear discriminant analysis and logistic regression is that in linear discriminant analysis, the predictors are assumed to be normally distributed, whereas in logistic regression, no assumption about the distribution is made. Thus, logistic regression seems to be more robust. A comparison study of several methodologies for probabilistic quantitative precipitation forecasts (Applequist et al. 2002) showed logistic regression performed better than other models such as linear regression, linear discriminant analysis, neural networks, and a classifier system.

In this chapter, we will focus on the prediction of rapid intensification of TCs. As such, a binary logistic regression model (LRRI) and a neural network model (NNRI) to forecast RI of TCs over the western North Pacific will be developed and the results will be compared to models developed for the Atlantic and eastern Pacific ocean.

5.1 Model development

RI of TCs, as defined in chapter 3, refers to over-water samples with minimum central pressure fall in excess of 20 hPa over a 24-h period. The rest of the over-water samples are non-RI samples. The value of the dependent variable (Y, predictand) is 0 or 1, where the dependent variables of RI samples are given as 1 and the dependent variables of non-RI samples are given as 0 (see equation 2.4).

To solve the multicollinearity problem, a forward logistic stepwise method is utilized to select significant predictors from the same potential predictor pool (see Table 4.1). The significance level for a predictor to enter into the model is 0.01 and the significance level for a predictor to remove from the model is 0.05. The procedure results in five significant predictors (DMWS, POT, RHLO, REFC, and SHR) in the final LRRI model.

The data over the period 2000–2008 are divided into two parts: data from 2000 to 2007 that contains 1176 samples are used as training set and data in 2008 with 64 samples are used as the verification set. The regression coefficients and t-statistics of the LRRI model are shown in Table 5.1. The regression coefficients associated with the predictors are consistent with their physical reasoning. The TC with higher intensification rate in the previous 12 h and initial intensity further from maximum potential intensity, which is under the environment of higher lower-level relative humidity, larger upper-level momentum flux, and less vertical wind shear, is more likely to intensify rapidly. t-statistics indicate that the persistence term (DMWS), intensification potential (POT), and vertical wind shear (SHR) are the most important

predictors.

Table 5.1 LRRI predictor regression coefficients. The predictors are listed on the left side of the table. 1176 dependent samples are used to develop the model.

Predictor	Regression coefficient	t-statistics
Intercept	–4.57	–2.45
1) DMWS	0.13	9.05
2) POT	0.03	6.47
3) RHLO	0.05	1.96
4) REFC	–0.04	–2.90
5) SHR	–0.19	–4.81

The five predictors aforementioned are also used to develop the NNRI model, which has five neurons in input layer, five neurons in hidden layer and one neuron in output layer. The log-sigmoid transfer function is used from the input layer to the hidden layer and the tan-sigmoid transfer function is used from the hidden layer to the output layer. This combination of transfer functions allows the NNRI model output between 0 and 1 as the LRRI model, the output of the NNRI and LRRI models represent the probability of RI.

5.2 Model verification in 2008 typhoon season

In line with the earlier works using logistic regression, a threshold probability 0.5 is used for both of the LRRI and NNRI models. That is to say, a RI event is predicted if the probability of an event output by the model exceeds 0.5, the said probability

that is smaller than 0.5 indicates a non-RI event. The 2 × 2 contingency tables are employed to assess the performance of the LRRI and NNRI models in 2008.

Table 5.2 A 2 × 2 contingency table of the LRRI model forecasts in 2008. Threshold probability is set at 0.5.

Rapid intensification or not		Observed	
		Yes	No
Forecast	Yes	7	1
	No	9	53

Table 5.3 A 2 × 2 contingency table of the NNRI model forecasts in 2008. Threshold probability is set at 0.5.

Rapid intensification or not		Observed	
		Yes	No
Forecast	Yes	8	1
	No	8	53

Table 5.2 and Table 5.3 show the 2 × 2 contingency tables of the LRRI and NNRI models, respectively. The resulting skill scores of the LRRI and NNRI model performance in 2008 are indicated in Table 5.4. There are a total of 16 RI events and 54 non-RI events in 2008. The LRRI (NNRI) model makes 7 (8) forecasts of RI events and 9 (8) RI events are missed. The forecasts of non-RI events are quite good, 53 non-RI events are predicted in the both models. The number of false alarms from the both models is only 1. Consequently, the NNRI model is more skillful than the LRRI model. It is worthy to note that FAR of our models is much lower than that of the model developed by Kaplan et al. (2010).

Table 5.4 Skill scores of the LRRI and NNRI model. Probability of detection (POD), false alarm ratio (FAR), critical success index (CSI), and equitable threat score (ETS) are used to evaluate the model performance in 2008. Threshold probability is set at 0.5.

	LRRI	NNRI
POD	0.44	0.50
FAR	0.13	0.11
CSI	0.41	0.47
ETS	0.34	0.40

Table 5.5 Impact of varying threshold probability on the LRRI model.

Skill score / Threshold probability	POD	FAR	CSI	ETS
0.45	0.50	0.11	0.47	0.40
0.4	0.69	0.08	0.64	0.58
0.35	0.69	0.21	0.58	0.49
0.3	0.69	0.31	0.52	0.42

The cases are examined further. It is found that the LRRI and NNRI models issue false alarms for the same event, and there are 6 cases of detection of RI events by both the LRRI and NNRI model. If we combine both models, i.e., once a forecast of an event is a RI event in any of the both models, this forecast is RI. By this manner 9 out of 16 RI events are forecasted.

Table 5.6 Impact of varying threshold probability on the NNRI model.

Skill score / Threshold probability	POD	FAR	CSI	ETS
0.45	0.56	0.10	0.53	0.46
0.4	0.75	0.14	0.67	0.59
0.35	0.81	0.13	0.72	0.66
0.3	0.94	0.29	0.68	0.59

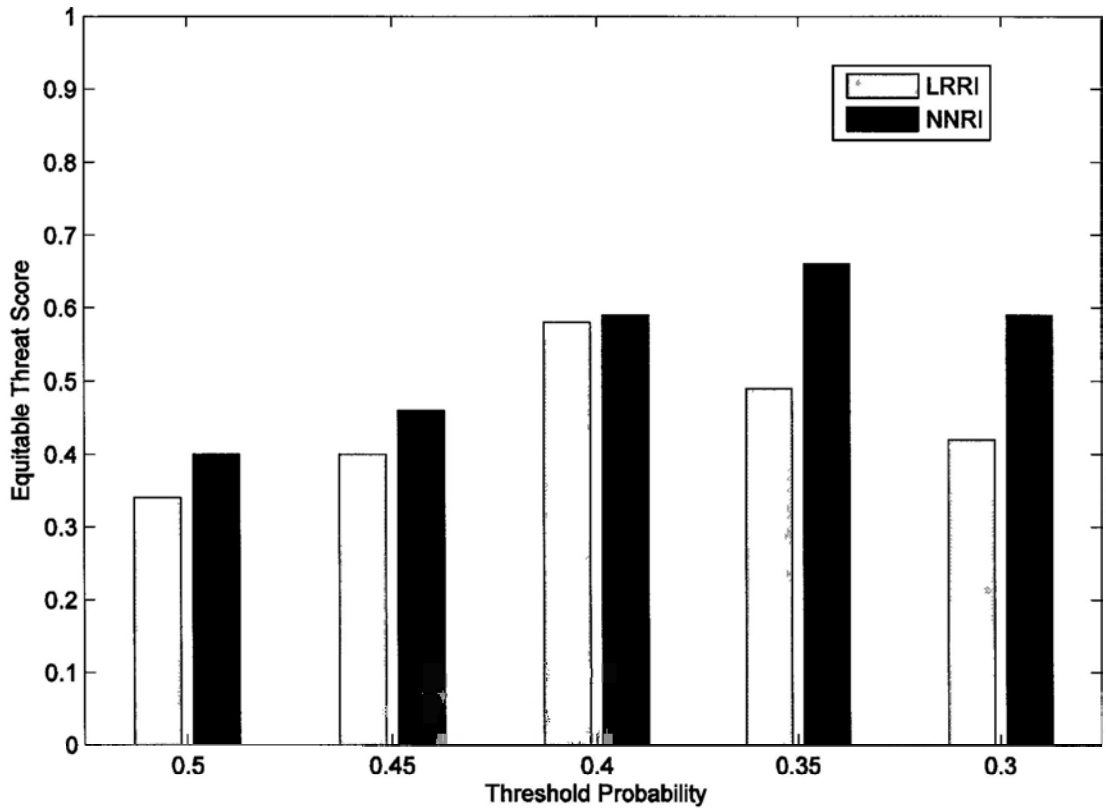

Figure 5.1 Equitable threat scores as a function of threshold probability for both LRRI and NNRI models.

The sensitivity of the prediction to varying threshold probability is examined. The resulting skill scores are shown in Table 5.5 for the LRRI model and Table 5.6 for the NNRI model. The NNRI model outperforms the LRRI model for all three values of threshold probability. As the threshold probability decreases from 0.5 to 0.4, POD,

CSI and ETS of the both models increase and FAR of the both models are nearly the same, indicating that the use of lower threshold probability can enhance the skill of RI detection. While the threshold probability decreases from 0.4 to 0.3, for the LRRI model POD remains the same and FAR becomes much larger, for the NNRI model both of POD and FAR increase.

The ETS is the more appropriate statistics to use since the proportion of RI is much less than 0.5. Figure 5.1 shows the ETS as a function of threshold probability for both LRRI and NNRI models. ETS is the highest when the threshold probability is set at 0.4 (0.35) for the LRRI (NNRI) model, thus 0.4 (0.35) is the optimal threshold probability for RI prediction using logistic regression (neural networks).

5.3 Summary

An attempt is made to predict RI of TCs using logistic regression and neural networks. Five variables (intensity change in the previous 12 h, intensification potential, lower-level relative humidity, eddy flux convergence at 200 hPa, and vertical wind shear) are included in the final set of predictors.

A verification result from 2008 typhoon season shows that the neural network model is superior to the logistic regression model for RI detection. A more satisfactory performance of the LRRI (NNRI) model is observed when the threshold probability is reduced to 0.4 (0.35) instead of the conventional 0.5.

CHAPTER 6 Conclusion and Discussion

6.1 Conclusion

First, OAFlux surface latent heat flux (SLHF) and TMPA rain rate data as well as JMA RSMC Tokyo best track data are used to examine SLHF and rainfall associated with rapidly intensifying western North Pacific tropical cyclones. In this study rapid intensification (RI) of tropical cyclones (TCs) is defined as over-water minimum central pressure fall in excess of 20 hPa over a 24-h period. Composite analysis on the initial (t = 0 h) SLHF and rainfall for four categories classified by moving direction over a 24-h period shows that RI samples are usually associated with an area of relatively high SLHF on the right-hand of TC track and with relatively high rainfall within inner-core regions. The significant difference between initial SLHF of RI and non-RI samples occurs on TCs' pathway, and this significant difference in SLHF is dominated by the air-sea humidity difference. The results suggest the potential usefulness of SLHF and inner-core rain rate (IRR) in the prediction of TC intensity over the western North Pacific.

Second, several linear regression models and neural network models are developed for the western North Pacific TC intensity prediction at 24-h, 48-h, and 72-h intervals using JMA RSMC Tokyo best track, NCEP GFS FNL analysis, TMI OI sea surface temperature (SST), OAFlux SLHF and TMPA rain rate data. A pool of 18 potential predictors contains 6 variables related to climatology and persistence, 10 variables related to atmospheric and oceanic environment, and 2 new satellite-based variables

(SLHF and IRR). The estimation of TC maximum potential intensity (MPI), which is a very important predictor, is improved by using TMI OI SST with higher temporal and spatial resolution. Four types of models are developed, linear regression models with climatology and persistence predictors (CLIPER) as a benchmark, linear regression models with climatology, persistence and environmental predictors (BASE), linear regression models with SLHF and IRR (STIPER) in addition to BASE predictors, and neural network (NN) models with the same predictors as STIPER. Analysis of the resulting models indicates that STIPER produces up to 6% improvement in performance for TC intensity forecasts out to 72 h compared to BASE. Further improvement of NN models over STIPER is up to 28%, and error reduction are found at all the TC stages and intensity changes. The most significant improvement is in forecasts of the rapidly intensifying and rapidly decaying storms.

Finally, for TC RI forecasting, a logistic regression model (LRRI) and a neural network model (NNRI) are developed using the same pool of potential predictors over the period 2000–2007. Five significant predictors include intensity change in the previous 12 h, intensification potential, lower-level relative humidity, eddy flux convergence at 200 hPa, and vertical wind shear. The verification of forecasts in 2008 typhoon season shows that NNRI outperforms LRRI for RI detection. The optimal threshold probabilities for NNRI and LRRI are 0.35 and 0.4, respectively.

6.2 Discussion

6.2.1 Potential for operational use

The ultimate goal of this study is to employ these models for operational forecast. The climatology, persistence and environmental predictors can be derived timely from numerical weather prediction (NWP) model forecast fields and TC track forecast, whereas timely satellite microwave observations of a TC for SLHF, IRR and SST retrieval may not be available. The availability of remote sensing products of IRR and SLHF are needed in real-time or near-real-time applications of these products in the STIPER and NN models.

6.2.2 Additional error source for operational use

All the potential predictors are derived along the TC track using a "perfect prog" approach, where the NCEP analysis and JMA RSMC Tokyo TC best track data are used to develop the statistical models. However, when the models are in operational use, NCEP NWP model forecast are used to compute the predictors along the TC track forecast by JMA RSMC Tokyo. As a result, errors in both the NCEP NWP forecast fields and the JMA RSMC Tokyo track forecast would produce additional intensity forecast errors.

6.2.3 Future work

Further improvement in intensity forecast may come from the use of consensus intensity forecasts (forecasts created by combining output from individual forecasts), as shown by Sampson et al. (2008). Consensus of both track forecasts and NWP forecasts could be tested.

OAFlux SLHF has relatively coarse temporal and spatial resolution (daily and 1

degree). Higher temporal and spatial resolution SLHF may provide a better understanding of TC-ocean interaction. The production in progress of the third version of the NASA/Goddard Space Flight Center Satellite based Surface Fluxes GSSTF3 (Shie et al. 2009) SLHF data with the resolution of 12 hourly and a quarter degree, which is retrieved from a number of satellite datasets, may be potentially used for typhoon forecast.

In the RI forecast, the variables selected are all prognostic variables, i.e. they depend on the prognostic models to provide good estimates of the atmospheric state variables. It might be advantageous to include SLHF since the SLHF is produced as a diagnostic variable in model analyses.

Another way to improve the resolution of SLHF is to retrieve it directly using brightness temperature measurements from TRMM Microwave Imager, as proposed by Lin and Tang (2000) as well as Lin and Fan (2005). These microwave satellite estimates can provide SLHF estimates with spatial and temporal resolutions compatible with the TMPA rainfall estimates and may provide a better estimate of the static predictors in the STIPER and NN models.

BIBLIOGRAPHY

Aberson, S. D., and J. L. Franklin, 1999: Impact on hurricane track and intensity forecasts of GPS dropwindsonde observations from the first-season flights of the NOAA gulfstream-IV Jet Aircraft. *Bull. Amer. Meteor. Soc.,* **80**, 421–427.

Agrawal, R., T. Imielinski, and A. Swami, 1993: Mining association rules between sets of items in large databases, paper presented at 1993 International Conference on Management of Data, Spec. Interest Group on Manage. of Data, Assoc. for Comput. Mach., Washington, D.C. May.

Ali, A. H., 2004: Application of neural network principal components to climate data. *J. Atmos. Oceanic Technol.*, **21**, 149–158.

Applequist, S., G. E. Gahrs, R. L. Pfeffer, and X.-F. Niu, 2002: Comparison of methodologies for probabilistic quantitative precipitation forecasting. *Wea. Forecasting*, **17**, 783–799.

Arkin, P. A., and B. N. Meisner, 1987: The relationship between large-scale convective rainfall and cold cloud over the Western Hemisphere during 1982–84. *Mon. Wea. Rev.*, **115**, 51–74.

Baik, J.-J., and J.-S. Paek, 2000: A neural network model for predicting typhoon intensity. *J. Meteor. Soc. Japan*, **78**, 857–869.

Bender, M., I. Ginis, R. Tuleya, B. Thomas, and T. Marchok, 2007: The operational GFDL coupled hurricane-ocean prediction system and a summary of its performance. *Mon. Wea. Rev.*, **135**, 3965–3989.

Bentamy, A., K. B. Katsaros, A. M. Mestas-Nuñez, W. M. Drennan, E. B. Forde, and H. Roquet, 2003: Satellite estimates of wind seed and latent heat flux over the global oceans. *J. Climate*, **16**, 637–656.

Berg, R., C. Sisko, and M. DeMaria, 2004: High resolution SST in the SHIPS model: Improving operational guidance of tropical cyclone intensity forecasts. Preprints, 26th Conf. on Hurricanes and Tropical Meteorology, Miami, FL, Amer. Meteor. Soc., 536–537.

Black, P. G., E. A. D'asaro, W. M. Drennan, J. R. French, P. P. Niiler, T. B. Sanford, E. J. Terrill, and J. A. Zhang, 2007: Air–sea exchange in hurricanes: Synthesis of observations from the Coupled Boundary Layer Air–Sea Transfer Experiment. *Bull. Amer. Meteor. Soc.*, **88**, 357–374.

Blackerby, J. S., 2005: Accuracy of western North Pacific tropical cyclone intensity guidance. M.S. thesis, Naval Postgraduate School, USA, 107pp.

Bosart, L. F., C. S. Velden, W. E. Bracken, J. Molinari, and P. G. Black, 2000: Environmental influences on the rapid intensification of Hurricane Opal (1995) over the Gulf of Mexico, *Mon. Wea. Rev.*, **128**, 322–352.

Briegel, L. M., and W. M. Frank, 1997: Large-scale influences on tropical cyclogenesis in the western North Pacific. *Mon. Wea. Rev.*, **125**, 1397–1413.

Bulmer, M. G., 1979: Principles of Statistics. New York: Dover Publications, 252 pp.

Burpee R. W., J. L. Franklin, S. J. Lord, R. E. Tuleya, and S. D. Aberson, 1996: The impact of Omega dropwindsondes on operational hurricane track forecast models. *Bull. Amer. Meteor. Soc.*, **77**, 925–933.

Chang, A. T. C., L. S. Chiu, G. R. Liu, and K. H. Wang, 1995: Analysis of 1994 typhoons in the Taiwan region using satellite data. COSPAR Colloquia Series Volume 8, Space Remote Sensing of Subtropical Oceans, 89–96, SRSSO, Taipei, Taiwan, Elsevier Science, 1995.

Charney, J. G., and A. Eliassen, 1964: On the growth of the hurricane depression. *J. Atmos. Sci.*, **21**, 68–75.

Chiu L. S., and Kadem B., 1990: Estimating the exceedance probability of rain rate by logistic regression. *J. Geophys. Res.*, **95**, 2217–2227.

Chou, S.-H., R. Atlas, C.-L. Shie, and J. Ardizzone, 1995: Estimates of surface humidity and latent heat fluxes over oceans from SSM/I data. *Mon. Wea. Rev.*, **123**, 2405-2425.

Chou, S.-H., C.-L. Shie, R. M. Atlas, and J. Ardizzone, 1997, Air-sea fluxes retrieved from special sensor microwave imager data. *J. Geophys. Res.*, **102**, 12706–12726.

Chou, S.-H., E. Nelkin, J. Ardizzone, R. M. Atlas, and C.-L. Shie, 2003: Surface turbulent heat and momentum fluxes over global oceans based on the Goddard satellite retrieval, version 2 (GSSTF2). *J. Climate*, **16**, 3256–3273.

Chu, J.-H., 1994: A regression model for the western North Pacific tropical cyclone intensity forecasts. NRL Memo. Rep. 7541-94-7215, Naval Research Laboratory, 33 pp.

Dasgupta, S., and U. K. De, 2007: Binary logistic regression models for short term prediction of premonsoon convective developments over Kolkata (India), *Int. J. Climatol.*, **27**, 831–836.

Davis, C., W. Wang, S. S. Chen, Y. Chen, K. Corbosiero, M. DeMaria, J. Dudhia, G. Holland, J. Klemp, J. Michalakes, H. Reeves, R. Rotunno, C. Snyder, and Q. Xiao, 2008: Prediction of landfalling hurricanes with the advanced hurricane WRF model. *Mon. Wea. Rev.*, **136**, 1990–2005.

DeCosmo, J., K. B. Katsaros, S. D. Smith, R. J. Anderson, W. A. Oost, K. Bumke, and H. Chadwick, 1996: Air-sea exchange of water vapor and sensible heat: The Humidity Exchange Over the Sea (HEXOS) results. *J. Geophys. Res.*, **101**, 12001–12016.

DeMaria, M., J.-J. Baik, and J. Kaplan, 1993: Upper-level eddy angular momentum fluxes and tropical cyclone intensity change. *J. Atmos. Sci.*, **50**, 1133-1147.

DeMaria, M., and J. Kaplan, 1994a: A statistical hurricane intensity prediction scheme (SHIPS) for the Atlantic basin. *Wea. Forecasting*, **9**, 209–220.

DeMaria, M., and J. Kaplan, 1994b: Sea surface temperature and the maximum intensity of Atlantic tropical cyclones. *J. Climate*, **7**, 1324–1334.

DeMaria, M., and J. Kaplan, 1999: An updated statistical hurricane intensity prediction scheme (SHIPS) for the Atlantic and eastern North Pacific basins. *Wea. Forecasting*, **14**, 326–337.

DeMaria, M., J. A. Knaff, and C. R. Sampson, 2007: Evaluation of long-term trend in tropical cyclone intensity forecasts. *Meteor. Atmos. Phys.*, **97**, 19-28.

DeMaria, M., M. Mainelli, L. K. Shay, J. Knaff, and J. Kaplan, 2005: Further improvements to the updated Statistical Hurricane Intensity Prediction Scheme (SHIPS). *Wea. Forecasting*, **20**, 531–543.

Demuth, H., M. Beale, and M. Hagan, 2009: Neural Network Toolbox User's Guide. The MathWorks, Inc, 901 pp.

Dvorak, V. F., 1982: Tropical cyclone intensity analysis and forecasting from satellite visible or enhanced infrared imagery. NOAA National Environmental Satellite Service, Applications Laboratory Training Notes, 42 pp.

Dvorak, V. F., 1984: Tropical cyclone intensity analysis using satellite data. NOAA Tech. Memo. NESDIS 11, 47 pp.

Elsberry, R. L., T. D. B. Lambert, and M. A. Boothe, 2007: Accuracy of Atlantic and Eastern North Pacific Tropical Cyclone Intensity Forecast Guidance. *Wea. Forecasting*, **22**, 747–762.

Emanuel, K. A., 1986: An air–sea interaction theory for tropical cyclones. Part I: Steady-state maintenance. *J. Atmos. Sci.*, **43**, 585–605.

Emanuel, K. A., 2003, Tropical cyclones. *Annu. Rev. Earth Sci.*, **31**, 75–104.

Evans, J. L., K. McKinley, 1998: Relative timing of tropical storm lifetime maximum intensity and track recurvature. *Meteor. Atmos. Phys.*, **65**, 241-245.

Fairall, C. W., E. F. Bradley, J. E. Hare, A. A. Grachev, and J. B. Edson, 2003: Bulk parameterization on air–sea fluxes: Updates and verification for the COARE algorithm. *J. Climate*, **16**, 571–591.

Fitzpatrick, P. J., 1997: Understanding and forecasting tropical cyclone intensity change with the Typhoon Intensity Prediction Scheme (TIPS). *Wea. Forecasting*, **12**, 826–846.

Fritz H. M., C. D. Blount, S. Thwin, M. K. Thu, and N. Chan, 2009: Cyclone Nargis storm surge in Myanmar. *Nat. Geosci.*, **2**, 448–449.

Fu, B., M. S. Peng, T. Li, and J. Hansen, 2010: A logistic regression model for WNP tropical cyclone formation forecast. 29th Conference on Hurricanes and Tropical Meteorology, 10–14 May 2010, Tucson, USA.

Gautam, R., G. Cervone, R. P. Singh, and M. Kafatos, 2005: Characteristics of meteorological parameters associated with Hurricane Isabel, *Geophys. Res. Lett.*, **32**, L04801, doi:10.1029/2004GL021559.

Gentemann, C. L., F. J. Wentz, C. A. Mears, and D. K. Smith, 2004: In situ validation of Tropical Rainfall Measuring Mission microwave sea surface temperatures, *J. Geophys. Res.*, **109**, C04021.

Gentemann, C. L., M. DeMaria, and F. J. Wentz, 2007: Improving predictions of hurricane intensity: new high-resolution sea surface temperatures from NASA's Aqua satellite. Remote Sensing Systems. Santa Rosa, USA, 14 pp. [Available online at http://www.remss.com/papers/gentemann/gentemann_etal_2007.pdf.]

Goerss, J. S., 2008: Impact of satellite observations on the tropical cyclone track forecasts of the Navy Operational Global Atmospheric Prediction System. *Mon. Wea. Rev.*, **137**, 41–50.

Grassl, H., V. Jost, R. Kumar, J. Schulz, P. Bauer, and P. Schlussel, 2000: The Hamburg Ocean-Atmosphere Parameters and Fluxes from Satellite Data (HOAPS): A Climatological Atlas of Satellite-Derived Air-Sea-Interaction Parameters over the Oceans. Rep. 312, ISSN 0937-1060, Max Planck Institute for Meteorology,

Hamburg, Germany, 130 pp.

Grimes, D. I. F., E. Coppola, M. Verdecchia, and G. Visconti, 2003: A neural network approach to real-time rainfall estimation for Africa using satellite Data. *J. Hydrometeor.*, **4**, 1119-1133.

Haddad, Z. S., E. A. Smith, C. D. Kummerow, T. Iguchi, M. R. Farrar, S. L. Durden, M. Alves, and W. S. Olson, 1997: The TRMM "day-1" radar/radiometer combined rain-profiling algorithm. *J. Meteor. Soc. Japan*, **75**, 799–809.

Heymsfield, G. M., J. B. Halverson, J. Simpson, L. Tian, and T. P. Bui, 2001: ER-2 Doppler radar investigations of the eyewall of Hurricane Bonnie during the Convection and Moisture Experiment-3. *J. Appl. Meteor.*, **40**, 1310–1330.

Hinton, G. E., 1992: How neural networks learn from experience. *Scient. Amer.*, **267**, 145–151.

Holland, G. J., and R. T. Merill, 1984: On the dynamics of tropical cyclone structure changes. *Quart. J. Roy. Meteor. Soc.*, **110**, 723–745.

Holliday, C. R., and A. H. Thompson, 1979: Climatological characteristics of rapidly intensifying typhoons, *Mon. Wea. Rev.*, **107**, 1022–1034.

Hollinger, J., R. Lo, G. Poe, R. Savage, and J. Peirce, 1987: Special Sensor Microwave/Imager user's guide. Naval Research Laboratory, Washington, DC, USA, 177 pp.

Huffman, G. J., R. F. Adler, D. T. Bolvin, G. Gu, E. J. Nelkin, K. P. Bowman, Y. Hong, E. F. Stocker, and D. B. Wolff, 2007: The TRMM Multisatellite Precipitation Analysis (TMPA): quasi-global, multiyear, combined-sensor precipitation estimates at fine scales. *J. Hydrometeor.*, **8**, 38–55.

Janowiak, J. E., R. J. Joyce, and Y. Yarosh, 2001: A real-time global half-hourly pixel-resolution infrared dataset and its applications. *Bull. Amer. Meteor. Soc.*, **82**, 205–217.

Jarvinen, B. R., and C. J. Neumann, 1979: Statistical forecasts of tropical cyclone intensity change. NOAA Tech. Memo. NWS NHC-10, 22 pp.

Jiang, H., J. B. Halverson, and J. Simpson, 2008: On the differences in storm rainfall from hurricanes isidore and lili. part i: satellite observations and rain potential. *Wea. Forecasting*, **23**, 29–43.

Jin, L., 2004: Modeling Theory Method and Application for Weather Forecast Based

on Neural Network (in Chinese). China Meteorological Press, 218 pp.

Jin, L., C. Yao, and X. Y. Huang, 2008: A Nonlinear Artificial Intelligence Ensemble Prediction Model for Typhoon Intensity. *Mon. Wea. Rev.*, **136**, 4541–4554.

Joint Typhoon Warning Center, 1988: Annual Tropical Cyclone Report, U. S. Naval Oceanography Command Center, Guam, Mariana Islands. 216 pp.

Jones, T. A., D. Cecil, and M. DeMaria, 2006: Passive-microwave enhanced Statistical Hurricane Intensity Prediction Scheme. *Wea. Forecasting*, **21**, 613–635.

Kalnay, E., M. Kanamitsu, R. Kistler, W. Collins, D. Deaven, L. Gandin, M. Iredell, S. Saha, G. White, J. Woollen, Y. Zhu, A. Leetmaa, B. Reynolds, M. Chelliah, W. Ebisuzaki, W. Higgins, J. Janowiak, K. Mo, C. Ropelewski, J. Wang, R. Jenne, and D. Joseph, 1996: The NCEP/NCAR 40-Year Reanalysis Project. *Bull. Amer. Meteor. Soc.*, **77**, 437–471.

Kanamitsu, M., W. Ebisuzaki, J. Woolen, J. Potter and M. Fiorino, 2002: NCEP/DOE AMIP-II Reanalysis (R-2). *Bull. Amer. Met. Soc.*, **83**, 1631–1643.

Kaplan, J., and M. DeMaria, 2003: Large-scale characteristics of rapidly intensifying tropical cyclones in the North Atlantic basin. *Wea. Forecasting*, **18**, 1093–1108.

Kaplan, J., M. DeMaria, and J. A. Knaff, 2010: A revised tropical cyclone rapid intensification index for the Atlantic and eastern North Pacific basins. *Wea. Forecasting*, **25**, 220-241.

Knabb, R. D., J. R. Rhome, and D. P. Brown, 2005: Tropical cyclone report, Hurricane Katrina, 23–30 August 2005. National Hurricane Center, 43 pp. [Available online at http://www.nhc.noaa.gov/pdf/TCR-AL122005_Katrina.pdf.]

Knaff, J. A., 2009: Revisiting the maximum intensity of recurving tropical cyclones. *Int. J. Climatol.*, **29**: 827–837.

Knaff, J. A., M. DeMaria, C. R. Sampson, and J. M. Gross, 2003: Statistical 5-day tropical cyclone intensity forecasts derived from climatology and persistence. *Wea. Forecasting*, **18**, 80–92.

Knaff, J. A., C. R. Sampson, and M. DeMaria, 2005: An operational statistical typhoon intensity prediction scheme for the western North Pacific. *Wea. Forecasting*, **20**, 688–699.

Koba, H., T. Hagiwara, S. Osano, and S. Akashi, 1990: Relationships between CI Number from Dvorak's technique and minimum sea level pressure or maximum speed of tropical cyclone (in Japanese). *J. Meteor. Res.*, **42**, 59–67.

Kubota, M., N. Iwasaka, S. Kizu, and M. Knoda, 2002: Japanese Ocean Flux Data Sets with Use of Remote Sensing Observations (J–OFURO). *J. Oceanogr.*, **58**, 213–225.

Kummerow, C., W. Barnes, T. Kozu, J. Shiue, and J. Simpson, 1998: The Tropical Rainfall Measuring Mission (TRMM) sensor package. *J. Atmos. Oceanic Technol.*, **15**, 809–817.

Kuo, H., 1965: On formation and intensification of tropical cyclones through latent heat release by cumulus convection. *J. Atmos. Sci.*, **22**, 40–63.

Kurihara Y., Bender M. A., Tuleya R. E., and Ross R. J., 1998: The GFDL hurricane prediction system and its performance in the 1995 hurricane season. *Mon. Wea. Rev.*, **126**, 1306–1322.

Lee, T. F., F. J. Turk, J. Hawkins, and K. Richardson, 2002: Interpretation of TRMM TMI images of tropical cyclones. *Earth Interactions*, **6**, 1–17.

Levitus, S., 1982: Climatological Atlas of the World Oceans. NOAA Prof. Paper 13, U.S. Government Printing Office, 173pp.

Lin B., and A. Fan, 2005: Validating of satellite retrieved latent heat fluxes over tropical oceans. Ninth Symposium on Integrated Observing and Assimilation Systems for the Atmosphere, Oceans, and Land Surface, The 85th AMS Annual Meeting, 8–14 January 2005, San Diego, USA.

Lin, I.-I., C.-H. Chen, I.-F. Pun, W. T. Liu, and C.-C. Wu, 2009: Warm ocean anomaly, air sea fluxes, and the rapid intensification of tropical cyclone Nargis (2008), *Geophys. Res. Lett.*, **36**, L03817, doi:10.1029/2008GL035815.

Liu, W. T., and W. Tang, 2000: Direct retrieval of ocean surface evaporation and latent heat flux from the spacebased observations. PORSEC 2000, 5–8 December 2000, Goa, India.

Lungu, T., 2001: QuikSCAT science data product user's manual: Overview and geophysical data products. JPL D-18053, Version 2.2, Jet Propulsion Laboratory, Pasadena, USA, 95 pp.

Mainelli, M., M. DeMaria, L. K. Shay, and G. Goni, 2008: Application of oceanic heat content estimation to operational forecasting of recent Atlantic category 5 hurricanes. *Wea. Forecasting*, **23**, 3–16.

Mazany R. A., Businger S., Gutman S. I., and Roeder W., 2002: A lightning index that utilizes GPS integrated precipitable water vapor. *Wea. Forecasting*, **17**,

1034–1048.

Molinari, J., and D. Vollaro, 1989: External influences on hurricane intensity. Part I: Outflow layer angular momentum fluxes. *J. Atmos. Sci.*, **46**, 1093–1105.

Mundhenk B. D., 2009: A statistical-dynamical approach to intraseasonal prediction of tropical cyclogenesis in the western North Pacific. M.S. thesis. Naval Postgraduate School, Monterey, USA, 107pp.

Neumann, C. J., 1993: Global overview. *Global Guide to Tropical Cyclone Forecasting*. G. J. Holland, Ed., WMO Tech. Doc. 560, Rep. TCP-31, 1.1–1.43.

Olander, T. L., and C. S. Velden, 2007: The advanced Dvorak technique: Continued development of an objective scheme to estimate tropical cyclone intensity using geostationary infrared satellite imagery, *Wea. Forecasting*, **22**, 287–298.

Panofsky, H. A., and G. W. Brier, 1968: Some Applications of Statistics to Meteorology. The Pennsylvania State University Press, 224 pp.

Pielke R. A. Jr., J. Gratz, C. W. Landsea,D. Collins, M. A. Saunders, and R. Musulin, 2008: Normalized Hurricane Damage in the United States: 1900–2005. *Nat. Hazards Rev.*, **9**, 29–42.

Ramirez-Beltran, N. D., W. K. M. Lau, A. Winter, J. M. Castro, and N. R. Escalante, 2007: Empirical Probability Models to Predict Precipitation Levels over Puerto Rico Stations, *Mon. Wea. Rev.*, **135**, 877–890.

Rao, G. V., and P. D. Macarthur, 1994: The SSM/I Estimated Rainfall Amounts of Tropical Cyclones and Their Potential in Predicting the Cyclone Intensity Changes. *Mon. Wea. Rev.*, **122**, 1568–1574.

Reynolds, R. W., N. A. Rayner, T. M. Smith, D. C. Stokes, and W. Wang, 2002: An improved in situ and satellite SST analysis for climate. *J. Climate*, **15**, 1609–1625.

Reynolds, R. W., T. M. Smith, C. Liu, D. B. Chelton, K. S. Casey, and M. G. Schlax, 2007: Daily high-resolution-blended analyses for sea surface temperature. *J. Climate*, **20**, 5473–5496.

Riehl, H., 1972: Intensity of recurved typhoons. *J. Appl. Meteor.*, **11**, 613–615.

Riehl, H., and J. Malkus, 1961: Some aspects of Hurricane Daisy, 1958. *Tellus*, **13**, 181–213.

Ritchie, E. A., and G. J. Holland, 1999: Large-scale patterns associated with tropical cyclogenesis in the western Pacific. *Mon. Wea. Rev.*, **127**, 2027-2043.

Rodgers, E. B., S. W. Chang, and H. F. Pierce, 1994: A satellite observational and numerical study of the precipitation characteristics in western north Atlantic tropical cyclones. *J. Appl. Meteor.*, **33**, 573-593.

Rodgers, E. B., and H. F. Pierce, 1995: Environmental influence on Typhoon Bobbie's precipitation distribution. *J. Appl. Meteor.*, **34**, 2515–2532.

Rodgers, E. B., W. S. Olson, V. M. Karyampudi, and H. F. Pierce, 1998: Satellite-derived latent heating distribution and environmental influences in Hurricane Opal (1995). *Mon. Wea. Rev.*, **126**, 1229–1247.

Rodgers, E. B., W. S. Olson, J. Halverson, J. Simpson, and H.F. Pierce, 2000: Environmental forcing of Supertyphoon Paka's (1997) latent heat structure. *J. Appl. Meteor.*, **39**, 1983–2006.

Rumelhart, D. E., G. E. Hinton, and R. J. Williams, 1986: Learning internal representations by error propagation. Parallel Distributed Processing, D. E. Rumelhart, J. L. McClelland, and P. R. Group, Eds., Vol. 1, MIT Press, 318–362.

Sadler, J. C., 1976: A role of the tropical upper tropospheric trough in early season typhoon development. *Mon. Wea. Rev.*, **104**, 1266–1278.

Sadler, J. C., 1978: Mid-season typhoon development and intensity changes and the tropical upper tropospheric trough. *Mon. Wea. Rev.*, **106**, 1137–1152.

Sampson C. R., J. L. Franklin, J. A. Knaff, and M. DeMaria, 2008: Experiments with a simple tropical cyclone intensity consensus. *Wea. Forecasting*, **23**, 304–312.

Shay, L. K., G. J. Goni, and P. G. Black, 2000: Effects of a warm oceanic feature on Hurricane Opal. *Mon. Wea. Rev.*, **128**, 1366–1383.

Shie, C.-L., L. S. Chiu, R. Adler, E. Nelkin, I.-I. Lin, P. Xie, F.-C. Wang, R. Chokngamwong, W. Olson, and D. A. Chu, 2009: A note on reviving the Goddard Satellite-based Surface Turbulent Fluxes (GSSTF) dataset. *Adv. Atmos. Sci.*, **26**, 1071–1080.

Simpson, J., J. B. Halverson, B. S. Ferrier, W. A. Petersen, R. H. Simpson, R. Blakeslee, and S. L. Durden, 1998: On the role of"hot towers in tropical cyclone formation. *Meteorol. Atmos. Phys.*, **67**, 15–35.

Soden B. J., C. S. Velden, and R. E. Tuleya, 2001: The impact of satellite winds on experimental GFDL hurricane model forecasts. *Mon. Wea. Rev.*, **129**, 835–852.

Song, J.-J., Y. Wang, and L. Wu, 2010: Trend discrepancies among three best track data sets of western North Pacific tropical cyclones, *J. Geophys. Res.*, **115**, D12128, doi:10.1029/2009JD013058.

Surgi, N., R. Tuleya, Q. Lui, V. Tallapragada, and Y. Kwon, 2008: Advancement of the HWRF for the Next Generation Prediction at NCEP's Environmental Modeling Center. Proc. 62nd Interdepartmental Hurricane Conf., Charleston, SC, Office of the Federal Coordinator for Meteorology, 32pp. [Available online at http://www.ofcm.gov/ihc08/linking_file_ihc08.htm.]

Takemura, Y., and S. Osano, 1989: Estimation of typhoon intensity from meteorological satellite data, WMO Typhoon Committee, 22nd Session, 30 Oct–6 Nov 1989, Tokyo, Japan.

Tatsumi, Y., 1986: A spectral limited area model with time dependent lateral boundary condition and its application to a multi-level primitive equation model. *J. Meteor. Soc. Japan*, **64**, 637–664.

Tuleya R. E., and Lord S. J., 1996: The impact of dropwindsonde data on GFDL hurricane model forecasts using global analyses. *Wea. Forecasting*, **12**, 307–323.

Uppala, S. M., P. W. KÅllberg, A. J. Simmons, U. Andrae, V. Da Costa Bechtold, M. Fiorino, J. K. Gibson, J. Haseler, A. Hernandez, G. A. Kelly, X. Li, K. Onogi, S. Saarinen, N. Sokka, R. P. Allan, E. Andersson, K. Arpe, M. A. Balmaseda, A. C. M. Beljaars, L. Van De Berg, J. Bidlot, N. Bormann, S. Caires, F. Chevallier, A. Dethof, M. Dragosavac, M. Fisher, M. Fuentes, S. Hagemann, E. Hólm, B. J. Hoskins, L. Isaksen, P. A. E. M. Janssen, R. Jenne, A. P. Mcnally, J.-F. Mahfouf, J.-J. Morcrette, N. A. Rayner, R. W. Saunders, P. Simon, A. Sterl, K. E. Trenberth, A. Untch, D. Vasiljevic, P. Viterbo, and J. Woollen, 2005: The ERA-40 re-analysis. *Quart. J. Roy. Meteor. Soc.*, **131**, 2961–3012.

Velden, C. S., T. L. Olander, and R. M. Zehr, 1998: Development of an objective scheme to estimate tropical cyclone intensity from digital geostationary satellite infrared imagery, *Wea. Forecasting*, **13**, 172–186.

Ventham, J. D., and B. Wang, 2007: Large scale flow patterns and their influence on the intensification rates of western North Pacific tropical storms. *Mon. Wea. Rev.*, **135**, 1110–1127.

Wang B., and X. Xu, 1997: Northern Hemispheric summer monsoon singularities and climatological intraseasonal oscillation. *J. Climate*, **10**, 1071–1085.

Wang, Y., 2002: Vortex Rossby waves in a numerically simulated tropical cyclone. Part II: The role in tropical cyclone structure and intensity change. *J. Atmos. Sci.*,

59, 1239–1262.

Weissmann M., F. Harnisch, C.-C. Wu, P.-H. Lin, Y. Ohta, K. Yamashita, Y.-K. Kim, E.-H. Jeon, T. Nakazawa, and S. Aberson, 2010: The influence of dropsondes on typhoon track and mid-latitude forecasts. *Mon. Wea. Rev., in press.*

Weng, F. W., L. Zhao, R. Ferraro, G. Pre, X. Li, and N. C. Grody. 2003. Advanced Microwave Sounding Unit (AMSU) cloud and precipitation algorithms. *Radio Sci.*, **38**, 8068–8079.

Wentz, F. J., 1997: A well-calibrated ocean algorithm for SSM/I. *J. Geophys. Res.*, **102**, 8703-8718.

Wentz, F. J., and R. W. Spencer, 1998: SSM/I rain retrievals within a unified all-weather ocean algorithm. *J. Atmos. Sci.*, **55**, 1613–1627.

Wentz, F. J., and T. Meissner, 2000: AMSR Ocean Algorithm Theoretical Basis Document, Version 2. Remote Sensing Systems, Santa Rosa, USA.

Wilheit, T., C. Kummerow, and R. Ferraro, 2003: Rainfall algorithms for AMSR-E. *IEEE Trans. Geosci. Remote Sens.*, **41**, 204–214.

Wilks, D. S., 2006: Statistical Methods in the Atmospheric Sciences, 2nd edition. Academic Press, 627 pp.

Willoughby, H. E., J. A. Clos, and M. G. Shoreibah, 1982: Concentric eyewalls, secondary wind maxima, and the evolution of the hurricane vortex. *J. Atmos. Sci.*, **39**, 395–411.

Wu, C.-C., P.-H. Lin, S. Aberson, T.-C. Yeh, W.-P. Huang, K.-H. Chou, J.-S. Hong, G.-C. Lu, C.-T. Fong, K.-C. Hsu, I.-I. Lin, P.-L. Lin, and C.-H. Liu, 2005: Dropwindsonde Observations for Typhoon Surveillance near the Taiwan Region (DOTSTAR): An overview. *Bull. Amer. Meteor. Soc.*, **86**, 787–790.

Xiao Q., X. Zhang, C. Davis, J. Tuttle, G. Holland, and P. J. Fitzpatrick, 2009; Experiments of Hurricane Initialization with Airborne Doppler Radar Data for the Advanced Research Hurricane WRF (AHW) Model. *Mon. Wea. Rev.*, **137**, 2758–2777.

Xie X., W. T. Liu, and B. Tang, 2008: Spacebased estimation of moisture transport in marine atmosphere using support vector regression. *Remote Sens. Environ.*, **112**, 1846–1855.

Yang, B., Y. Wang, and B. Wang, 2007: The Effect of internally generated inner–core

asymmetries on tropical cyclone potential intensity. *J. Atmos. Sci.*, **64**, 1165–1188.

Yang, F., H.-L. Pan, S. K. Krueger, S. Moorthi, and S. J. Lord, 2006: Evaluation of the NCEP Global Forecast System at the ARM SGP site. *Mon. Wea. Rev.*, **134**, 3668–3690.

Yang, R., J. Tang, and M. Kafatos, 2007: Improved associated conditions in rapid intensifications of tropical cyclones. *Geophys. Res. Lett.*, **34**, L20807, doi:10.1029/2007GL031241.

Yang, R., D. Sun, and J. Tang, 2008: A "sufficient" condition combination for rapid intensifications of tropical cyclones. *Geophys. Res. Lett.*, **35**, L20802, doi:10.1029/2008GL035222.

Yu, H., C. Hu, and L. Jiang, 2007: Comparison of three tropical cyclone intensity datasets. *Acta Meteorol. Sin.*, **21**, 121–128.

Yu, H. and H. J. Kwon, 2005: Effect of TC–Trough interaction on the intensity change of two typhoons. *Wea. Forecasting*, **20**, 199–211.

Yu, L., X. Jin, and R. A. Weller, 2008: Multidecade Global Flux Datasets from the Objectively Analyzed Air-sea Fluxes (OAFlux) Project: Latent and sensible heat fluxes, ocean evaporation, and related surface meteorological variables. Woods Hole Oceanographic Institution, OAFlux Project Tech. Rep. OA-2008-01, 64 pp.

Zehr, R. M., 1992: Tropical cyclogenesis in the western North Pacific. NOAA Tech. Rep. NESDIS 61, 181 pp.

Zhang, Q., L. Wu, and Q. Liu, 2009: Tropical cyclone damages in China 1983–2006. *Bull. Amer. Meteor. Soc.*, **90**, 489–495.

Appendix A suite of sample codes

To extract parameters from NCEP GFS FNL 12-hourly analysis data (in GRIB1 format) and convert them to BINARY format:

For example, the following codes are used to extract 400-hPa relative humidity in 2008, which is the 88th record in the GRIB1 data with filename such as 'fnl_200801_01_00', 'fnl_200801_01_12', and so on. The output data file is named as 'RH400_08.dat'. To run this code in WINDOWS operating system, save the codes in a BAT file and open the BAT file directly.

```
@echo off
for %%i in (01_00 01_12 02_00 02_12 03_00 03_12 04_00 04_12 05_00 05_12 06_00 06_12 07_00 07_12 08_00 08_12 09_00 09_12 10_00 10_12 11_00 11_12 12_00 12_12 13_00 13_12 14_00 14_12 15_00 15_12 16_00 16_12 17_00 17_12 18_00 18_12 19_00 19_12 20_00 20_12 21_00 21_12 22_00 22_12 23_00 23_12 24_00 24_12 25_00 25_12 26_00 26_12 27_00 27_12 28_00 28_12 29_00 29_12 30_00 30_12 31_00 31_12) do wgrib -bin -nh F:\ds083.2\200801\fnl_200801%%i_00 -d 88 -append -o F:\stips\RH400_08.dat

for %%i in (01_00 01_12 02_00 02_12 03_00 03_12 04_00 04_12 05_00 05_12 06_00 06_12 07_00 07_12 08_00 08_12 09_00 09_12 10_00 10_12 11_00 11_12 12_00 12_12 13_00 13_12 14_00 14_12 15_00 15_12 16_00 16_12 17_00 17_12 18_00 18_12 19_00 19_12 20_00 20_12 21_00 21_12 22_00 22_12 23_00 23_12 24_00 24_12 25_00 25_12 26_00 26_12 27_00 27_12 28_00 28_12 29_00 29_12) do wgrib -bin -nh F:\ds083.2\200802\fnl_200802%%i_00 -d 88 -append -o F:\stips\RH400_08.dat

for %%i in (01_00 01_12 02_00 02_12 03_00 03_12 04_00 04_12 05_00 05_12 06_00 06_12 07_00 07_12 08_00 08_12 09_00 09_12 10_00 10_12 11_00 11_12 12_00 12_12 13_00 13_12 14_00 14_12 15_00 15_12 16_00 16_12 17_00 17_12 18_00 18_12 19_00 19_12 20_00 20_12 21_00 21_12 22_00 22_12 23_00 23_12 24_00 24_12 25_00 25_12 26_00 26_12 27_00 27_12 28_00 28_12 29_00 29_12 30_00 30_12 31_00 31_12) do wgrib -bin -nh F:\ds083.2\200803\fnl_200803%%i_00 -d 88 -append -o F:\stips\RH400_08.dat

for %%i in (01_00 01_12 02_00 02_12 03_00 03_12 04_00 04_12 05_00 05_12 06_00 06_12 07_00 07_12 08_00 08_12 09_00 09_12 10_00 10_12 11_00 11_12 12_00 12_12 13_00 13_12 14_00 14_12 15_00 15_12 16_00 16_12 17_00 17_12 18_00 18_12 19_00 19_12 20_00 20_12 21_00 21_12 22_00 22_12 23_00 23_12 24_00 24_12 25_00 25_12 26_00 26_12 27_00 27_12 28_00 28_12 29_00 29_12 30_00 30_12) do wgrib -bin -nh F:\ds083.2\200804\fnl_200804%%i_00 -d 88 -append -o F:\stips\RH400_08.dat

for %%i in (01_00 01_12 02_00 02_12 03_00 03_12 04_00 04_12 05_00 05_12 06_00 06_12 07_00 07_12 08_00 08_12 09_00 09_12 10_00 10_12 11_00 11_12 12_00 12_12
```

13_00 13_12 14_00 14_12 15_00 15_12 16_00 16_12 17_00 17_12 18_00 18_12 19_00 19_12 20_00 20_12 21_00 21_12 22_00 22_12 23_00 23_12 24_00 24_12 25_00 25_12 26_00 26_12 27_00 27_12 28_00 28_12 29_00 29_12 30_00 30_12 31_00 31_12) do wgrib -bin -nh F:\ds083.2\200805\fnl_200805%%i_00 -d 88 -append -o F:\stips\RH400_08.dat

for %%i in (01_00 01_12 02_00 02_12 03_00 03_12 04_00 04_12 05_00 05_12 06_00 06_12 07_00 07_12 08_00 08_12 09_00 09_12 10_00 10_12 11_00 11_12 12_00 12_12 13_00 13_12 14_00 14_12 15_00 15_12 16_00 16_12 17_00 17_12 18_00 18_12 19_00 19_12 20_00 20_12 21_00 21_12 22_00 22_12 23_00 23_12 24_00 24_12 25_00 25_12 26_00 26_12 27_00 27_12 28_00 28_12 29_00 29_12 30_00 30_12) do wgrib -bin -nh F:\ds083.2\200806\fnl_200806%%i_00 -d 88 -append -o F:\stips\RH400_08.dat

for %%i in (01_00 01_12 02_00 02_12 03_00 03_12 04_00 04_12 05_00 05_12 06_00 06_12 07_00 07_12 08_00 08_12 09_00 09_12 10_00 10_12 11_00 11_12 12_00 12_12 13_00 13_12 14_00 14_12 15_00 15_12 16_00 16_12 17_00 17_12 18_00 18_12 19_00 19_12 20_00 20_12 21_00 21_12 22_00 22_12 23_00 23_12 24_00 24_12 25_00 25_12 26_00 26_12 27_00 27_12 28_00 28_12 29_00 29_12 30_00 30_12 31_00 31_12) do wgrib -bin -nh F:\ds083.2\200807\fnl_200807%%i_00 -d 88 -append -o F:\stips\RH400_08.dat

for %%i in (01_00 01_12 02_00 02_12 03_00 03_12 04_00 04_12 05_00 05_12 06_00 06_12 07_00 07_12 08_00 08_12 09_00 09_12 10_00 10_12 11_00 11_12 12_00 12_12 13_00 13_12 14_00 14_12 15_00 15_12 16_00 16_12 17_00 17_12 18_00 18_12 19_00 19_12 20_00 20_12 21_00 21_12 22_00 22_12 23_00 23_12 24_00 24_12 25_00 25_12 26_00 26_12 27_00 27_12 28_00 28_12 29_00 29_12 30_00 30_12 31_00 31_12) do wgrib -bin -nh F:\ds083.2\200808\fnl_200808%%i_00 -d 88 -append -o F:\stips\RH400_08.dat

for %%i in (01_00 01_12 02_00 02_12 03_00 03_12 04_00 04_12 05_00 05_12 06_00 06_12 07_00 07_12 08_00 08_12 09_00 09_12 10_00 10_12 11_00 11_12 12_00 12_12 13_00 13_12 14_00 14_12 15_00 15_12 16_00 16_12 17_00 17_12 18_00 18_12 19_00 19_12 20_00 20_12 21_00 21_12 22_00 22_12 23_00 23_12 24_00 24_12 25_00 25_12 26_00 26_12 27_00 27_12 28_00 28_12 29_00 29_12 30_00 30_12) do wgrib -bin -nh F:\ds083.2\200809\fnl_200809%%i_00 -d 88 -append -o F:\stips\RH400_08.dat

for %%i in (01_00 01_12 02_00 02_12 03_00 03_12 04_00 04_12 05_00 05_12 06_00 06_12 07_00 07_12 08_00 08_12 09_00 09_12 10_00 10_12 11_00 11_12 12_00 12_12 13_00 13_12 14_00 14_12 15_00 15_12 16_00 16_12 17_00 17_12 18_00 18_12 19_00 19_12 20_00 20_12 21_00 21_12 22_00 22_12 23_00 23_12 24_00 24_12 25_00 25_12 26_00 26_12 27_00 27_12 28_00 28_12 29_00 29_12 30_00 30_12 31_00 31_12) do wgrib -bin -nh F:\ds083.2\200810\fnl_200810%%i_00 -d 88 -append -o F:\stips\RH400_08.dat

```
for %%i in (01_00 01_12 02_00 02_12 03_00 03_12 04_00 04_12 05_00 05_12 06_00
06_12 07_00 07_12 08_00 08_12 09_00 09_12 10_00 10_12 11_00 11_12 12_00 12_12
13_00 13_12 14_00 14_12 15_00 15_12 16_00 16_12 17_00 17_12 18_00 18_12 19_00
19_12 20_00 20_12 21_00 21_12 22_00 22_12 23_00 23_12 24_00 24_12 25_00 25_12
26_00 26_12 27_00 27_12 28_00 28_12 29_00 29_12 30_00 30_12) do wgrib -bin -nh
F:\ds083.2\200811\fnl_200811%%i_00 -d 88 -append -o F:\stips\RH400_08.dat

for %%i in (01_00 01_12 02_00 02_12 03_00 03_12 04_00 04_12 05_00 05_12 06_00
06_12 07_00 07_12 08_00 08_12 09_00 09_12 10_00 10_12 11_00 11_12 12_00 12_12
13_00 13_12 14_00 14_12 15_00 15_12 16_00 16_12 17_00 17_12 18_00 18_12 19_00
19_12 20_00 20_12 21_00 21_12 22_00 22_12 23_00 23_12 24_00 24_12 25_00 25_12
26_00 26_12 27_00 27_12 28_00 28_12 29_00 29_12 30_00 30_12 31_00 31_12) do
wgrib -bin -nh F:\ds083.2\200812\fnl_200812%%i_00 -d 88 -append -o
F:\stips\RH400_08.dat
```

To read OAFlux data (in NetCDF format) and convert them to BINARY format:

The following FORTRAN codes are used to convert OAFlux daily SLHF data in NetCDF format to BINARY format. The codes are generated by using free software named 'nc2f90.exe' obtained online from http://www.whigg.ac.cn/yanhm/fortran.htm.

The NetCDF library is needed to run this FORTRAN program.

```
      include 'netcdf.inc'
!-----------------------------------------------------
!     Define Variables.
!     Variable ids run sequentially from 1 to nvars=5 ! number of variables
      integer,parameter :: ix=360, jy=180, nrec=365  ! change this to generalize
      integer*4  ncid, status    ! file control
      integer*4 recdim   ! record dimension
!-------------------------------------------------------------
 !     Below 5 variables is the data in netCDF file
      real*4          ::  lon( ix )
      real*4          ::  lat( jy )
      integer*4       ::  time(nrec)
      integer*2       ::  tmpsf( ix, jy, nrec )
      integer*2       ::  err( ix,jy, nrec )
!     above 5 variables is the data in netCDF file
!-------------------------------------------------------------
      integer*4   :: start(10)
      integer*4   :: count(10)
      integer*4   :: dimids(10)! allow up to 10 dimensions
      integer*4   :: dimid, xtype
      character(len=31) :: dummy
!-------------------------------------------------------------
!  Define "scale_factor" and "add_offset" variables
      real*8      ::  scale4(1), add4(1)
      real*8      ::  scale5(1), add5(1)
!-------------------------------------------------------------
      real        ::  Ta, q, qs( ix, jy, nrec )
! Open netCDF file.
      status=nf_open('f:\oaflux\lh_oaflux_2008.nc',nf_nowrite,ncid)
          if ( status/=nf_noerr ) write (*,*) nf_strerror(status)
!-------------------------------------------------
!   Retrieve data for Variable 'lon'
!   Long_name of 'lon' is 'longitude'
!   Units of 'lon' is 'degrees'
      status=nf_inq_var(ncid,    1,dummy,xtype,ndim,dimids,natts)
          if ( status/=nf_noerr ) write (*,*) nf_strerror(status)
      do j=1,ndim
```

```
      status=nf_inq_dim(ncid,dimids(j),dummy,len)
          if ( status/=nf_noerr ) write (*,*) nf_strerror(status)
      start(j)=1 ; count(j)=len
      end do
      status=nf_get_vara_real(ncid,    1,start,count,lon)
!-------------------------------------------------
!   Retrieve data for Variable 'lat'
!   Long_name of 'lat' is 'latitude'
!   Units of 'lat' is 'degrees'
      status=nf_inq_var(ncid,    2,dummy,xtype,ndim,dimids,natts)
          if ( status/=nf_noerr ) write (*,*) nf_strerror(status)
      do j=1,ndim
      status=nf_inq_dim(ncid,dimids(j),dummy,len)
          if ( status/=nf_noerr ) write (*,*) nf_strerror(status)
      start(j)=1 ; count(j)=len
      end do
      status=nf_get_vara_real(ncid,    2,start,count,lat)
!-------------------------------------------------
!   Retrieve data for Variable 'time'
!   Units of 'time' is 'day'
      status=nf_inq_var(ncid,    3,dummy,xtype,ndim,dimids,natts)
          if ( status/=nf_noerr ) write (*,*) nf_strerror(status)
      do j=1,ndim
      status=nf_inq_dim(ncid,dimids(j),dummy,len)
          if ( status/=nf_noerr ) write (*,*) nf_strerror(status)
      start(j)=1 ; count(j)=len
      end do
      status=nf_get_vara_int(ncid,    3,start,count,time)
!-------------------------------------------------
!   Retrieve data for Variable 'tmpsf'
!   Units of 'tmpsf' is 'W/m^2'
      status=nf_inq_var(ncid,    4,dummy,xtype,ndim,dimids,natts)
          if ( status/=nf_noerr ) write (*,*) nf_strerror(status)
      do j=1,ndim
      status=nf_inq_dim(ncid,dimids(j),dummy,len)
          if ( status/=nf_noerr ) write (*,*) nf_strerror(status)
      start(j)=1 ; count(j)=len
      end do
      status=nf_get_vara_int2(ncid,    4,start,count,tmpsf)
      scale4(1) =0.0 ; add4(1) =0.0
! Scale_factor and add_offset for variable 'tmpsf'
      status=nf_get_att_double(ncid,    4,'scale_factor',scale4(1))
! add scale_factor and add_offset to get true value
! Caution: variable type of 'tmpsf' may not as the same as the type of
! 'scale4(1)' and 'add4(1)', you must change it youself!
```

```
      tmpsf=tmpsf*scale4(1)+add4(1)
!-----------------------------------------------------
!   Retrieve data for Variable 'err'
!   Units of 'err' is 'W/m^2'
      status=nf_inq_var(ncid,    5,dummy,xtype,ndim,dimids,natts)
          if ( status/=nf_noerr ) write (*,*) nf_strerror(status)
      do j=1,ndim
      status=nf_inq_dim(ncid,dimids(j),dummy,len)
           if ( status/=nf_noerr ) write (*,*) nf_strerror(status)
      start(j)=1 ; count(j)=len
      end do
      status=nf_get_vara_int2(ncid,    5,start,count,err)
      scale5(1) =0.0 ; add5(1) =0.0
! Scale_factor and add_offset for variable 'err'
      status=nf_get_att_double(ncid,    5,'scale_factor',scale5(1))
! add scale_factor and add_offset to get true value
! Caution: variable type of 'err' may not as the same as the type of
! 'scale5(1)' and 'add5(1)', you must change it youself!
      err=err*scale5(1)+add5(1)
! ----------   Some useful advices  -------------
! If dimensions of a variable exceed 3, there can be an error (or warning)
! "warning LNK4084: total image size 382214144 exceeds max (268435456); image may not
run"
! when link this program. The best way to resolve it: decrease dimensions
! of the variable, use "do ...  end do" cycle to get little data at one time.
! See NetCDF mannual to look for how to control the dimensions.
!------------   End suggestions   -------------
!-----------------------------------------------------
!  Begin writing statements to use the data.
!     Here write your own code please!
   open(11,file='f:\oaflux\lh_2008.dat',access='direct',form='binary',recl=4*ix*jy
)
      do k=1,nrec
      write(11,rec=k) ((real(tmpsf(i,j,k)),i=1,ix),j=1,jy)
      enddo
   close(11)
!-----------------------------------------------------
!  End Program
      End
```

To calculate area-averaged SLHF within a 5° × 5° box for each TC sample during 2000–2008.

```
      integer, parameter :: ix=360, jy=180, nt=366, tyno=211, max=200
      integer id(tyno), line(tyno), seri(tyno), grade(tyno, max), ilat(tyno, max)
      integer ilon(tyno, max), drad50(tyno, max), r50l(tyno, max), r50s(tyno, max)
      integer drad30(tyno, max), r30l(tyno, max), r30s(tyno, max)
      integer vmax(tyno, max), mslp(tyno, max), yr, mon, dy, hr
      real lat(tyno, max), lon(tyno, max), lh(ix, jy, nt), lhf(tyno, max)
      character*20 tcname(tyno)
      character*2 year(tyno, max), month(tyno, max), day(tyno, max), hour(tyno, max)

! Read RMSC Tokyo best track
      open(3, file='f:\stips\bst00-08_12h.txt', status='old')
      do n=1, tyno
      read (3, 11) ind1, id(n), line(n), seri(n), tcname(n)
11    format(i5, 1x, i4, 2x, i3, 1x, i4, 10x, a20, 22x)
      if (ind1==66666) then
      do i = 1, line(n)
      read (3, 101) year(n, i), month(n, i), day(n, i), hour(n, i), ind2, grade(n, i), &
      ilat(n, i), ilon(n, i), mslp(n, i), vmax(n, i), drad50(n, i), r50l(n, i), r50s(n, i), &
      drad30(n, i), r30l(n, i), r30s(n, i)
101   format(4a2, 1x, i3, 1x, i1, 1x, i3, 1x, i4, 1x, i4, 5x, i3, 5x, i1, i4, 1x, i4, 1x, i1, i4, 1x, i4)
      lat(n, i)=ilat(n, i)/float(10)
      lon(n, i)=ilon(n, i)/float(10)
      enddo
      endif
      enddo
      close(3)

      do n=1, tyno
      do m=1, line(n)

      read( year(n, m),  '(i2)' )  yr
      read( month(n, m), '(i2)' )  mon
      read( day(n, m),   '(i2)' )  dy
      read( hour(n, m),  '(i2)' )  hr

      call leap_year(yr, log)
      if (log==1) then
      nn=nt-1
      else
      nn=nt
      endif
```

```
open(11,file='f:\oaflux\lh_20'//year(n,m)//'.dat',access='direct',&
form='binary',recl=4*ix*jy)
do k=1,nn
read(11,rec=k) ((lh(i,j,k),i=1,ix),j=1,jy)
enddo
close(11)

call datetojday(yr,mon,dy,jday)
lhf(n,m)=0.
j1=nint(lat(n,m))+91; i1=nint(lon(n,m))+1
dd=0.; ll=0
do j=-2,2
do k=-2,2
i2=i1+j;j2=j1+k;k2=jday
if (lh(i2,j2,k2)/=32766.) then
ll=ll+1
dd=dd+lh(i2,j2,k2)
endif
enddo
enddo

if (ll>0) then
lhf(n,m)=dd/float(ll)
else
lhf(n,m)=32766.
endif

enddo
enddo

open(31,file='f:\stips\LHF_00-08.txt')
do n=1,tyno
write (31,11) ind1,id(n),line(n),seri(n),tcname(n)
if (ind1==66666) then
do i = 1, line(n)
write (31,103) year(n,i),month(n,i),day(n,i),hour(n,i),ind2,grade(n,i),&
lat(n,i),lon(n,i),mslp(n,i),vmax(n,i),lhf(n,i)
enddo
103 format(4a2,1x,i3,1x,i1,1x,f4.1,1x,f5.1,1x,i4,5x,i3,5x,f5.1)
endif
enddo
close(31)
end
```

To calculate area-averaged TMPA rain rate within a 110km circle for each TC sample during 2000–2008:

```
      integer, parameter :: ix=1440, jy=400, tyno=211, max=200
      integer id(tyno), line(tyno), seri(tyno), grade(tyno, max), ilat(tyno, max)
      integer ilon(tyno, max), drad50(tyno, max), r501(tyno, max), r50s(tyno, max)
      integer drad30(tyno, max), r301(tyno, max), r30s(tyno, max)
      integer vmax(tyno, max), mslp(tyno, max)
      real*8 lat(tyno, max), lon(tyno, max), out2, angle2, lat2(ix, jy), lon2(ix, jy)
      character*20 tcname(tyno)
      character*1 cvarin(4), cvar(4)
      character*2 year(tyno, max), month(tyno, max), day(tyno, max), hour(tyno, max)
      real rr(ix, jy), irr(tyno, max), varin, var, ill, idd
      equivalence (cvarin, varin)
      equivalence (cvar, var)

! Read RMSC Tokyo best track
      open(3, file='f:\stips\bst00-08_12h.txt', status='old')
      do n = 1, tyno
      read (3, 11) ind1, id(n), line(n), seri(n), tcname(n)
11    format(i5, 1x, i4, 2x, i3, 1x, i4, 10x, a20, 22x)
      if (ind1==66666) then
      do k = 1, line(n)
      read (3, 101) year(n, k), month(n, k), day(n, k), hour(n, k), ind2, grade(n, k), &
      ilat(n, k), ilon(n, k), mslp(n, k), vmax(n, k), drad50(n, k), r501(n, k), r50s(n, k), &
      drad30(n, k), r301(n, k), r30s(n, k)
101   format(4a2, 1x, i3, 1x, i1, 1x, i3, 1x, i4, 1x, i4, 5x, i3, 5x, i1, i4, 1x, i4, 1x, i1, i4, 1x, i4)
      lat(n, k)=ilat(n, k)/float(10)
      lon(n, k)=ilon(n, k)/float(10)
      enddo
      endif
      enddo
      close(3)

      do n=1, tyno
      do k=1, line(n)

       open(11, file='f:\trmm\20'//year(n, k)//''//month(n, k)//'\3b42.'//year(n, k)&
       //''//month(n, k)//''//day(n, k)//'.'//hour(n, k)//'z.6.precipitation.bin', &
       access='direct', form='binary', recl=4*ix*jy)
       read(11, rec=1) ((rr(i, j), i=1, ix), j=1, jy)
       close(11)

! The data has been read into the array, swap the byte order to get the rain rate.
        do i = 1, ix
```

```
      do j = 1, jy
       varin = rr (i, j)
       cvar (1) = cvarin (4)
       cvar (2) = cvarin (3)
       cvar (3) = cvarin (2)
       cvar (4) = cvarin (1)
       rr (i,j) = var
      enddo
      enddo

      idd=0.; ill=0.
      do i=1,ix
      do j=1,jy
       if (i<=720) then
       lon2(i,j)=-179.875+(i-1)*0.25+360
       else
       lon2(i,j)=-179.875+(i-1)*0.25
       endif
      lat2(i,j)=-47.875+(j-1)*0.25
      call distance(lon(n,k),lat(n,k),lon2(i,j),lat2(i,j),out2,angle2)
        if (out2<=110d0 .and. rr(i,j)/=-9999.) then
        idd=idd+rr(i,j)
        ill=ill+1
        endif
      enddo
      enddo
     irr(n,k)=idd/ill
     enddo
     enddo

     open(31,file='f:\stips\IRR_00-08.txt')
     do n=1,tyno
     write (31,11) ind1,id(n),line(n),seri(n),tcname(n)
     if (ind1==66666) then
     do k = 1, line(n)
     write (31,103) year(n,k),month(n,k),day(n,k),hour(n,k),ind2,grade(n,k),&
     lat(n,k),lon(n,k),mslp(n,k),vmax(n,k),irr(n,k)
     enddo
103  format(4a2,1x,i3,1x,i1,1x,f4.1,1x,f5.1,1x,i4,5x,i3,5x,f5.1)
     endif
     enddo
     close(31)
     end
```

To get the SST at the center of each TC sample during 2000–2008:

```
      integer, parameter :: ix=1440, jy=720, tyno=211, max=200
      integer id(tyno), line(tyno), seri(tyno), grade(tyno, max), ilat(tyno, max)
      integer ilon(tyno, max), drad50(tyno, max), r501(tyno, max), r50s(tyno, max)
      integer drad30(tyno, max), r301(tyno, max), r30s(tyno, max)
      integer vmax(tyno, max), mslp(tyno, max), yr, mon, dy, hr, jday
      real*8 lat(tyno, max), lon(tyno, max), out, angle
      real*8 out2, angle2, lat2(ix, jy), lon2(ix, jy)
      character*20 tcname(tyno)
      character*1 cvarin(4), cvar(4)
      character*2 year(tyno, max), month(tyno, max), day(tyno, max), hour(tyno, max)
      character*3 jdy
      real varin, var, ill, idd, sst(tyno, max)
      character(len=150)          :: file_name
      real*4, dimension(ix, jy) :: sst_data
      integer*4                   :: iexist

! Read RSMC best track
      open(3, file='f:\stips\bst00-08_12h.txt', status='old')
      do n=1, tyno
      read (3, 11) ind1, id(n), line(n), seri(n), tcname(n)
11    format(i5, 1x, i4, 2x, i3, 1x, i4, 10x, a20, 22x)
      if (ind1==66666) then
      do k = 1, line(n)
      read (3, 101) year(n, k), month(n, k), day(n, k), hour(n, k), ind2, grade(n, k), &
      ilat(n, k), ilon(n, k), mslp(n, k), vmax(n, k), drad50(n, k), r501(n, k), r50s(n, k), &
      drad30(n, k), r301(n, k), r30s(n, k)
101   format(4a2, 1x, i3, 1x, i1, 1x, i3, 1x, i4, 1x, i4, 5x, i3, 5x, i1, i4, 1x, i4, 1x, i1, i4, 1x, i4)
      lat(n, k)=ilat(n, k)/float(10)
      lon(n, k)=ilon(n, k)/float(10)
      enddo
      endif
      enddo
      close(3)

      do n=1, tyno
      do k=1, line(n)

      read( year(n, k),  '(i2)' )   yr
      read( month(n, k), '(i2)' )   mon
      read( day(n, k),   '(i2)' )   dy
      call datetojday(yr, mon, dy, jday)
      write( jdy, '(i3)' )   jday
```

```
if (jday<=9) then
file_name='f:\SST\tmi.fusion.20'//year(n,k)//'.00'//trim(adjustl(jdy))//'.v01'
elseif (jday>9 .and. jday<100) then
file_name='f:\SST\tmi.fusion.20'//year(n,k)//'.0'//trim(adjustl(jdy))//'.v01'
else
file_name='f:\SST\tmi.fusion.20'//year(n,k)//'.'//jdy//'.v01'
endif

  CALL READ_RSS_OISST_V2(file_name,sst_data,iexist)
  if(iexist.ne.0) stop

  i = nint ( ( lon(n,k)+0.125 ) / 0.25  )
  j = nint ( ( lat(n,k)+90.125 ) / 0.25 )

  sst(n,k) = sst_data(i,j)
  write(*,*) sst(n,k)

  enddo
  enddo

  open(10,file='f:\stips\SST_00-08.txt')
  do n=1,tyno
  write (10,11) ind1,id(n),line(n),seri(n),tcname(n)
  if (ind1==66666) then
  do i = 1, line(n)
  write (10,103) year(n,i),month(n,i),day(n,i),hour(n,i),ind2,grade(n,i),&
   lat(n,i),lon(n,i),mslp(n,i), vmax(n,i),sst(n,i)
  enddo
103  format(4a2,1x,i3,1x,i1,1x,f4.1,1x,f5.1,1x,i4,5x,i3,1x,f7.2)
  endif
  enddo

  end
```

To obtain the parameters from 12-hourly NCEP BINARY data (taking area-averaged (200–800 km) temperature at 200 hPa as an example) for each TC sample during 2000–2008:

```
      integer, parameter :: ix=360, jy=181, nt=732, tyno=211, max=200
      integer id(tyno), line(tyno), seri(tyno), grade(tyno, max), ilat(tyno, max)
      integer ilon(tyno, max), drad50(tyno, max), r501(tyno, max), r50s(tyno, max)
      integer drad30(tyno, max), r301(tyno, max), r30s(tyno, max)
      integer vmax(tyno, max), mslp(tyno, 200), yr, mon, dy, hr, log
      real lh(ix, jy, nt), t200(tyno, max)
      real*8 lat(tyno, max), lon(tyno, max), out2, angle2, lat2(ix, jy), lon2(ix, jy)
      character*20 tcname(tyno)
      character*2 year(tyno, max), month(tyno, max), day(tyno, max), hour(tyno, max)

! Read RMSC Tokyo best track
      open(3, file='f:\stips\bst00-08_12h.txt', status='old')
      do n=1, tyno
      read (3, 11) ind1, id(n), line(n), seri(n), tcname(n)
11    format(i5, 1x, i4, 2x, i3, 1x, i4, 10x, a20, 22x)
      if (ind1==66666) then
      do i = 1, line(n)
      read (3, 101) year(n, i), month(n, i), day(n, i), hour(n, i), ind2, grade(n, i), &
      ilat(n, i), ilon(n, i), mslp(n, i), vmax(n, i), drad50(n, i), r501(n, i), r50s(n, i), &
      drad30(n, i), r301(n, i), r30s(n, i)
101   format(4a2, 1x, i3, 1x, i1, 1x, i3, 1x, i4, 1x, i4, 5x, i3, 5x, i1, i4, 1x, i4, 1x, i1, i4, 1x, i4)
      lat(n, i)=ilat(n, i)/float(10)
      lon(n, i)=ilon(n, i)/float(10)
      enddo
      endif
      enddo
      close(3)

      do n=1, tyno
      do m=1, line(n)

      read( year(n, m),  '(i2)' )  yr
      read( month(n, m), '(i2)' )  mon
      read( day(n, m),   '(i2)' )  dy
      read( hour(n, m),  '(i2)' )  hr

      call leap_year(yr, log)
      if (log==1) then
      nn=nt-2
      else
      nn=nt
```

```
      endif

      open(11,file='f:\stips\T200_'//year(n,m)//'.dat',access='direct',&
      form='binary',recl=4*ix*jy)
      do k=1,nn
      read(11,rec=k) ((lh(i,j,k),i=1,ix),j=1,jy)
      enddo
      close(11)

      call datetono(yr,mon,dy,hr,no)

        dd=0.;ll=0
        do i=1,ix
        do j=1,jy
        lon2(i,j)=i-1; lat2(i,j)=91-j
        call distance(lon(n,m),lat(n,m),lon2(i,j),lat2(i,j),out2,angle2)
          if (out2<=800D0 .and. out2>=200D0) then
          dd=dd+lh(i,j,no)
          ll=ll+1
          endif
        enddo
        enddo

      T200(n,m)=dd/float(ll)

      enddo
      enddo

      open(31,file='f:\stips\T200_00-08.txt')
      do n=1,tyno
      write (31,11) ind1,id(n),line(n),seri(n),tcname(n)
      if (ind1==66666) then
      do i = 1, line(n)
      write (31,103) year(n,i),month(n,i),day(n,i),hour(n,i),ind2,grade(n,i),&
      lat(n,i),lon(n,i),mslp(n,i),vmax(n,i),T200(n,i)
      enddo
103   format(4a2,1x,i3,1x,i1,1x,f4.1,1x,f5.1,1x,i4,5x,i3,5x,f5.1)
      endif
      enddo
      close(31)

      end
```

Some subtoutines used in the above FORTRAN codes.

```
      subroutine read_rss_oisst_v2(file_name, sst_data, file_exists)
!     This routine reads version-2 RSS OI SST daily files made from tmi and/or amsre data
!     You must UNZIP FILES before reading them
!
!     INPUT
!     file_name  with path in form satnames.yyyy.doy.v02
!     where satname  = name of satellite (tmi_amsre, amsre, or tmi)
!           yyyy = year
!           doy  = day of year(Julian day)
!
!     OUTPUT
!     sst_data  (a 1440x720 array of data)
!       file_exits  =0 if file read and data returned,  =-1 if no file
!
!     xdim=1440, ydim=720
!     Longitude  is 0.25*xdim-0.125    degrees east
!     Latitude   is 0.25*ydim-90.125
!
!      Values (251 - 255) have special meanings:
!      251 = missing data
!      252 = sea ice
!      253 = missing data
!      254 = missing data
!      255 = land mass

!     Please read the data description on www.remss.com
!     To contact RSS support:
!     http://www.remss.com/support

      character(len=150)                 :: file_name
      real(4), dimension(1440, 720)      :: sst_data
      integer(4)                         :: file_exists
      character(len=1), dimension(1440, 720) :: buffer
      logical lexist
      real(4), parameter                 :: scale  =  0.15
      real(4), parameter                 :: offset = -3.0

!     check to see if file exists -- if not return a -1 in file_exists
      file_exists=0
      inquire(file=file_name, exist=lexist)
      if(.not. lexist) then
          file_exists = -1
          return
```

```
      endif

!     open the file and read in character data
      write(*,*) 'reading sst file: ', file_name
      open(3,file=file_name,status='OLD',RECL=1036800,access='DIRECT',&
       form='UNFORMATTED')
      read(3,rec=1) buffer

!     convert character data to real SSTs using byte scaling and offset parameters
      sst_data = real(ichar(buffer))
      where(sst_data<=250)
          sst_data = (sst_data * scale) + offset
      endwhere

!     close the file and return
      close(3)

      return
      end


      subroutine datetono(year,mon,day,hour,no)
      !to convert date to sequence number of record for 12 hourly data
      integer year,yr,mon,day,hour,jday
      call datetojday(year,mon,day,jday)
      if (hour==0) then
      no=(jday-1)*2+1
      else if (hour==12) then
      no=(jday-1)*2+2
      endif
      return
      end


      subroutine datetojday(year,mon,day,jday)
      !To convert a date to Julian day, 2-digit years will be transformed to 4-digit years.
      integer year,mon,day,jday,log
      if (year>=50) then
      year=year+1900
      elseif (year<=10) then
      year=year+2000
      endif
      call leap_year(year,log)
      if (log==1) then
      select case (mon)
```

```
case (1)
jday=day
case (2)
jday=31+day
case (3)
jday=60+day
case (4)
jday=91+day
case (5)
jday=121+day
case (6)
jday=152+day
case (7)
jday=182+day
case (8)
jday=213+day
case (9)
jday=244+day
case (10)
jday=274+day
case (11)
jday=305+day
case (12)
jday=335+day
end select
else
select case (mon)
case (1)
jday=day
case (2)
jday=31+day
case (3)
jday=59+day
case (4)
jday=90+day
case (5)
jday=120+day
case (6)
jday=151+day
case (7)
jday=181+day
case (8)
jday=212+day
case (9)
jday=243+day
```

```
case (10)
jday=273+day
case (11)
jday=304+day
case (12)
jday=334+day
end select
endif

return
end


subroutine leap_year(yr,log)
! To determine if a year is a leap year or not, 1 for leap year,3 for not
integer yr,log
if(mod(yr,4)/=0) then
log=3
else if(mod(yr,100)/=0) then
log=1
else if(mod(yr,400)/=0) then
log=3
else
log=1
endif

return
end


    subroutine distance(lonA,latA,lonB,latB,out,angle)
! Input: lonA,latA,lonB,latB (longitude and latitude of point A and point B on the Earth)
! Output: out(distance between point A and point B)
! Output: angle (azimuth angle of point B relative to point A)
! If point B is to the east of point A, then the azimuth angle is 90 degree;
! If point B is to the south of point A, then the azimuth angle is 180 degree;
! If point B is to the west of point A, then the azimuth angle is 270 degree;
! If point B is to the north of point A, then the azimuth angle is 0 degree;
    real*8 :: lonA,latA,lonB,latB,out,angle
    real*8 :: RadLoA,RadLaA,RadLoB,RadLaB
    real*8 :: Ec,Ed,dx,dy,dLo,dLa,pi
    real*8, parameter :: Rc=6378.137D0,Rj=6356.752D0

    PI = 4.D0*atan(1.)
    RadLoA = lonA * PI / 180.D0
```

```
    RadLaA = latA * PI / 180.D0
    RadLoB = lonB * PI / 180.D0
    RadLaB = latB * PI / 180.D0
    Ec = Rj + (Rc - Rj) * (90.D0 - latA) / 90.D0
    Ed = Ec * cos(RadLaA)
    dy = (RadLaB - RadLaA) * Ec
    dx = (RadLoB - RadloA) * Ed
    out = sqrt(dx * dx + dy * dy)
    angle = atan(abs(dx/dy)) * 180.D0 / PI
! To determine the quadrant
    dLo = lonB - lonA
    dLa = latB - latA
    if(dLo > 0 .and. dLa < 0) then
    angle = 360.D0 - angle
    else if (dLo <= 0 .and. dLa <= 0) then
    angle = angle + 180.D0
    else if (dLo < 0 .and. dLa > 0) then
    angle = 180.D0 - angle
    endif

    return
    end
```

To develop three linear regression models (CLIPER, BASE, and STIPER):
The following MATLAB codes show an example of developing the 24-hr models using data from 2000 to 2007 and verifying the models using data in 2008. Each of 'all_08p_24.txt' and 'all_08_24.txt' data file contains an n-by-19 matrix of 1 predictand (the 1st column) and 18 predictors (the 2nd to the 19th column) at each of n observations.

```
clear;
clc;

A = load('all_08p_24.txt');
B = load('all_08_24.txt');

%standardization (this part of codes are only used to get normalized
regression coefficients)
% for i = 1:19
% result = ( A(:,i) - mean( A(:,i) ) ) / std(A(:,i),1);
% A(:,i) = result;
% result2 = ( B(:,i) - mean( B(:,i) ) ) / std(B(:,i),1);
% B(:,i) = result2;
% end

Y = A(:,1);
y = B(:,1);

% Select significant predictors suing stepwise regression
X=[ones(size(A,1),1) A(:,2:17)];
stepwisefit(X,Y,'penter',0.01,'premove',0.02)

% BASE model formulation and verification
X1 = [ones(size(A,1),1) A(:,2:4) A(:,6) A(:,8:10) A(:,15)];
[b,bint,r,rint,stats] = regress(Y,X1);
Y1 = X1*b;
MAE = mean(abs(Y1-Y));
RS = 1 - (Y1-Y)'*(Y1-Y) / ( var(Y)*size(A,1) );

X2 = [ones(size(B,1),1) B(:,2:4) B(:,6) B(:,8:10) B(:,15)];
Y2 = X2*b;
MAEt = mean(abs(Y2-y));
RSt = 1 - (Y2-y)'*(Y2-y) / ( var(y)*size(B,1) );

% STIPER model formulation and verification
X3 = [ones(size(A,1),1) A(:,2:4) A(:,6) A(:,8:10) A(:,15) A(:,18:19)];
[b2,bint2,r2,rint2,stats2] = regress(Y,X3);
```

```
Y3 = X3*b2;
MAE2 = mean(abs(Y3-Y));
RS2 = 1 - (Y3-Y)'*(Y3-Y) / ( var(Y)*size(A,1) );

X4 = [ones(size(B,1),1) B(:,2:4) B(:,6) B(:,8:10) B(:,15) B(:,18:19)];
Y4 = X4*b2;
MAEt2 = mean(abs(Y4-y));
RSt2 = 1 - (Y4-y)'*(Y4-y) / ( var(y)*size(B,1) );

%CLIPER model formulation and verification
X5 = [ones(size(A,1),1) A(:,2:4) A(:,6)];
[b3,bint3,r3,rint3,stats3] = regress(Y,X5);
Y5 = X5*b3;
MAE3 = mean(abs(Y5-Y));
RS3 = 1 - (Y5-Y)'*(Y5-Y) / ( var(Y)*size(A,1) );

X6 = [ones(size(B,1),1) B(:,2:4) B(:,6)];
Y6 = X6*b3;
MAEt3 = mean(abs(Y6-y));
RSt3 = 1 - (Y6-y)'*(Y6-y) / ( var(y)*size(B,1) );
```

To train a neural network (NN) model using the same predictors as STIPER:
The following MATLAB codes show an example of developing the 24-hr NN model using data from 2000 to 2007 and verifying the models using data in 2008. Each of 'all_08p_24.txt' and 'all_08_24.txt' data file contains an n-by-19 matrix of 1 predictand (the 1st column) and 18 predictors (the 2nd to the 19th column) at each of n observations.

```
clear;
clc;

A = load( 'all_08p_24.txt' );
B = load( 'all_08_24.txt' );

p = [A(:,2:4) A(:,6) A(:,8:10) A(:,15) A(:,18:19)];
t = A(:,1);
P = p';
T = t';

% train the neural network
net = newff(P,T,7,{'tansig','purelin'},'traincgf');
net.trainParam.epochs = 3000;
net.trainParam.goal = 0.1;
net.trainParam.lr=0.5;
net = init(net);
[net,tr] = train(net,P,T);
Y = sim(net,P);

MAE = mean(abs(T-Y))
R2 = 1 - (Y-T)*(Y-T)' / ( var(T)*size(A,1) )

% verification
P2 = [B(:,2:4) B(:,6) B(:,8:10) B(:,15) B(:,18:19)]';
T2 = B(:,1)';
Y2 = sim(net,P2);
MAE = mean(abs(T2-Y2));
R2t = 1 - (Y2-T2)*(Y2-T2)' / ( var(T2)*size(B,1) );
```

A MATLAB function for multinomial logistic regression:

```
function result = logit(y,x,maxit,tol)
% PURPOSE: computes Logit Regression
%---------------------------------------------------
% USAGE: results = logit(y,x,maxit,tol)
% where: y = dependent variable vector (nobs x 1)
%        x = independent variables matrix (nobs x nvar)
%    maxit = optional (default=100)
%      tol = optional convergence (default=1e-6)
%---------------------------------------------------
% RETURNS: a structure
%        result.meth   = 'logit'
%        result.beta   = bhat
%        result.tstat  = t-stats
%        result.yhat   = yhat
%        result.resid  = residuals
%        result.sige   = e'*e/n
%        result.r2mf   = McFadden pseudo-R^2
%        result.rsqr   = Estrella R^2
%        result.lratio = LR-ratio test against intercept model
%        result.lik    = unrestricted Likelihood
%        result.cnvg   = convergence criterion, max(max(-inv(H)*g))
%        result.iter   = # of iterations
%        result.nobs   = nobs
%        result.nvar   = nvars
%        result.zip    = # of 0's
%        result.one    = # of 1's
%        result.y      = y data vector
% -------------------------------------------------
% SEE ALSO: prt(results), probit(), tobit()
%---------------------------------------------------
% References: Arturo Estrella (1998) 'A new measure of fit
% for equations with dichotmous dependent variable', JBES,
% Vol. 16, #2, April, 1998.


% written by:
% James P. LeSage, Dept of Economics
% Texas State University-San Marcos
% 601 University Drive
% San Marcos, TX 78666
% jlesage@spatial-econometrics.com
if (nargin < 2); error('Wrong # of arguments to logit'); end;
if (nargin > 4); error('Wrong # of arguments to logit'); end;
```

```
% check for all 1's or all 0's
tmp = find(y ==1);
chk = length(tmp);
[nobs junk] = size(y);
if chk == nobs
   error('logit: y-vector contains all ones');
elseif chk == 0
   error('logit: y-vector contains no ones');
end;


% maximum likelihood logit estimation
result.meth = 'logit';

res = ols(y,x); % use ols values as start
[t k] = size(x);
b = res.beta;

if nargin == 2
tol = 0.000001;
maxit = 100;
elseif nargin ==3
tol = 0.000001;
end;

crit = 1.0;
i = ones(t,1);
tmp1 = zeros(t,k);
tmp2 = zeros(t,k);

iter = 1;
while (iter < maxit) & (crit > tol)

tmp = (i+exp(-x*b));
pdf = exp(-x*b)./(tmp.*tmp);
cdf = i./(i+exp(-x*b));

tmp = find(cdf <=0);
[n1 n2] = size(tmp);
if n1 ~= 0; cdf(tmp) = 0.00001; end;

tmp = find(cdf >= 1);
[n1 n2] = size(tmp);
if n1 ~= 0; cdf(tmp) = 0.99999; end;
```

```
% gradient vector for logit
term1 = y.*(pdf./cdf); term2 = (i-y).*(pdf./(i-cdf));
for kk=1:k;
tmp1(:,kk) = term1.*x(:,kk);
tmp2(:,kk) = term2.*x(:,kk);
end;
g = tmp1-tmp2; gs = (sum(g))';
delta = exp(x*b)./(i+exp(x*b)); % see page 883 Green, 1997

H = zeros(k,k);
for ii=1:t;
xp = x(ii,:)';
H = H - delta(ii,1)*(1-delta(ii,1))*(xp*x(ii,:));
end;

db = -inv(H)*gs;
% stepsize determination
s = 2;
term1 = 0; term2 = 1;
while term2 > term1
 s = s/2;
 term1 = lo_like(b+s*db,y,x);
 term2 = lo_like(b+s*db/2,y,x);
end;

bn = b + s*db;
crit = abs(max(max(db)));
b = bn;
iter = iter + 1;
end; % end of while

% compute Hessian for inferences
delta = exp(x*b)./(i+exp(x*b)); % see page 883 Green, 1997
H = zeros(k,k);
for i=1:t;
xp = x(i,:)';
H = H - delta(i,1)*(1-delta(i,1))*(xp*x(i,:));
end;

% now compute regression results
covb = -inv(H);
stdb = sqrt(diag(covb));
result.tstat = b./stdb;
```

```
% fitted probabilities
prfit = ones(t,1)./( ones(t,1)+exp(-x*b));
result.resid = y - prfit;
result.sige = (result.resid'*result.resid)/t;

% find ones
tmp = find(y ==1);
P = length(tmp);
cnt0 = t-P;
cnt1 = P;
P = P/t; % proportion of 1's
like0 = t*(P*log(P) + (1-P)*log(1-P)); % restricted likelihood
like1 = lo_like(b,y,x); % unrestricted Likelihood

result.r2mf = 1-(abs(like1)/abs(like0)); % McFadden pseudo-R2
term0 = (2/t)*like0;
term1 = 1/(abs(like1)/abs(like0))^term0;
result.rsqr = 1-term1;  % Estrella R2

result.beta = b;
result.yhat = prfit;
result.lratio = 2*(like1-like0); % LR-ratio test against intercept model
result.lik   = like1;% unrestricted Likelihood
result.nobs  = t;    % nobs
result.nvar  = k;    % nvars
result.zip   = cnt0; % number of 0's
result.one   = cnt1; % number of 1's
result.iter  = iter; % number of iterations
result.convg = crit; % convergence criterion max(max(-inv(H)*g))
result.y = y;        % y data vector
```